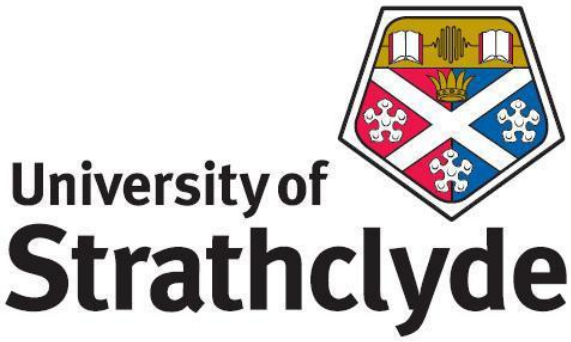

University of Strathclyde

Department of Electronic and Electrical Engineering

Future Power System Dynamic Frequency Response Under High Penetration Levels of Wind

JUN XIA

MSc

A thesis presented in fulfilment of the requirements for the requirement of degree in PhD of Engineering

MARCH 2015

ABSTRACT

Due to environmental concerns, offshore wind plant will play an important role in next decades for meeting the requirement of carbon emission and renewable energy target. The variable speed wind turbine will not have a load-frequency response similar with traditional synchronous generator which may cause the inertia less problems in the system. The UK National Grid has developed scenarios where high wind power penetration levels are considered which are likely to change the patterns of UK transmission network operation and dynamic performance. Therefore, it is necessary to develop an analytical capability which can assess the system dynamic performance ahead of the anticipated changes. Although some work has been reported in this area, the studies are either based on very simple network representations or involve very complex proprietary network modelling not publically available and with results which are often difficult to interpret. This thesis aims to develop appropriate ways of deriving a representative dynamic system model using UK transmission system as a benchmark. The methodology "Individual channel analysis and design (ICAD)" is utilized to realise the trade-off between plant dynamical requirements (feedback design) and the limitations (coupling effects) on achieving such requirements in multivariable system. A representative 21 bus dynamic model of the entire UK transmission system based on Ten Year Statement has been developed and implemented in Power System Simulator (PSS/E). A few recent system-wide events, captured by the existing Phasor Measurement Units (PMU), have been used to validate the frequency response of the model. Moreover, the General Electric (GE) type DFIG models are added for the purpose of analysing the future system performance with the increasing penetration levels of wind energy. The case study reveals that improvements are to be had by transmission line reinforcements under appropriate wind energy distribution scenarios with system transient stability largely improved. The impact of key influencing factors such as the size of the largest generating unit for *n*-1 contingency, amount of primary system response, frequency dependency of load, and others are presented. The study concludes that none of the individual factors can provide a complete solution and that careful cost benefit analysis is needed to determine the proper mix of services and reinforcements needed in the future.

ACKNOWLEDGEMENTS

I would like to express my sincerest thanks to my supervisor, Dr Adam Dyśko and Dr Campbell Booth for accepting me as a PhD student. I would like to give my special thanks to Dr Adam Dyśko for his continued guidance, sincere encouragement, patience, thoughtful support, and understanding during my doctoral studies.

I have also greatly benefited from many intellectual conversations with Prof. W.E. Leithead and Prof. John O'Reilly. I would like to thank for their technical support during my PhD studies.

Finally, to my family, especially my wife, Ji ChenChen, I express my deepest thanks for her unending love, encouragement and support. Thank you my new born baby, Xia YanMing, to give me the strength and motivation to get things done. Thanks to my parents, for their support and understanding.

CONTENTS

LIST OF FIGURES

LIST OF TABLES

LIST OF ABBREVIATIONS AND SYMBOLS

List of abbreviations

AD	Average distribution
AG	Accelerated Growth
AVR	Automation voltage regulator
BMRS	Balancing mechanism reporting system
CFCT	Critical Fault Clearance Time
DFIG	Doubly fed induction generator
EMTDC	Electromagnetic transients program for dc application
ETYS	Electricity Ten Year Statement
FRC	Full rated converter
FRTSG	Frequency response technical subgroup
FSIG	Fixed speed induction generator
GE	General electric
GG	Gone Green
GPS	Global positioning system
HVDC	High voltage direct current
ICAD	Individual channel and design
LFDD	Low frequency demand disconnection
LOM	Loss of Main
MPT	Maximum power track
NETA	New electricity trading arrangement
NG	National Grid
NS	10% North and 70% South distribution
PAC	Pitch angle control
PLL	Phase locked loop
PMU	Phasor measurement unit
PSS	Power system stabiliser
PWM	Pulse width modulation
ROCOF	Rate of change of frequency

RSC	Rotor speed control
RTDS	Real time digital simulator
SG	Slow progression
STATCOM	Static synchronous compensator
SVC	Static var compensator
VS	Voltage vector shift
VSC	Voltage source converter
WTG	Wind turbine generator

List of symbols

Synchronous generator

J	Total moment of inertia of generator
a_{ac}	Rotor angular acceleration
T_m	Mechanical torque
T_e	Electrical torque
T_a	Accelerating torque
ω_m	Rotor velocity
θ_m	Rotor angular position
H	Inertia time constant
R	Speed drop gain
P_e	Electrical power
T_e	Electrical torque
P_m	Mechanical power

Wind Generator

β	Pitch angle
λ_T	Tip ratio
C_p	Power coefficient
R_s	Stator Resistance
R_r	Rotor Resistance
L_s	Stator Leakage Induction
L_r	Rotor Leakage Induction

L_m	Mutual Induction
u_s	Stator Voltage
u_r	Rotor Voltage
ψ_s	Stator flux
ψ_r	Rotor flux
ω_s	Synchronous speed
ω_r	Rotor speed
i_s	Stator current
i_r	Rotor current
s	Slip
D	Damping torque
d-q	d-q transformation, d-axis & q-axis
E_{dc}	Energy stored in dc-link capacitor
Others	
$\{R\}$	Nodes need to be retained
$\{E\}$	Nodes need to be eliminated
V_s	Sending end voltage
V_R	Receiving end voltage
T_1	Governor time constant
T_2/T_3	Fraction of turbine power developed by high-pressure turbine
T_3	Reheater time constant
$\dot{x}_i$	System state variables
u	System inputs
y	System outputs
A,B,C,D	Transfer matrix
λ	Eigenvalues

CHAPTER 1: INTRODUCTION

1.1 Backgroud

Although techniques used in conventional electricity generation are considered reliable nowadays, a number of negative environmental impacts exist, such as greenhouse effect and nuclear radiation which limit their future development. Several renewable energy resources are introduced to replace conventional generation to a certain extent. Wind energy is one of the feasible choices at this moment which has led to the great expansion of wind power generation during the past decade. Some countries, including Germany and Denmark, have already reached, what can be considered, a very high level of wind energy integration. For example, the installed wind power capacity in Germany already reached 20,621MW which is an increase of more than 40% compared with the capacity in 2003 [1]. The typical size of wind turbine unit has reached 5 MW, and what's more, new larger machines are being developed with capacities up to 7-8 MW. Percentage wise, the total renewable energy in Germany is projected to increase from 12.5% in 2010 to at least 20% by 2020 [2]. Danish government has also prepared a plan to build large scale wind farms which will reach a total capacity of 1500 MW in the Eastern part of the country by 2030 [3]. The UK government expects that around 30% of the country's electricity will come from renewable energy by 2020. The total capacity of renewables in 2020 is projected to reach approximately 30GW according to Gone Green scenario [4].

Wind turbines can be divided into two categories: fixed-speed and variable speed drives [5]. The fixed speed induction generator (FSIG) is directly connected to the grid whereas the doubly fed induction generator (DFIG) or fully rated converter (FRC) based wind turbine are decoupled from the grid frequency due to the back-to-back voltage source converter (VSC) connection. When the amount of wind power is relatively low the system frequency and voltage can be maintained without difficulty within statutory limits using conventional synchronous generators. However, the influence of non-synchronous sources can no longer be ignored when the amount of wind power increases beyond certain level. It is known that large scale wind power will increase the difficulties in operation of the power system as a whole. Thus, a

new set of problems related to system load flow as well as dynamic behaviour need to be researched and addressed [6].

Recently, the DFIG or FRC have become the standard wind generating technologies on the market, at least for larger units [7]. Several investigations have already been performed and shown that when wind farms are connected to the network, 3-phase faults can cause a wide area voltage collapse due to the influence of induction machines; frequency and voltage stability deteriorates and network losses increase significantly [1, 8-9]. Paper [10] analyses the dynamic contribution of DFIG-based wind farms to system frequency response in detail. The converter connected wind power plants have no inertia response during network disturbance. In [11-13] the methodologies used to extract kinetic energy with their impact on the system dynamic frequency performance are introduced. The frequency supportive techniques called de-load are mentioned as well. The dynamic oscillatory performance with different types of wind turbines integrated in the system is presented in [6]. The limitations of the voltage support capability of wind turbines at different penetration levels are mentioned in [14]. The impacts of extra FACT devices (SVC or STACOM) on voltage stability are tested. However, either the test systems used in these analyses are very simple containing only one or two generators or they use the IEEE standard networks. None of the investigations use a real representative and properly validated dynamic model.

The work described in [15] investigates the impact of large wind power generation on both the steady state and transient voltage stability. The electromechanical oscillations performances are discussed in paper [1]. Also the steeper frequency drop due to smaller overall system inertia caused by the presence of the wind turbines is reported. In [16], the impact of increased penetration of DFIG is analysed by small signal and transient stability study. Both the beneficial and detrimental impacts are discussed. However, only a limited number of studies from these papers analysed the network frequency response with high penetration level of wind. Furthermore, all of the research studies based on the real test systems involve access to detailed proprietary network data which is not publically available. The results of these tests are also difficult to interpret. Therefore, there is still insufficient amount of research focused on the systematic quantification of the influence of

increasing wind penetration levels on power systems frequency performance, especially in a large power system.

1.2 Motivation: future UK power system challenges

For the purposes of meeting the targets for the reduction of carbon emissions, each country in Europe has established their individual scenarios to replace the conventional generation plant with the renewable energy sources such as wind and solar power plant. Especially regarding the wind energy, the National Grid in Great Britain indicated in their Ten Year Statement (ETYS) in 2014 that the capacity of wind is expected to reach a high percentage (28.5% in 2020 and finally increasing to 43% in 2035) of the total power capacity under the assumed energy scenarios [4]. Although these renewable sources offer many benefits, the applied non-synchronous generating technologies cannot provide inertia or frequency response to the network. This issue has been highlighted in the recently released System Operability Framework document by National Grid [17]. Thus, the future system stability is likely to face new challenges:

Frequency management: The UK National Grid has been evaluating the influence of future frequency response services during the past years with the purpose to secure the system in the future. There will be a significant change of generation portfolio in the coming years [18]:

- Increase in renewable generation (wind) to 29 GW
- The installed wind capacity exceeding the summer minimum demand
- Increased size of the largest unit for *n*-1 contingency (from 1320 MW to 1800 MW)

Due to these changes, the rate of change of frequency (RoCoF) technique which is typically utilized in loss of mains (LOM) protection of distributed generation will face serious challenges in the future. High RoCoF values in the system can temporarily occur over the entire network in the event of loss of large infeed (generation or import) or demand (export). Once the measured RoCoF reaches the value of the relay setting according to each distributed generation protection, the generators will stop generating which may cause the operation of Low Frequency Demand Disconnection (LFDD). In these circumstances, a large number of

electricity consumers can lose their electricity supply. This happened once in UK on 27th May 2008 when 546 MW of demand had to be shed to preserve system stability.

The current balancing strategies are established for the purpose of ensuring that the existing recommended RoCoF setting is not exceeded. This can be achieved by two actions: pay for additional synchronous generators to run partly de-loaded during the high renewable generation and low demand periods, or limit the largest infeed loss. However, the increasing capacities of non-synchronous generators make these conventional solutions less and less economically viable. The UK National Grid is therefore seriously concerned about potential LFDD situations in the future especially under following two conditions:

1) High import or windy conditions during summer minimum demand
2) Largest infeed loss increased of 1800 MW

Under these conditions, LFDD is very likely to be triggered without any prevention policies being developed in the future [19]. In order to secure the network frequency performance, the preventing actions must be decided. In the National Grid document "Future Frequency Response Services" published by the Grid Code Review Panel [18], the possible impact of the significant changes in the mix of UK electricity generation on frequency requirements were discussed; in later August 2013, the Frequency Response Technical subgroup (FRTSG) [19] presented their conclusions with two main proposals for preventing the risks in RoCoF:

The first action is to change the current RoCoF setting: this is achieved by either disabling the relay or setting the threshold at a relatively higher value to ensure LOM protection stability during system wide frequency deviations. The anticipated recommended setting would be in the order of 1 Hzs^{-1} and possibly with additional time delay.

The second action is related to the sufficient amount of primary frequency response: additional synchronous generators are paid to limit the speed of change of frequency, or new control technologies applied in the non-synchronous generators (DFIG or inverter connected power plants) which allow these generators to provide fast response following frequency deviation which is often termed as "Synthetic Inertia".

Reactive power management: According to the future plan that with the increasing amount of renewable energy, many coal plants will be decommissioned especially in the centre of the UK network. Although large offshore wind farms can provide local reactive power support through HVDC connection, this reactive power support is only available at the point of connection. Low MVAr capability of onshore DFIG based generation is also likely to result in shortage of reactive power control capability in the future. These changes lead to new challenges related to reactive power compensation in the centre of the network, negative influence on the boundary transfer capability near the centre, and the transient stability issues.

Power flow volatility: The varying wind speed distribution across the country during normal operation conditions may lead to significantly different wind power output distribution. This changes the pattern of the power flow throughout the UK which historically was largely unidirectional. Such variations may enhance or worsen the transmission capacity across each critical boundary.

As mentioned earlier, although several research projects have been undertaken in the past, none of them tested the system frequency performance based on a large power network, or else, the testing network involves proprietary network data which is not publically available, and the results are difficult to interpret. Hence, the main motivation of the thesis is to explore and quantify the level of potential risk in the system with the increasing penetration level of wind power plants. A validated dynamic model which can represent the UK transmission network is needed. The results are intended to offer enhanced understanding and provide suggestions for power system stability and security issues of UK in the future through a number of case studies based on the different future wind distribution scenarios.

1.3 Research objectives

In order to analyse the potential risks in the UK transmission system in the near future, the main objectives of the research carried out in this thesis are as follows:

- To investigate and develop appropriate network reduction methodology in power system modelling.
- To develop aggregated representative models of the UK transmission system. The model should be capable of performing both steady-state power flow

studies and dynamic simulations. An important aspect of the model is its flexibility and ease of parameter adjustment for the purposes of exploring a variety of future system scenarios.

- To investigate possible oscillation phenomena in the UK transmission system. Suitable control system design methods should be utilized to determine the appropriate locations and parameter tuning of the control devices.
- To propose a practical methodology for the validation of the established equivalent dynamic model. The validation should include several aspects: 1) validity under different operating conditions; 2) good accuracy in power flow results; 3) good system dynamic frequency response, which can accurately replicate similar swing curves recorded from the real system events.
- To analyse and quantify the transient stability and frequency profiles of the system with high penetration levels of wind. Find out the critical operating conditions (operating limits) which may cause the system to become unstable. Point out the possible solutions on how to ensure continuing safe operation of the system.

1.4 Research contribution

In order to address the main objectives outlined in the previous section, the following points highlight the key research contributions of this thesis:

- A novel power network reduction method has been developed and demonstrated. It was identified that the existing techniques for obtaining network equivalent model developed in 1980s have many disadvantages and limitations. The proposed method is suitable for all types of power systems. An approach to achieve model flexibility in changing the system operating conditions is also presented.
- A systematic comparison between the proposed network reduction method and earlier established methods is presented. The improved accuracy of the proposed method is demonstrated not only in steady state analysis but also through transient simulation.

- A representative UK system model based on the publically accessible information included in “Ten Year Statement” [4] has been developed using the proposed network reduction method.
- Through small signal analysis, one unstable and two lightly damped system inter-area modes were initially identified using the reduced equivalent UK system model. The Bode-type frequency response analysis, as well as the individual channel and design (ICAD) analysis have been both applied to achieve adequate oscillatory stability. Eight appropriate locations were found to equip existing generators with power system stabilizers (PSS).
- The UK system future transient stability performance is investigated by way of assessing the potential risks (caused by different wind penetration scenarios) and benefits (result from transmission line reinforcements). Moreover, the analyses of the possibility of increasing the critical fault clearance time (CFCT) by introducing additional reactive power compensators are also included.
- With regards to system RoCoF under high wind penetration, detailed evaluation of the impact of the three major influencing factors has been performed: amount of maximum generation loss, fast frequency response reserve, and characteristic of frequency dependent demand. This realistic quantification is intended to inform cost benefit analysis of potential alternative solutions to UK transmission system challenges in the future.

1.5 Thesis organization

The thesis includes seven chapters and is organized as follows:

Chapter 1 introduces the motivation, key objective and contributions of the thesis.

Chapter 2 summarises the background knowledge related to power system analysis. Furthermore, it focuses on the wind energy generating systems especially the doubly fed induction generator (DFIG). The introduction of the theoretical principles of the wind power plant control system is presented. In addition, the assessment of the GE WT3 model which is utilized in PSS/E software is also included.

In Chapter 3, the three major network reduction methodologies are first introduced. Due to their limitations and the need of full detail dynamic network data when applying these methods, a new practical equivalent model method is presented. The method is explained by using the UK transmission system as an example. The network impedance data of the equivalent model for load flow studies is calculated.

In Chapter 4, unstable or lightly damped system inter-area modes are identified by small signal analysis. The individual channel analysis and design (ICAD) method is highlighted as an optimal tool for improving system oscillatory stability. With the help of ICAD, the coupling effects among control devices are identified by decomposing the original multivariable system into several single-input single-output channels. Then, appropriate power system stabiliser (PSS) locations are found and controller parameters tuned. The effects of applying these control devices are also verified through time domain simulations.

Chapter 5 validates the proposed method in two ways: 1) comparing system frequency response with the previously established Ward method using the well-known IEEE 14 bus system as a benchmark; 2) comparing the reduced UK dynamic system frequency performance with the historical real events data records obtained from the existing Phasor Measurement Units (PMU). The processes of extending the equivalent model to represent future scenarios in the UK transmission system are also described.

In Chapter 6, the system transient stability is discussed where different wind penetration levels, wind speed distribution conditions and load conditions are considered. The necessity of adding additional reactive power compensators is mentioned in order to satisfy the minimum 80 ms (CFCT) requirement. The system RoCoF is characterised through the evaluation of various influencing factors including: frequency dependent load, fast frequency response reserve and amount of maximum generation loss in a single event.

Chapter 7 presents the conclusion of the work and provides several suggestions for the future research work.

Publications

The following publications were produced during the development of the research presented in the thesis:

[1] J. Xia, A. Dyśko, J. O'Reilly, "Impact of induction machine based wind generation on power system voltage and oscillatory stability", *Universities Power Engineering Conference (UPEC), Soest, Germany*, 5–8 September 2011, paper 233, published on CD

[2] J. Xia, A. Dyśko, "UK transmission system modelling and validation for dynamic studies," *Innovative Smart Grid Technologies Europe (ISGT EUROPE)*, 4th IEEE/PES , Copenhagen, Denmark, 6-9 Oct.2013, pp.1-5

[3] J. Xia, A. Dyśko, J. O'Reilly, "Future stability challenges for the UK network with high wind penetration levels," *IET Generation, Transmission & Distribution*, accepted on 19th Dec 2014

References

[1] I. Erlich, F. Shewarega, "Insert impact of large-scale wind power generation on the dynamic behaviour of interconnected systems," *Bulk Power System Dynamics and Control - VII. Revitalizing Operational Reliability, 2007 iREP Symposium* , Charleston, USA, 19-24 Aug. 2007, pp.1-7

[2] Tennet, "*Germany Grid Code*", Dec.2012. http://www.tennet.eu/de/en/customers/grid-customers/grid-connection-regulations.html

[3] M. Bruntt, J. Havsager, H. Knudsen, "Incorporation of wind power in the east Danish power system," *Electric Power Engineering, 1999. PowerTech Budapest 99. International Conference,* Gentofte, Denmark, Aug.1999, pp.54

[4] National Grid, "*Electricity Ten Year Statement 2014*", 2014 http://www2.nationalgrid.com/UK/Industry-information/Future-of-Energy/Electricity-Ten-Year-Statement/

[5] M. Eremia, M. Shahidehpour, "*Wind Power Generation*", John Wiley & Sons, Inc, Hoboken, NJ, USA, 2013.

[6] J.G. Slootweg, W.L. Kling, "The impact of large scale wind power generation on power system oscillations", *Electric Power Systems Research*, Vol. 67, Issue 1, October 2003, pp. 9-20

[7] T. Thiringer, A. Petersson, T. Petru, "Grid disturbance response of wind turbines equipped with induction generator and doubly-fed induction generator," IEEE *Power Engineering Society General Meeting*, Toronto, Canada, 13-17 July 2003, pp.1542-1547

[8] V.V. Thong, D.V. Dommelen, R. Belmans, "Penetration level of distributed energy resources with anti-islanding criteria and secure operation of power system," IEEE *Power Engineering Society General Meeting*, Montreal, Canada, 18-22 June 2006, pp.1-7

[9] H. Shien, W. Weizhou, J. Huaisen; C. Gang, *et al*, "Integration of wind farm into Gansu power grid and its operation," *SUPERGEN, International Conference on Sustainable Power Generation and Supply*, Nanjing, China, 6-7 April 2009, pp.1-5

[10] M. Kayikci, J.V. Milanović, "Dynamic Contribution of DFIG-Based Wind Plants to System Frequency Disturbances," *IEEE Transactions on Power Systems*, vol.24, no.2, May 200, pp.859-867

[11] G. Ramtharan, J.B. Ekanayake, N. Jenkins, "Frequency support from doubly fed induction generator wind turbines," *Renewable Power Generation, IET*, vol.1, no.1, March 2007, pp.3-9

[12] H.T. Ma, B.H. Chowdhury, "Working towards frequency regulation with wind plants: Combined control approaches," *Renewable Power Generation, IET*, vol.4, no.4, July 2010, pp.308-316

[13] Z.S. Zhang, Y.Z. Sun, J. Lin, *et al*, "Coordinated frequency regulation by doubly fed induction generator-based wind power plants," *Renewable Power Generation, IET* , vol.6, no.1, January 2012, pp.38-47

[14] M. J. Hossain, H.R. Pota, M.A Mahmud, *et al*, "Impacts of large-scale wind generators penetration on the voltage stability of power systems," *Power and Energy Society General Meeting, 2011 IEEE* , San Diego, Canada, 24-29 July 2011, pp.1-8

[15] C. Yongning, L. Yanhua, W. Weisheng, *et al*, "Voltage Stability Analysis of Wind Farm Integration into Transmission Network," *Power System Technology International Conference*, Chongqing, 22-26 Oct. 2006, pp.1-7

[16] M. J. Hossain, H.R. Pota, M.A. Mahmud, *et al*, "Investigation of the Impacts of Large-Scale Wind Power Penetration on the Angle and Voltage Stability of Power Systems," *Systems Journal, IEEE* , vol.6, no.1, March 2012, pp.76-84

[17] National Grid, "*Future Operability Framework*", Sep. 2014, pp.1-34

[18] National Grid, "*Future Frequency Response Services*", Grid Code Review Panel, Sep 2010, pp.10-21

[19] National Grid, "*Frequency Change during Large Disturbances and their Impact on the Total System*", Industry consultation report, Aug. 2013, pp.1-45

CHAPTER 2 POWER SYSTEM AND WIND TRUBINE ANALYSIS BACKGROUND

2.1 Introduction

The burning of fossil fuels is having a significant influence on the global climate. Hence, the use of low-carbon electricity generation sources such as wind is becoming one of the most important topics in many countries. The classification of wind turbines from the geographical expression is divided into two parts, onshore and offshore wind turbines [1]. The cheaper foundation of onshore wind turbine is attractive to us, however, visual and noise impacts are not welcomed from social publics. The characteristics of lower wind turbulence with higher average wind speeds of offshore wind farms make this type of wind farm be widely used although its capacity cost is probably 30%-50% higher than onshore wind farm.

The most of variable-speed wind turbines are converter-connected to the grid. Therefore, it cannot provide the similar frequency response to the network during disturbances as synchronous generators do. There will be a new set of challenges related to system stability performances in the near future. For example, high rate of change of frequency, reactive power control, system load flow balancing and transient stability [2-3]. Thus, it is necessary to gain the background knowledge of the power system analysis and have a good understanding of the frequency performance of wind turbine.

In this chapter, the international dynamic frequency response requirements are introduced in section 2.2; the background knowledge of power system stability analysis are mentioned in 2.3; section 2.4 introduces the general mechanical structure and aerodynamic characteristics of the wind turbine; section 2.5 gives a detailed explanations of the control systems used in the variable speed based wind turbine; in section 2.6, the introduction of the GE 1.5 MW WTG model used in PSS/E software is presented; section 2.7 gives the summary.

2.2 The International Dynamic Frequency Response Requirements.

The power systems up to date are mostly consisted by thermal plants with relative high inertia constants and have ability to provide primary and secondary

frequency response during frequency deviations. All the register generators should meet the requirement to provide frequency response capability during network disturbances according to the grid code proposed by their countries. Several grid codes of Europe countries are introduced:

The *German grid code* pointed out that every generator should be capable at a reduced power output and to allow constant power control of 1% of its rated power per minute. All the generators with a registered rating larger than 100 MW should be able to provide primary frequency response. No generator is allowed to be disconnected from the grid automatically while the frequency is between 47.5-51.5 Hz [4-5]. The wind power plant operators must contract frequency control services from other power plants to provide frequency response during disturbances.

The *Danish grid code* defined the normal full-load frequency operating range between 49.0 Hz-50.5 Hz. If the frequency is lower than 49.0 Hz, the power station unit must be able to supply the reduced power to the grid (15% of normal maximum power at 47.5 Hz and 0% at 49.0 Hz). All the power stations are equipped with excitation system to ensure a constant voltage in the point of common coupling. The power stations should be able to use/produce reactive power under any fault or disturbance [6]. The wind power plants must stay connected to the grid if they are operating in the range between cut-in and cut-out wind speed. For the purpose of preventing instability, the wind generators are required to equip with the de-load function.

The *Great Britain grid code* stated that the system frequency must be maintained as close to 50 Hz and with an operational limit of 0.2 Hz. The infrequent infeed loss limit in the network is 49.2 Hz. The system frequency is permitted to raise to52 Hz and fall to 47 Hz in exceptional circumstances. The voltage should be within $\pm$ 10% of its normal value during normal operating conditions. Each generating unit, onshore/offshore power park (not less than 50 MW) or DC converter should equipped with a fast acting frequency controller to provide frequency response during normal operating conditions. For conventional generation units, the frequency control device should be designed with the speed droop characteristic between 3% and 5%. The onshore/offshore power park should also have an equivalent speed droop setting between 3% and 5% [7].

In UK, the network frequency control is regulated by the National Grid in the way of three contracts: mandatory frequency response, frequency control by demand management (FCDM) and firm frequency response [8].

Mandatory frequency response means that the generators should have capability of changing theirs active power automatically in response to a frequency change according to the requirement of grid code CC 6.3.7 as shown in Figure 2.1 [7-8]: the generation unit with a completion date after 1st January 2001 must provide:

- Primary frequency response: the additional active power in response to frequency deviation must be achieved in 10s and sustained for a further 30s.
- Secondary frequency response: provision of additional active power within 30 s and sustained for 30 mins.
- High frequency response: the reduction of active power for a generation within 10 s and sustainable thereafter.

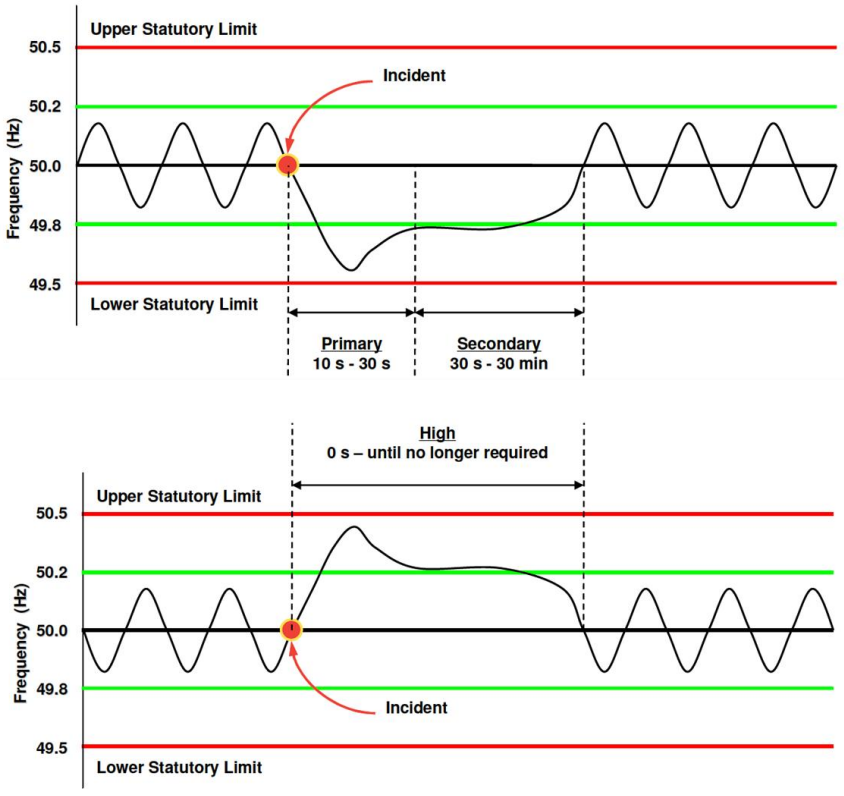

Figure 2-1. Frequency response profile [8]: a) Primary and Secondary frequency response; b) High frequency response

FCDM provides non-dynamic frequency response by the interruption of demand. The customers should be able to interrupt their demand for 30 minutes. Firm frequency response is also referred to as commercial frequency response. The providers must be contracted by participating in the tender process.

The minimum frequency response requirement for a 0.5 Hz frequency change is demonstrated in Figure 2.2. All the generation units should provide frequency response according to the solid boundaries. For example, if the disturbance causes the frequency drop was 0.5 Hz, assumed that the power plant was generating at 85% of its registered capacity, the generator should provide 7% active power of its registered capacity for primary frequency response; if the frequency drop was 0.2 Hz while the power plant was generating at 55% (minimum operating level), the minimum frequency response is 4% (10%*0.2/0.5).

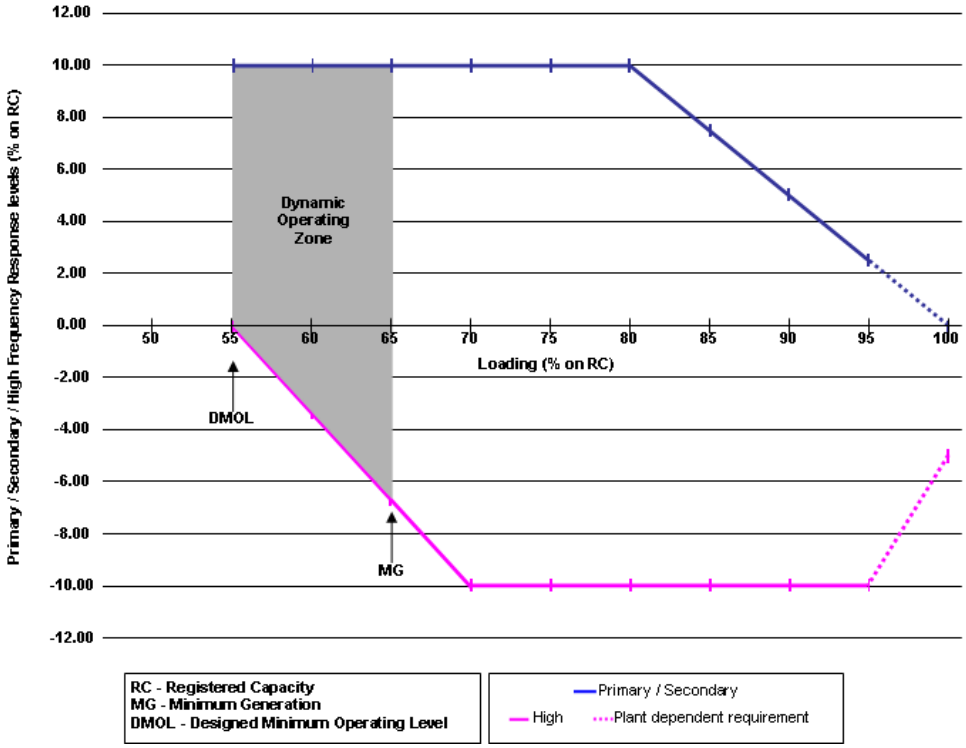

Figure 2-2. Minimum frequency response requirements for a 0.5 Hz frequency change [7]

2.3 Power System Stability Analysis

2.3.1 Inertia response: swing equation

In power system stability refers to the ability of synchronous generators move from one steady state operating point to another steady state operating point without

losing synchronism [9]. The rotor dynamics of synchronous machines are determined by the rotational swing equations which describe the unbalance performance between generators' mechanical power and electrical power. Under steady state condition, each individual generator should have equal electrical power and mechanical power. If disturbances occur at the network, for example: sudden loss of one major power plant, the system frequency will drop. The largest frequency drops as well as the rate of change of frequency are defined in each country's grid code to ensure the system to remain stable during the events. The frequency performances are largely dependent on the inertia of the power system. The swing equation of the synchronous generator is explained below.

Considering a normal synchronous generator unit, its rotor motion can be expressed as (2.1) according to Newton's second law:

$$Ja_{ac}(t) = T_m(t) - T_e(t) = T_a(t) \tag{2.1}$$

where: J is total moment of inertia of generator, $k_g m^2$; a_{ac} is rotor angular acceleration, rad/s^2; $T_m$is mechanical torque, Nm; T_e is electrical torque, Nm and T_a is accelerating torque, Nm.

The rotor angular acceleration can be expressed as:

$$a_{ac}(t) = \frac{d\omega_m(t)}{dt} = \frac{d^2\theta_m(t)}{dt} \tag{2.2}$$

$$\omega_m(t) = \frac{d\theta_m(t)}{dt} \tag{2.3}$$

where: ω_m is the rotor velocity, rad/s; θ_m is the rotor angular position in radians with respect to a synchronous rotating reference.

In power system analysis, it is always easier to work with per unit than actual unit and use power rather than torque. The inertia equation can be then expressed as:

$$\frac{J\omega_m(t)}{S_{rated}}\frac{d^2\theta_m(t)}{dt} = \frac{\omega_m(t)T_m(t) - \omega_m(t)T_e(t)}{S_{rated}} = \frac{P_m - P_e}{Srated} \tag{2.4}$$

$$\frac{2H}{\omega_{syn}}\omega_{p.u}\frac{d^2\theta_m(t)}{dt} = P_{m\,p.u} - P_{e\,p.u} = P_{a\,p.u} \tag{2.5}$$

$$H = \frac{\frac{1}{2}J\omega_{msyn}^2}{S_{rated}} = \text{Joules/VA or per unit seconds}$$

$$= \frac{\text{stored kinetic energy at synchronous pseed}}{\text{generator votampere rating}} \quad (2.6)$$

Equation (2.5) is called the swing equation and *H* is the inertia constant which is normally between 1-10 s.

2.3.2 Speed drop control

In power system, the turbine governor adjusts its valve or gate following the frequency disturbances in order to compensate the power imbalance of the network. According to the swing equation, if there is an increase in load, the electrical power will increase while the mechanical power is still remain constant initially. The deceleration torque causes a reduction in rotor speed while the kinetic energy is released to compensate the increased load. Usually the measured rotor speed signal ω_r is compared with the reference value ω_0. The error signal $\Delta\omega_r$ is sent to create the control signal of valves/gates of the turbines. The rotor speed and frequency return to its reference value if the amount of turbine mechanical power increased equal to the additional load [10].

However this control strategy can be applied if only one generator is required to response to the change in load in multi-generator system. When the power loads are shared between a number of generators connected to the system, they might fight each other to control the frequency. Therefore, the speed droop control is introduced.

The control loop of the speed droop control is demonstrated in Figure 2.3:

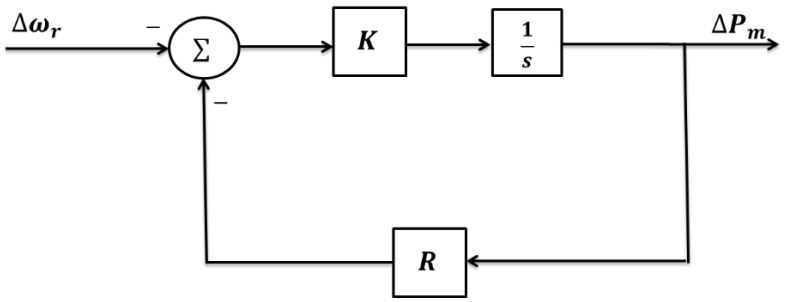

Figure 2-3. Speed Droop Control

The speed droop gain value *R* determines the characteristic between speed deviations and active power changes in the network. It is equal to the ratio of percent frequency change to the percent power output change:

$$R = \frac{percent\ frequency\ change}{percent\ power\ change} = (\frac{\omega_{NL}-\omega_{FL}}{\omega_0})/\Delta P \quad (2.7)$$

$$\Delta P_m = \Delta P_{ref} - \frac{1}{R}\Delta f \quad (2.8)$$

where ω_{NL} is the no load speed; ω_{FL} is the full load speed and $\omega_0$is the normal rated speed.

Figure 2.4 shows the characteristic of network frequency versus active power output. For example, a 2% droop means that if there is a 2% frequency deviation, the generator output will have a 100% change from no load condition to full load condition.

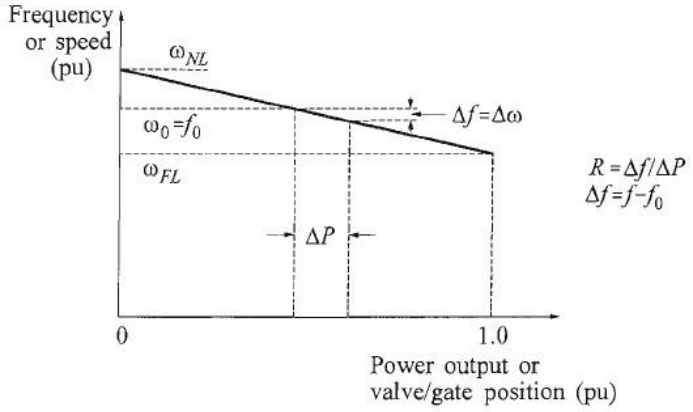

Figure 2-4. Characteristic of frequency versus power [10]

2.3.3 Loss of mains protection

In power system operation, if one part of the network loss connection to the main utility network, it is referred to as loss of mains (LOM) or islanding. If such situation is not detected, the generators inside this part may remain connected which will cause safety hazards in the system. Hence, the loss of mains protection is of one the most important safety requirements in all countries. There are various techniques used in detecting the islanding issues such as RoCoF; voltage vector shift (VS); rate of change of power or direct intertrip, etc. Paper [11] provides a detailed explanation and literature reviews on islanding detecting methods. Among these methods, the RoCoF is widely used in detecting the LOM in many countries for example: UK, Austria, Belgium and Italy since it can provide a fast, reliable and economical detection.

Rate of change of frequency: RoCoF estimates the rate of change of frequency according to the local measurement of the voltages. The measured values are

compared with a pre-set threshold. In some cases, additional time delay is applied. The RoCoF is defined as:

$$RoCoF(t) = \frac{df(t)}{dt} \tag{2.9}$$

$$f(\mathrm{t}) = f_0 + \Delta f(t) \tag{2.10}$$

The existing recommended setting of the RoCoF in UK is 0.125 $\mathrm{Hz\,s^{-1}}$. However, if there is a large infeed (generation or import interconnection) or off take (demand or export interconnection) loss exists, the value of the RoCoF can be relatively high at the very beginning of the disturbance. The distribution network may have high risk of spurious disconnection from the grid caused by the RoCoF based protection relays. Therefore, accurate RoCoF settings are necessary in order to ensure a reliable system operating conditions in the future.

2.3.4 Reactive power compensation

In power system, the stabilization of system voltages is achieved by the reactive power control. The most of electric equipment need to be operated within a specific voltage range. Inadequate or excessive reactive power may cause voltage instability problems. High or low voltage does harmful to equipment's life if the equipment operates outside the required range with a long time (for example 15min).

However reactive power does not transmit over long distance due to the huge losses consumed on the wires. The voltage control must be realized locally by using specific control devices dispersed throughout the network. This is not similar to the frequency management which can be regulated by the global active power dispatch. Hence, to determine the locations and types of the reactive power compensator is one of the most important tasks in power system analysis. The commonly used reactive power compensators are: series compensator, shunt compensator, static var compensator and STATCOM [10].

2.3.5 Critical fault clearance time (CFCT)

In order to understand the transient performance of the system, plots of the electrical power P_e and mechanical power P_m versus power angle δ are first introduced as shown in Figure 2.5. Assume the system is operating in steady-state where P_e=P_m=P_{m0} and $\delta = \delta_0$. If one major disturbance occurred at t=0 for example:

one three-phase-to ground fault reduced the electrical power P_e output to zero and remained zero until the fault was cleared. The acceleration power described above P_a (0^+) was positive since P_m (0^+) was greater than P_e (0^+) after the fault had happened. The rotor started to accelerate and δ increased. When δ reached δ_1, P_e=P_m=P_{m1}. However, the speed of acceleration $d\delta/dt$ was still positive and rotor would continue to increase. When δ was greater than δ_1, P_e was greater than P_m. The acceleration power P_a was negative and rotor started to decelerate. Finally, δ reached the maximum value δ_2 and swing back. If δ exceeded δ_3, P_m was greater than P_e again and the rotor would accelerate again. This caused a further increase in δ and the system lost stability finally.

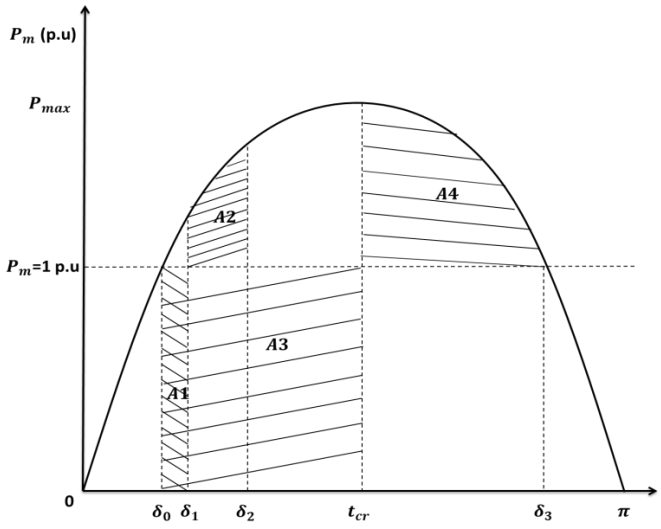

Figure 2-5. Power System Equal Area Criterion

Theoretically, the method used for determining the stability of the system can be achieved by the *equal area criterion*: the system can remain stable if the shaded acceleration area A1 is equal to the shaded deceleration area A2. The critical clearing time (t_{cr}) is the maximum fault duration which allows the A3=A4 [9] as shown in Figure 2.5.

2.4 Wind Generation

The typical wind turbine system is consisted by rotor blades, a gear box and generator. They are all located inside a nacelle on the top of the tower. Wind is the fluid which contains a lot of quickly moved particles. These particles make the

blades begin to turn. Then, the rotating blades turn the shaft and the gearbox increases the rotational speed until it is appropriate for the generator [12].

2.4.1 Aerodynamic characteristics in wind turbine

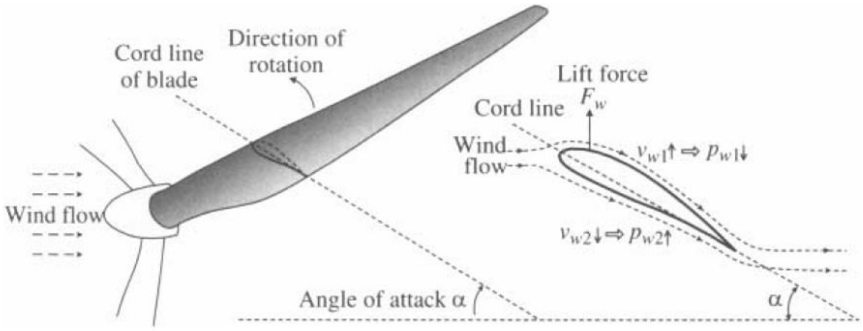

Figure 2-6. Wind turbine blade aerodynamics [13]

The aerodynamic characteristics in wind turbines are shown in Figure 2.6. The difference between wind speed v_{w1} (above) and v_{w2} (below) creates the lift force F_w on the blade which makes the blade rotate [13-14]. The tip speed ratio λ is defined as the ratio of the rotational speed of blade tip to the wind speed as given by:

$$\lambda_T = \frac{\omega_M r_T}{v_w} \tag{2.11}$$

where v_w is the wind speed; r_T is the radius of turbine rotor and ω_M is rotating speed of blade. The lift force is normally controlled by the angle of attack α or the pitch angle β, where α is the angle between the direction of wind speed and cord line of the blade; β is the angle between the centreline and the horizon.

The relations between wind turbine mechanical power and wind speed can be explained by introducing the power curve which is characterised by three wind speeds: cut-in wind speed, rated wind speed and cut-out wind speed as shown in Figure 2.7.

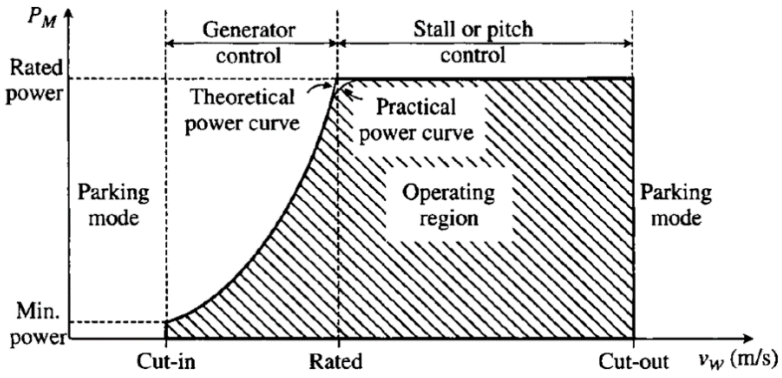

Figure 2-7. Power curve: wind turbine mechanical power versus wind speed [13]

The cut-in speed is the speed which enables turbine start to operate since the enough power should be captured by the blade for compensating the losses. The rated speed is the speed which wind turbine produces the rated output power, most of the wind generators operate at its rated capacity at wind speed between 12m/s to 16m/s. If the wind speed exceeds the cut-out speed for example (20m/s to 25m/s), the turbine must be forced to shut down.

Power coefficient C_p: The air mass power flowing at the speed v_w across an area *A* can be calculated:

$$P_w = \frac{1}{2}\rho A v_w^3 \tag{2.12}$$

where ρ is the air density (kg/m^3); *A* is the area swept by the rotor blades (m^2) and v_w is the wind speed. However, wind energy cannot be entirely transferred into mechanical energy, the mechanical power is calculated with an efficiency parameters: power coefficient C_p.

$$P_w = \frac{1}{2}\rho A v_w^3 C_p \tag{2.13}$$

The value of power coefficient C_p is depended on wind speed, turbine rotational speed and pitch angle. Figure 2.8 demonstrates the relationship between power coefficient in terms of pitch angle β and speed ratio λ [14]. The maximum power can be captured at optimal tip speed ratio λ with a given value of β. Hence, wind plant should be equipped with the control mechanisms to regulate its generation output with the variation of wind speeds. The control procedures are achieved by stall control or pitch control.

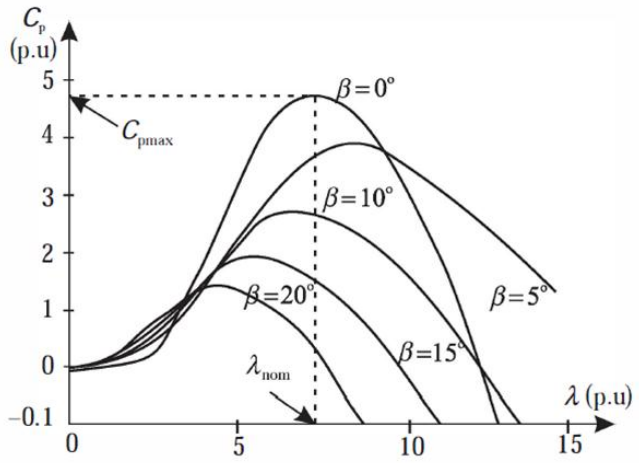

Figure 2-8. Power coefficient C_p characteristic [14]

Stall control. The stall control is to keep blade at an optimal angle of attack, so the blade can capture maximum power under wind speed which is below its rated value. If the wind speed exceeds rated speed, turbulence caused by strong wind will make the blade not facing the wind which leads lift force decrease and finally becomes zero. This phenomenon is referred to as stall [13].

Pitch control. Similar to the stall control, pitch control have adjustable blades to capture maximum power when the wind speed is at or below its rated value. However, it turns the blade out of the wind when wind speed exceeds rated value to reduce lift force. Hence, it is possible to maintain the rated power above the rated wind speed.

2.4.2 Fixed speed induction generator (FSIG)

The squirrel cage induction generator is used in fixed speed wind generator. Figure 2.9 introduces the basic structure of FSIG. It includes: aerodynamic turbine rotor, gearbox, blade control system (stall control), induction generator and reactive power compensator [12].

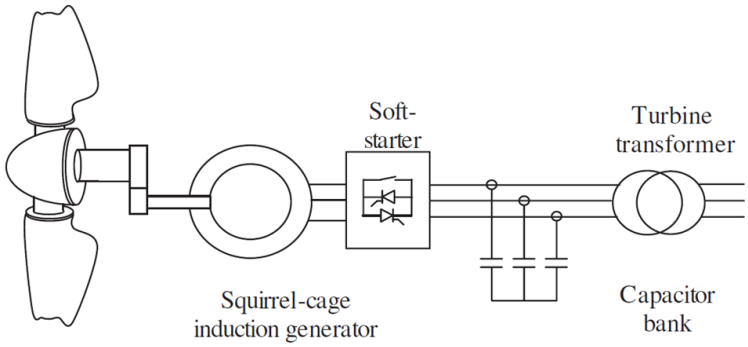

Figure 2-9. Fixed speed induction generator [12]

The FSIG is directly connected into the network. As a result, the turbine has to operate at constant speed. Usually, the device refers to soft-starter unit is equipped to the FSIG to minimize transient currents during energization of the generator [12, 14].

Most induction generators need the support from the reactive power compensators. Otherwise the FSIG based wind turbine may have difficulties in meeting the requirement relates to the voltage control capability. Figure 2.10 shows the characteristic between reactive power absorbed by induction generator and slip *s* [15]. It demonstrates that during the disturbance such as a network fault or a sudden increase of load, the slip of induction generator may increase which results a

significant increase of the reactive power absorbed by induction generator. In most of cases, the reactive power compensators relate to capacitor bank, static var compensator or STATOM are employed to provide reactive power support to FSIG.

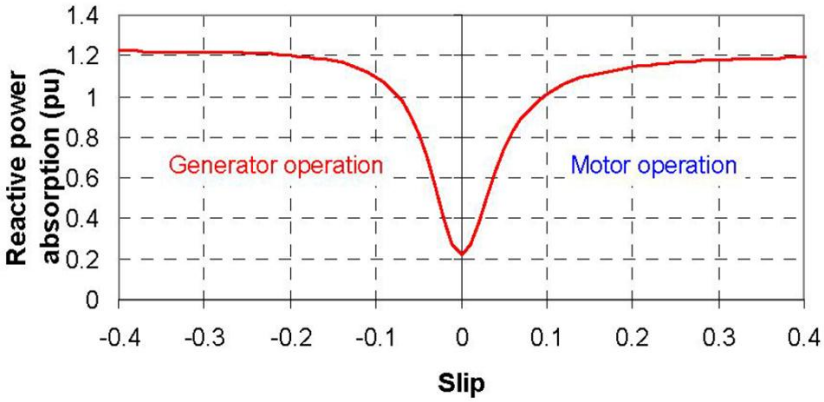

Figure 2-10. Reactive power absorbed by an induction generator [15]

2.5 Variable Speed Wind Turbine

With the increasing requirements of the renewable energy, the control technology changes from fixed speed into variable speed since it can not only import / export reactive power to the grid but also be able to remain synchronized while wind turbine speed varies. There are two types of variable speed wind power plants: double fed induction generator (DFIG) and fully rated converter wind turbine (FRC) based on a synchronous generator. In this chapter, the detailed theory of doubly fed induction generator is explained. The dynamic modelling of DFIG with its control policies are illustrated as well.

2.5.1 DFIG configuration

The typical DFIG is consisted with a wound rotor induction generator where its stator is directly connected to the grid and rotor side is connected via a back-to-back voltage source converter. Nowadays, the most commonly used power converter is IGBT-based voltage source converter (VSC) [16]. The variable-speed operation is achieved by injecting a controllable voltage into the rotor at the desired slip frequency. Therefore, the magnetic field created in the rotor is not fixed. It rotates at the frequency f_{rotor} (Hz) which is proportional to the frequency of the current on the rotor side winding. The relationship between rotor rotation speed n_{rotor} (r/min), rotor magnetic field rotation speed f_{rotor} and frequency of rotating magnetic field on stator winding f_{stator} (Hz) can be determined as follow[17]:

$$f_{stator} = \frac{n_{rotor} * N_{poles}}{120} + f_{rotor} \quad (2.14)$$

where N_{poles} is the number of poles in DFIG per phase. Due to the stator is directly connected into the grid, f_{stator} pass through the stator should always equal to the network frequency $f_{network}$. To achieve this target, the f_{rotor} should adjust its value continually to compensate any variation of rotor speed caused by the fluctuations of wind speed. This control approach decouples the rotor speed from the grid frequency. Hence, the variable speed operation of DFIG can be achieved.

According to this control strategy, it is possible to model the FRC turbine which is connected to the grid through AC/DC/AC converter directly. In this case, the electronic device should have the capability to transfer 100% of the generating power to the grid where only a part of the rated power is transferred in DFIG through the power converter link. Normally in DFIG, the maximum slip limit is set to 0.3 [18]. In other words, the DFIG inverter has the ability to transfer power up to 30% of its machine rating.

Figure 2.11 gives a general configuration of the DFIG model and torque-slip characteristic of an induction machine. DFIG can transmit power to the grid from both stator and grid side converter. Since the power convertor can operate in bidirectional way, the DFIG can either deliver power or absorb power by operating at sub-synchronous or super-synchronous operational mode. The power is delivered to the network if DFIG is operated under super-synchronous (rotor speed is beyond synchronous speed) mode and absorb power under sub-synchronous mode (rotor speed is below synchronous speed).

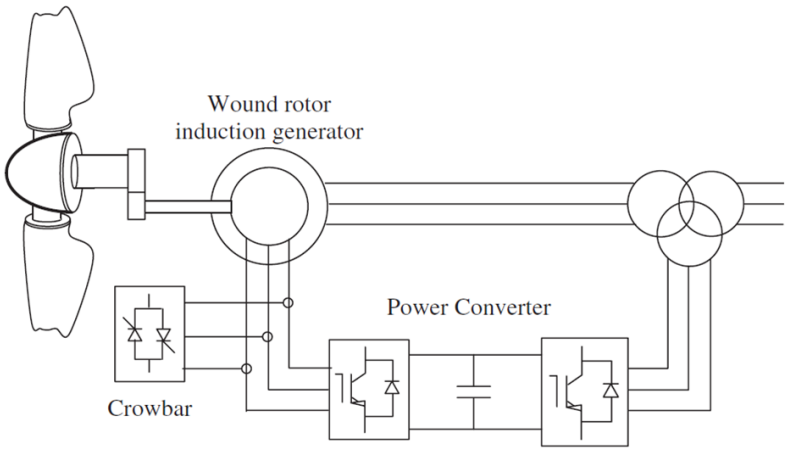

(a) Configuration of DFIG wind turbine

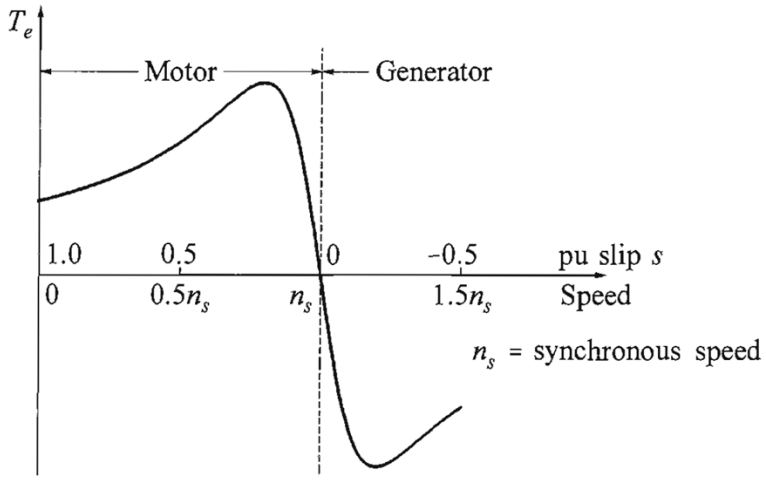

(b) Torque speed characteristic

Figure 2-11. DFIG model: a) Configuration of DFIG wind turbine [12]; b) Torque speed characteristic [10]

2.5.2 Dynamic circuit of induction machine

The dynamic T-circuit equivalent induction machine model is presented in Figure 2.12. By applying the Kirchhoff's voltage law, the stator voltage and rotor voltage can be written as:

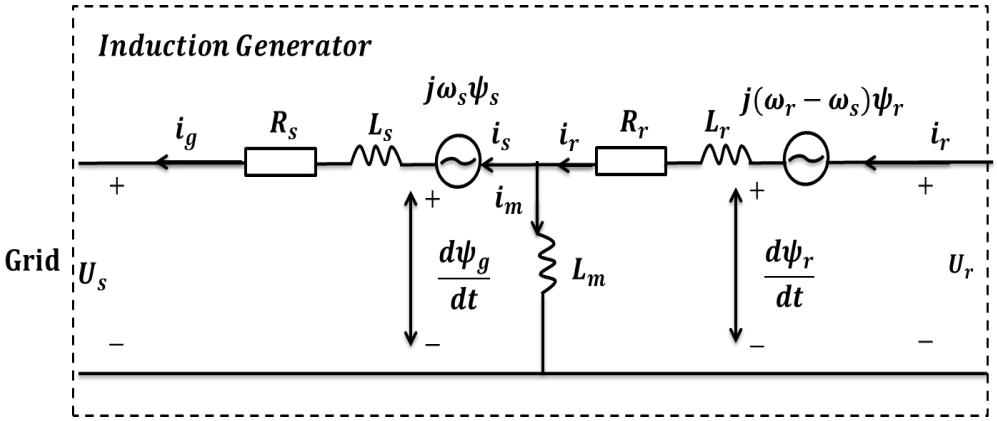

Figure 2-12. Dynamic equivalent circuit of an induction machine

$$u_s = R_s i_s + \frac{d\psi_s}{dt} + j\omega_s\psi_s \tag{2.15}$$

$$u_r = R_r i_r + \frac{d\psi_r}{dt} + j(\omega_s - \omega_r)\psi_r \tag{2.16}$$

$$\psi_s = (L_s + L_m)i_s + L_m i_r \tag{2.17}$$

$$\psi_r = (L_r + L_m)i_r + L_m i_s \tag{2.18}$$

where:

R_s: Stator Resistance	ψ_s: stator flux
R_r: Rotor Resistance	ψ_r: rotor flux
L_s: Stator Leakage Induction	ω_s: synchronous speed
L_r: Rotor Leakage Induction	ω_r: rotor speed
L_m: Mutual Induction	i_s: stator current
u_s: Stator Voltage	i_r: rotor current
u_r: Rotor Voltage	$s = \frac{\omega_s - \omega_r}{\omega_s}$: slip

The d-q transformation: Usually in synchronous generation models, the axes which rotating with the rotor is chosen through d-q transformation in order to simplify the power system analysis [10]. For an induction generator, the reference axes are chosen to be the axes which rotating at synchronous speed [19]. In this chapter, the q-axis was assumed to be 90^o ahead of the d-axis in the direction of rotation. So the stator phase currents can be transferred into their d-q variables:

$$i_{ds} = \frac{2}{3}[i_a cos\omega_s t + i_b cos(\omega_s t - 120^o) + i_c \cos(\omega_s t + 120^o)] \quad (2.19)$$

$$i_{qs} = -\frac{2}{3}[i_a sin\omega_s t + i_b sin(\omega_s t - 120^o) + i_c \sin(\omega_s t + 120^o)] \quad (2.20)$$

$$i_{dr} = \frac{2}{3}[i_a cos\theta_r + i_b \cos(\theta_r - 120^o) + i_c \cos(\theta_r + 120^o)] \quad (2.21)$$

$$i_{qr} = -\frac{2}{3}[i_a sin\theta_r + i_b \sin(\theta_r - 120^o) + i_c \sin(\theta_r + 120^o)] \quad (2.22)$$

From equation (2.15) to (2.18), the d-q transformation of stator and rotor flux can be written as:

$$\psi_{ds} = (L_s + L_m) i_{ds} + L_m i_{dr} \quad (2.23)$$

$$\psi_{qs} = (L_s + L_m) i_{qs} + L_m i_{qr} \quad (2.24)$$

$$\psi_{dr} = (L_r + L_m) i_{dr} + L_m i_{ds} \quad (2.25)$$

$$\psi_{qr} = (L_r + L_m) i_{qr} + L_m i_{qs} \quad (2.26)$$

The stator and rotor voltage in terms of d-q components are calculated below:

$$u_{ds} = R_s i_{ds} + \frac{d\psi_{ds}}{dt} - \omega_s \psi_{qs} \quad (2.27)$$

$$u_{qs} = R_s i_{qs} + \frac{d\psi_{qs}}{dt} + \omega_s \psi_{ds} \quad (2.28)$$

$$u_{dr} = R_r i_{dr} + \frac{d\psi_{dr}}{dt} - s\omega_s \psi_{qr} \quad (2.29)$$

$$u_{qr} = R_r i_{qr} + \frac{d\psi_{qr}}{dt} + s\omega_s \psi_{dr} \quad (2.30)$$

As seen in equation (2.27-2.30), the voltage is consisted of three terms: resistance Ri drop, flux transient $\frac{d\psi}{dt}$ term and rotating speed voltage term. The speed voltage term in stator represents the voltage created by synchronously rotating flux wave. The rotor speed voltage term represents the voltage created by rotor winding which moves at the slip speed with respect to synchronously rotating flux.

The torque and power: The electrical active power and reactive power generated by the DFIG can be expressed as:

$$P_s = u_a i_a + u_b i_b + u_c i_c \quad (2.31)$$

$$P_s = \frac{3}{2}(u_{ds} i_{ds} + u_{qs} i_{qs}) \quad (2.32)$$

$$Q_s = \frac{3}{2}(u_{qs} i_{ds} - u_{ds} i_{qs}) \quad (2.33)$$

$$P_r = \frac{3}{2}(u_{dr} i_{dr} + u_{qr} i_{qr}) \quad (2.34)$$

$$Q_r = \frac{3}{2}(u_{qr} i_{dr} - u_{dr} i_{qr}) \quad (2.35)$$

The electromagnetic torque in DFIG is:

$$T_e = \frac{3}{2}(\psi_{qr} i_{dr} - \psi_{dr} i_{qr}) \quad (2.36)$$

The total power in a DFIG with its relationship to mechanical power, rotor power and stator power are shown in Figure 2.13 [20].

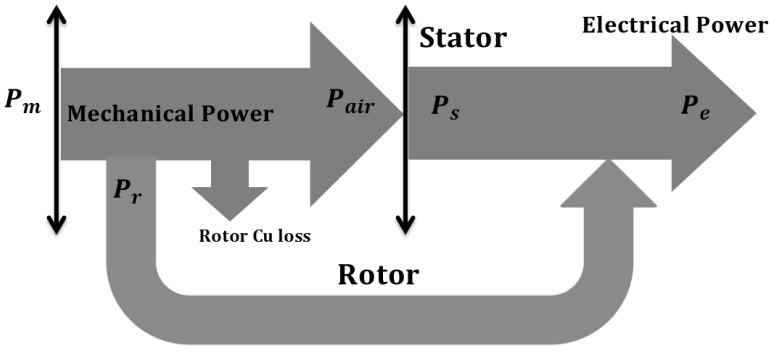

Figure 2-13. DFIG Power Relationships [20]

The stator power P_s can be expressed as equation (2.37) if stator losses are neglected:

$$P_s = P_m - P_r \tag{2.37}$$

$$P_r = -sP_s \tag{2.38}$$

$$P_g = P_s + P_r = (1 - s)P_s \tag{2.39}$$

So the total power transfer into the grid can be expressed in d-q elements:

$$P_g = \frac{3}{2}(u_{ds}i_{ds} + u_{qs}i_{qs} + u_{dr}i_{dr} + u_{qr}i_{qr}) \tag{2.40}$$

$$Q_g = \frac{3}{2}(u_{qs}i_{ds} - u_{ds}i_{qs} + u_{qr}i_{dr} - u_{dr}i_{qr}) \tag{2.41}$$

Figure 2.14 presents the relationship between slip, rotor speed, wind speed and mechanical power of a typical DFIG model [18]:

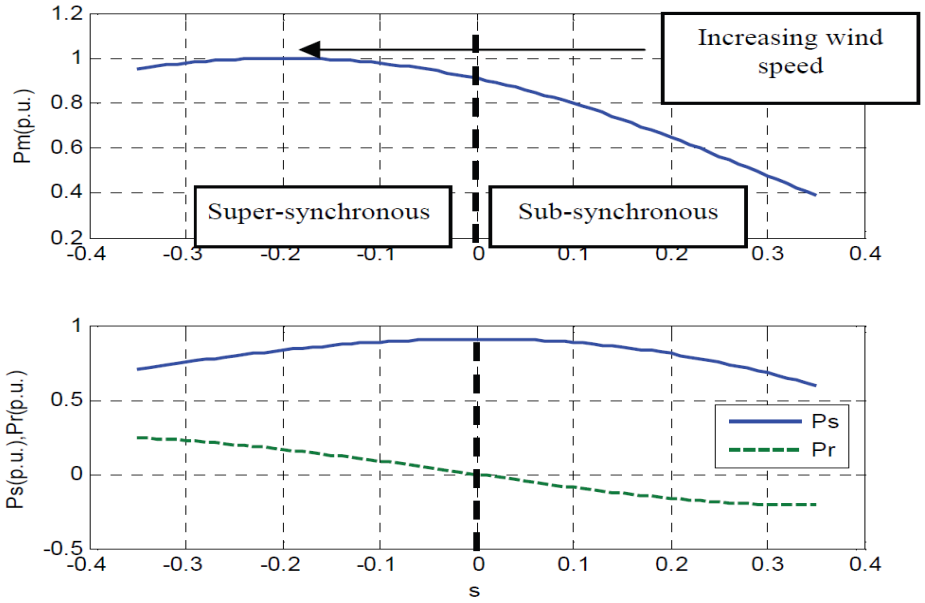

Figure 2-14. DFIG power flow versus slip [18]

It can be seen that the mechanical power reach its rated value with s = -0.2 in this case, that is ω_r =1.2 p.u. When the s = 0, the rotor is operating at synchronous speed. All the power is supplied via stator. If the wind speed increases, the machine operates at super-synchronous model (s < 0). In this condition, the mechanical power flows to the grid through both stator windings and rotor windings. If the wind speed is relatively low (s >0), the machine operates at sub-synchronous model. In this condition, the rotor converter system absorbs power from the grid.

2.5.3 Modelling the DFIG control system

Drive train model: In DFIG model, normally the two-mass drive train model is used as shown in Figure 2.15: the wind turbine rotor inertia constant H_t and induction generator rotor inertia constant H_g are connected through a spring (shaft).

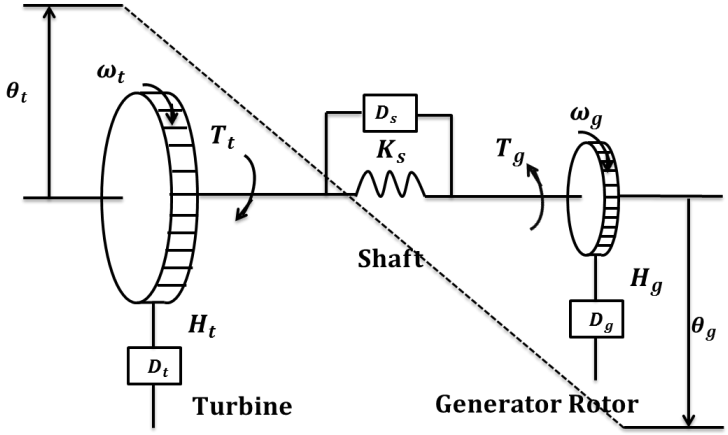

Figure 2-15. Two-mass model of a drive train [21]

The equations of the two-mass drive train are expressed as:

Induction Generator mass equation:

$$\begin{cases} 2H_g \frac{d\omega_g}{dt} = \omega_g \left(T_{shaft} - T_g\right) \\ \frac{d\theta_g}{dt} = \omega_g \end{cases} \tag{2.42}$$

Wind turbine mass equation:

$$\begin{cases} 2H_t \frac{d\omega_t}{dt} = \omega_t \left(T_t - T_{shaft}\right) \\ \frac{d\theta_t}{dt} = \omega_t \end{cases} \tag{2.43}$$

The shaft torque can be expressed as:

$$T_{shaft} = K_s\left(\theta_t - \theta_g\right) + D(\omega_t - \omega_g) \tag{2.44}$$

where the K_s is shaft stiffness and D is the damping torque; ω_t is the speed of wind turbine; ω_g is the speed of the induction machine; θ_g is the angular position of induction machine and θ_t is the angular position of wind turbine. The simulation control model of the drive train is shown in Figure 2.16.

Sometimes one-mass drive train model is used to simplified turbine structure by the way of replacing the two inertias to a single equivalent inertia. Therefore, the equation of one mass turbine as be expressed as:

$$2(H_t + H_g)\frac{d\omega_m}{dt} = \omega_m\left(T_t - T_g\right) \tag{2.45}$$

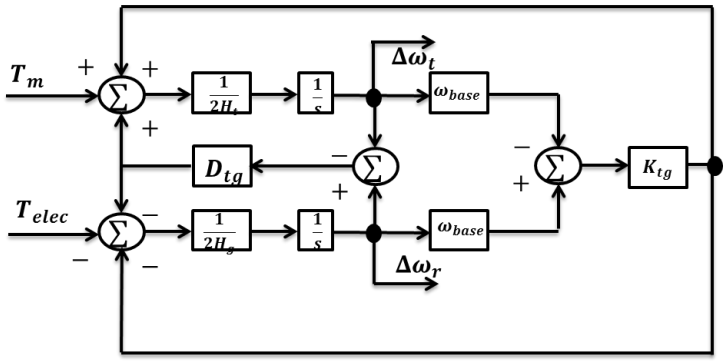

Figure 2-16. Simulation model of two-mass drive train

Pitch angle control: Based on the aerodynamic characteristics of the wind turbine, control actions must be taken to adjust the blade when wind speed exceeds rated value. An effective way to achieve this is related to the pitch angle control [4, 6, 11]. As mentioned in 2.4, the power coefficient C_p is significantly influenced by the pitch angle β. If the wind speed is below the rated value, the pitch angle is usually set to an optimal value to capture maximum power (for example 2^o [22]). Under high wind speed conditions, the pitch angle control is activated in order to reduce the lift force by increasing the pitch angle β. Figure 2.17 demonstrates the pitch control loop: The errors of rotor speed/aerodynamic power are used as the inputs of the control loop since the wind speed cannot be easily measured precisely. The P_{ref} of the upper part is the optimum power or rated power reference and P_g is the measured output power, ω_{ref} in the lower part is the rotor speed reference signal from the rotor sider convertor control model and ω_r is the measured rotor speed.

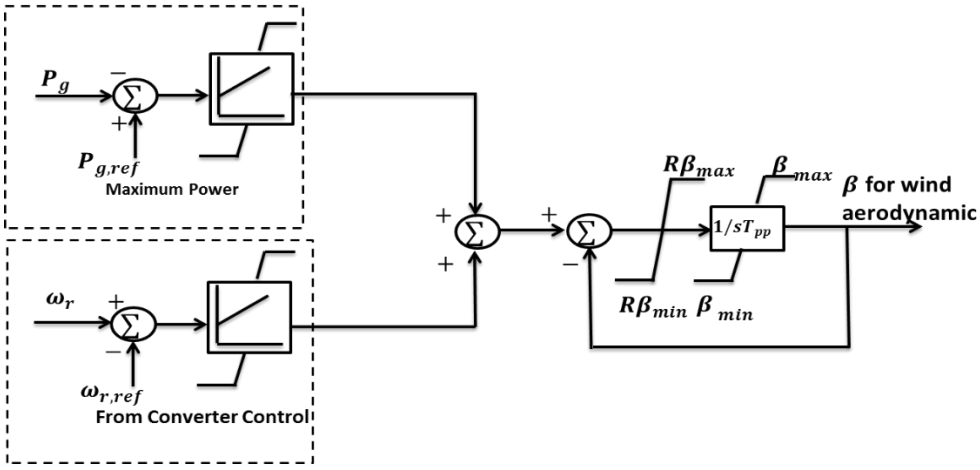

Figure 2-17. Pitch angle control model

Rotor side convertor control: The rotor side converter is used to control both active/reactive power. The active power is controlled according to power optimal strategy which enables the generator to capture the maximum power from wind. Figure 2.18 shows the general structure of the rotor side converter control [21]. The control model is analysed with the following several assumptions: the stator transients $d\psi_{ds}/dt$ is neglected since it does not vary much, the stator resistance $R_s$is also neglected, the d-axis is oriented along the stator flux which means the d-axis coincides with the maximum stator flux to make the u_{qs} equal to the terminal voltage u_{term} and u_{ds} equal to zero. The stator flux in d-q frame can be expressed as:

$$\psi_{ds} = \psi_s \tag{2.46}$$

$$\psi_{qs} = 0, \ \frac{d\psi_{qs}}{dt} = 0 \tag{2.47}$$

By substituting equation (2.46-2.47) in equation (2.23-2.28), we can achieve:

$$i_{qs} = -\frac{L_m}{L_s+L_m} i_{qr} \tag{2.48}$$

$$i_{ds} = -\frac{1}{L_s+L_m}(\psi_{ds} + L_m i_{dr}) \tag{2.49}$$

According to above assumption, the stator voltage in d-q frame is:

$$u_{ds} = 0, \ u_{qs} = \omega_s \psi_{ds} \tag{2.50}$$

Usually the rotor side converter is consisted with PWM-controlled voltage source converter [14], so it is necessary to further transfer the rotor current into rotor voltage by applying (2.48-2.49) into (2.29-2.30):

$$\begin{aligned} u_{qr} &= R_r i_{qr} + s\omega_s \psi_{dr} \\ &= R_r i_{qr} + s\omega_s [(L'_r - \frac{L_m^2}{L'_s}) i_{dr} - \frac{L_m}{\omega_s L'_s} u_{qs}] \end{aligned} \tag{2.51}$$

$$u_{dr} = R_r i_{dr} + s\omega_s \psi_{qr} = R_r i_{qr} + s\omega_s (L'_r - \frac{L_m^2}{L'_s}) i_{qr} \tag{2.52}$$

$$L'_r = L_r + L_m \tag{2.53}$$

$$L'_s = L_s + L_m \tag{2.54}$$

The active power and reactive power delivered by the stator can be rearranged as:

$$P_s = u_{qs} i_{qs} = -u_{qs} \frac{L_m}{L'_s} i_{qr} \tag{2.55}$$

$$Q_s = u_{qs} i_{ds} = -\frac{u_{qs}}{L_s + L_m} (\psi_{ds} + L_m i_{dr}) = -\frac{u_{qs}^2}{\omega_s L'_s} - \frac{L_m u_{qs}}{L'_s} i_{dr} \tag{2.56}$$

The rotor side converter control is then consists with four major parts: the active power control which transfers the active power order P_{order} signal into q-axis current signal i_{qref}; the q-axis current control calculates the u_{qref} which is send into rotor side converter; the reactive power control transfers the reactive power order Q_{order} into d-axis current signal i_{dref}; the d-axis current control computes the voltage signal v_{dref} and delivers it to the rotor side converter.

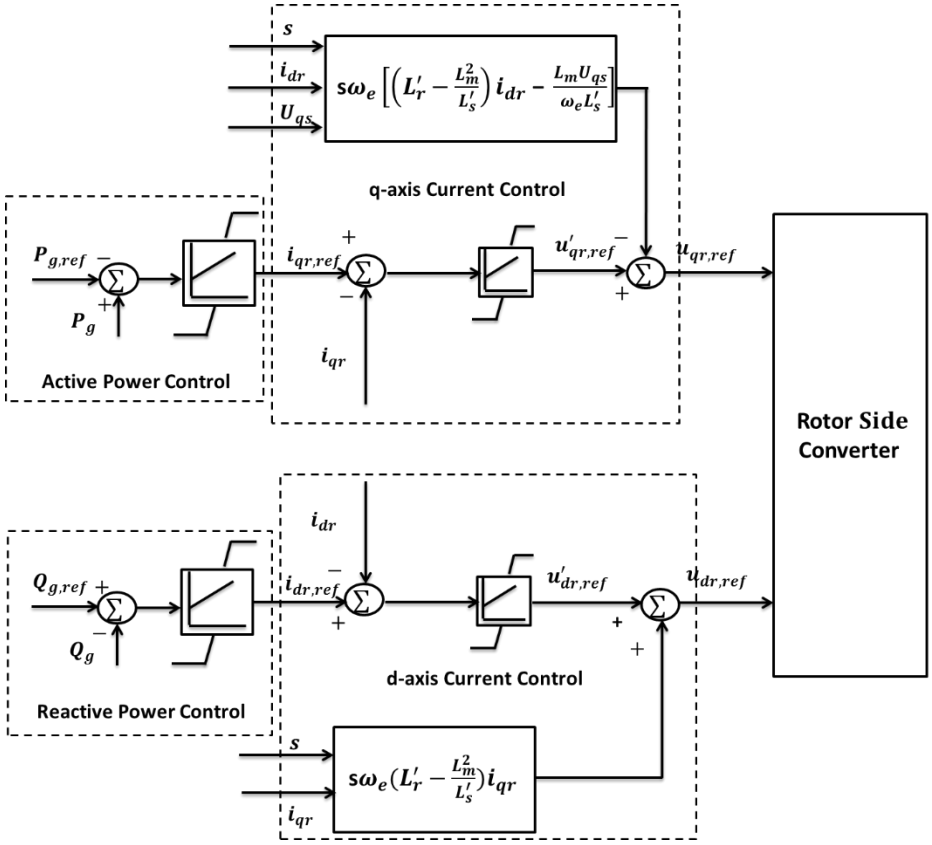

Figure 2-18. Rotor Side Converter Control

Maximum power track control: The active power reference signal is generated according to maximum power tracking control (MPT) curve (Figure 2.19). It demonstrates the relation between the mechanical power P_m and the rotor speed ω_m under the condition where the pitch angle is set to its optimal value. The turbine can capture the maximum power with the optimal tip speed ratio λ_{opt} under a given wind

speed. Usually, λ_{opt} is a constant value for a given blade. Therefore, the turbine speed ω_m must be adjusted according to the wind speed (referred to equation 2.11). The optimal power is given by [14]:

$$P_{opt} = K_{opt}\,\omega_r^3 \tag{2.57}$$

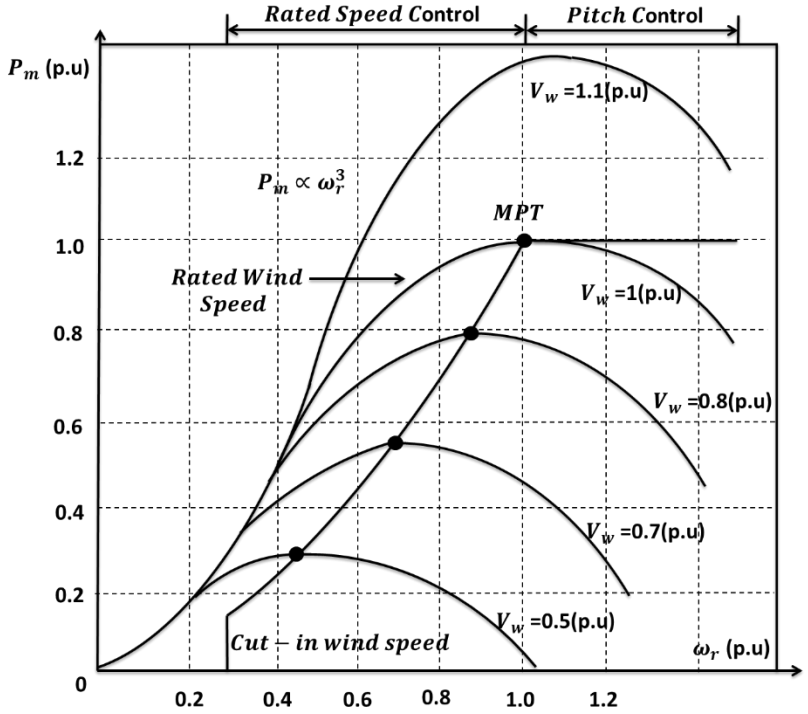

Figure 2-19. Maximum Power Track in DFIG

The optimal power curve can be further divided into several regions as shown in Figure 2.20: a) mechanical power versus wind speed; b) electrical power versus rotor speed.

Region A-B: Minimum Speed Operating

The turbine should operate above its cut-in speed normally around 30% below its rated speed. In this region, the turbine rotor speed is set to the minimum value. The optimum power is calculated by:

$$P_m^{opt} = \frac{1}{2}\rho\pi R^5 \frac{C_p^{opt}}{\lambda^3}\left[\omega_r^{min}\right]^3 \tag{2.58}$$

Region B-C: Optimal Speed Operating

In region (B-C), the turbine operates at different rotor speeds. The target in this region is to capture maximum power following by the optimal power curve. The

pitch angle is keep constant (zero) and in order to capture the optimal value, rotor speed ω_r should vary according to different wind speed for an optimal tip speed ratio λ_{opt}.

$$P_m^{opt} = \frac{1}{2}\rho\pi R^5 \frac{C_p^{opt}}{\lambda^3}\left[\omega_r^{ref}\right]^3 \quad (2.59)$$

Region C-D: Partial Load operating with rated rotor speed

The region (C-D) is designed to operate at the condition that wind speed is still below rated speed but the generator speed is reach its rated speed. In this situation, the generator speed is maintained at its rated speed while the power may be lower than the rated value. For a higher increasing of wind speed, the rotor speed may exceed the rated speed with a limitation range 15%-20% [13, 21]. The region B-C-D is control by rotor side converter control.

Region D-E: Full Load Operating

If the wind speed exceeds its rated speed, it is not possible for the rotor side converter to control the torque along. The pitch angle control is then activated to reduce the aerodynamic torque so that the rotor speed can be maintained at constant value until the wind speed reaches its cut-down limit (region D-E).

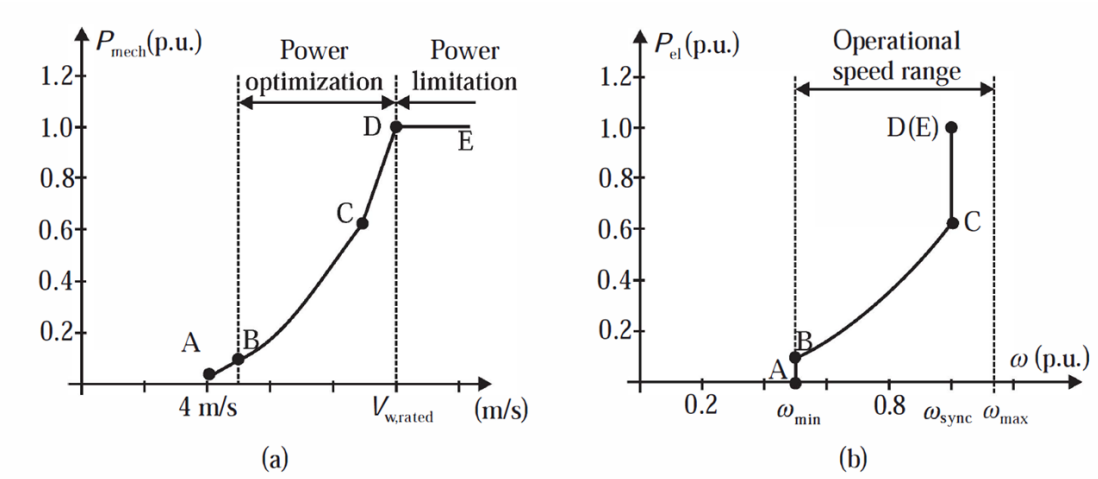

Figure 2-20. Maximum power track characteristics [14]: a) mechanical power versus wind speed; b) electrical power versus rotor speed

In order to provide a further explanation of the performance of rotor and pitch angle with the variation of wind speed, the characteristics of rotor speed and pitch angel versus wind speed is presented in Figure 2.21 [23]. At A-B-C-D regions, the

pitch angle is normally equal to zero. At high wind speed D-E condition, the pitch angle increases by a non-linear function based on wind speed variations. The rotor speed is only varying in the zone B-C. Otherwise it is maintained at constant values (either minimum value or rated value).

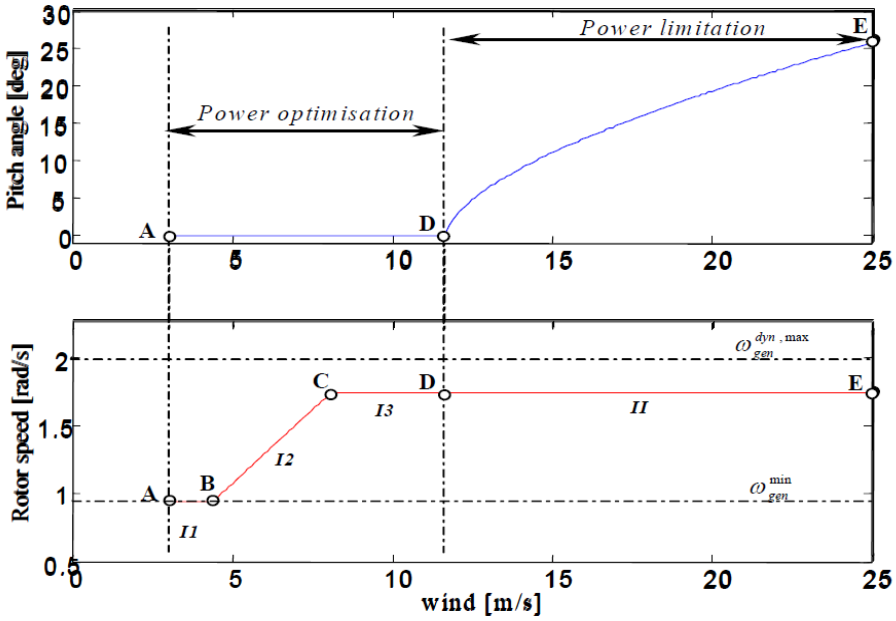

Figure 2-21. Characteristic of rotor speed and pitch angle versus wind speed [23]

Active Power Control: The active power control blocks in rotor side converter control can be realized in several ways as shown in Figure 2.22:

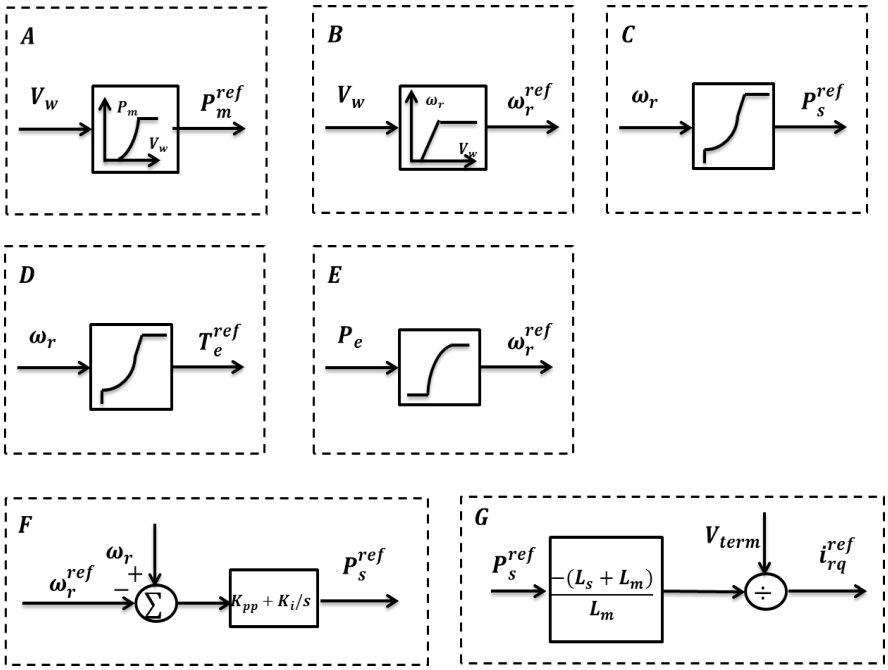

Figure 2-22. Rotor Side Converter Active Power Control combinations

A. Wind velocity versus mechanical power profile, the look up table in this block may transfer the measured wind velocity v_w into mechanical power reference signal P_{mref}.

B. Wind velocity versus rotor speed profile, the wind velocity v_w is converted into rotor speed signal $\omega_{rref}$by the look up table.

C. Rotor speed versus electrical power profile, this control scheme use the rotor speed ω_r as input and is sent into $\omega_r - P_s$ loop up table in order to deliver the electrical power reference signal P_{sref}.

D. Rotor speed versus electrical torque profile, sometimes the electrical power is replaced by electrical torque calculated by the $\omega_r - T_e$ look up table.

E. Electrical power versus rotor speed profile, the rotor speed is regulated using the$P_e - \omega_r$ look up table.

F. The block F compares the rotor speed reference ω_{rref} which comes from block B or E to the measured value ω_r to generate the error signal $\Delta\omega$. The $\Delta\omega$ is sent into a PI controller which creates the torque reference signal T_{sref}. If the stator resistance is assumed to be zero, the electrical power can be equal to the electromagnetic torque.

G. The block G finally calculates the q-axis current i_{qref} with equation (2.48) to be the input signal for v_q control.

There are two major combinations of these control blocks as shown in Figure 2.23:

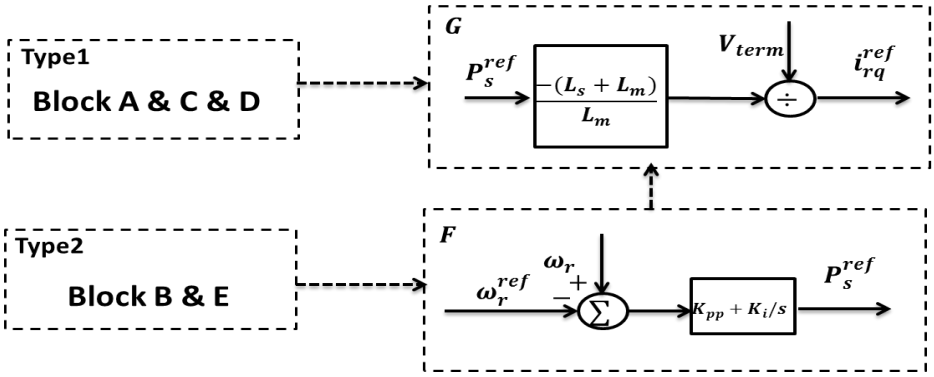

Figure 2-23. Different combinations of active power control in DFIG

1) Type 1 usually measured the rotor speed or wind speed to compute the reference electrical power or electrical torque. The application of this type of control can be found in [24-25].

2) Type 2 regulates the rotor speed and is usually used together with block F to compute the i_{qref}. This control strategy is used in GE Power System Energy Consulting's 1.5 MW wind turbine generators model. The application of type 2 control strategy can be found in [26-30].

Grid side convertor control: The main purpose of the grid side convertor control is to control the dc-voltage. Although it has the ability to support grid reactive power, it is seldom applied since a very large converter rating is needed [31]. The control strategy of grid side convertor is similar to rotor side convertor control, the active power and reactive power send to the grid is regulated by the d-q voltage. The grid side converter model is usually omitted by assuming a constant dc-link voltage which provides a path for rotor power to/from the grid at a unit power factor [32]. The detailed explanation of grid side convertor control can be found in [12, 14, 21].

2.5.4 Dynamic frequency response of DFIG

The crucial difference between DFIG and thermal power plants is explained to highlight the importance and necessity of the research. The DFIG rotor mechanical speed is decoupled from the grid due to the two AC/DC/AC converters. Therefore the rotor speed is set according to its maximum power tracking curve. It is only varied if the setting point changed caused by wind speed variation. The relationship between DFIG total output power, mechanical power, and stator power is described in equation (2.60): where the slip s is expressed in the way of rotor speed ω_r and synchronous speed ω_s:

$$P_{total} = P_s + P_r = \frac{\omega_r}{\omega_s} P_s \tag{2.60}$$

$$T_e = \frac{P_s}{\omega_s} \rightarrow P_{total} = \omega_r T_e \tag{2.61}$$

The control strategies used in active power control are achieved by either electrical torque T_e control or electrical power P_e control. If the electrical torque T_e is regulated, although the variation of network frequency will change the synchronous speed ω_s, the rotor speed ω_r is still unchanged. Therefore, the total power remains constant. The T_e regulated DFIG model has no inertia response to the grid. If the electrical power P_e is regulated, synchronous speed ω_s decreases during the

frequency drop. However in order to keep P_e constant, any change in ω_s is compensated by T_e. Therefore, T_e increases when frequency drops. The mechanical power remains unchanged and hence the rotor decelerates. The DFIG does not completely provide no inertia response to the system. However, this contribution is still inconsequential compared with the significant amount of kinetic energy released from synchronous generators [2]. Thus a conclusion can be made that DFIG model almost has no inertia contribution under frequency deviation conditions.

2.6 DFIG model built-in PSS/E

The General Electric (GE) Power Systems has been making effort on developing the GE wind turbine generator model (WTG) which is suitable in power system stability analysis [29]. The model is developed in time domain simulation software PSS/E. Some parts of the electric device are simplified according to the following assumption: it is assumed that the dynamic performance of the generator converter is very fast so it is modelled using algebraic approximations.

Figure 2.24 [33] shows the structure of GE 1.5 MW (or 3.6 MW) wind turbine generator. At rated wind speed, the DFIG will normally operate at 1.2pu speed (s = -0.2). The DFIG inverter has the ability to transfer power up to 30% of the machine rating. The active power of the DFIG is divided into stator power and rotor power which has the relationship in proportion to the slip s. The turbine control system contains two blocks: the blade pitch control and electrical converter control. The losses in the inverter are considered negligible and are not included in the model.

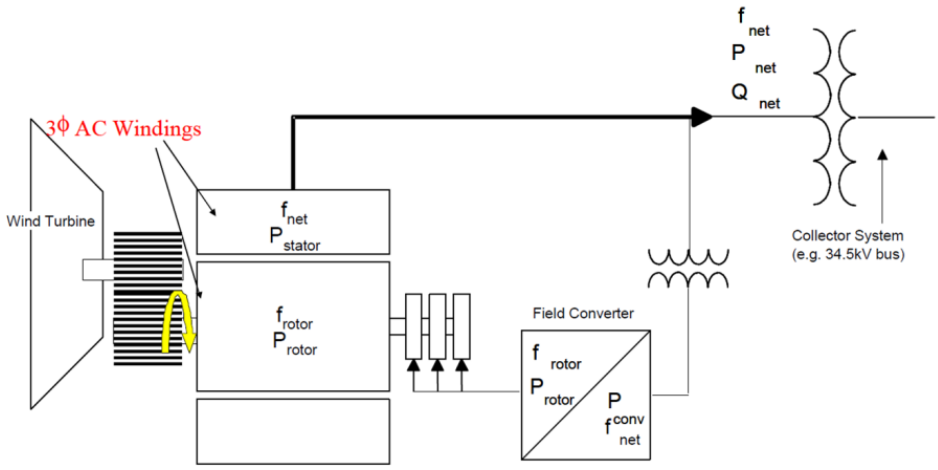

Figure 2-24. Double fed induction generator in PSS/E [33]

2.6.1 Load flow setup

The GE1.5 WTG Type3 model is used in this thesis to represent the DFIG model which has a rated power output of 1.5 MW. According to [29], the DFIG need to import reactive power from the grid side in most of cases since it has poor reactive power capability. Therefore, its power factor (pf) varies from 0.9 pf under-excited to 0.95 pf over-excited. The $Qmax$ = 0.49 MVAr and $Qmin$= -0.73 MVAr. In most cases, the wind farm always consists of a group of wind generators. It is necessary to simplify the group of wind generators with an approximation that all machines can be represented by a single large machine with an equivalent reactance. In PSS/E, this is realized by changing the parameter of MBASE and number of lumped WTG N with its MVA rating equal to N times the 1.5 MW rating.

In power flow studies, the GE1.5 WTG3 is modelled as a conventional generator which is connected to a PV bus. The P_{gen}, Q_{max} and Q_{min} should be set equal to the GE1.5 standard value multiplied by N. The reactive power control strategy in PSS/E is recommended as type 2 [Q_{max}, Q_{min}] [34] control.

2.6.2 WTG3 dynamic model built-in PSS/E

The dynamic model of WTG3 built-in PSS/E is consisted with four different parts as shown in Figure 2.25:

- WT3G: generator/converter model
- WT3E: electrical control model
- WT3T: mechanical control model
- WT3P: pitch control model

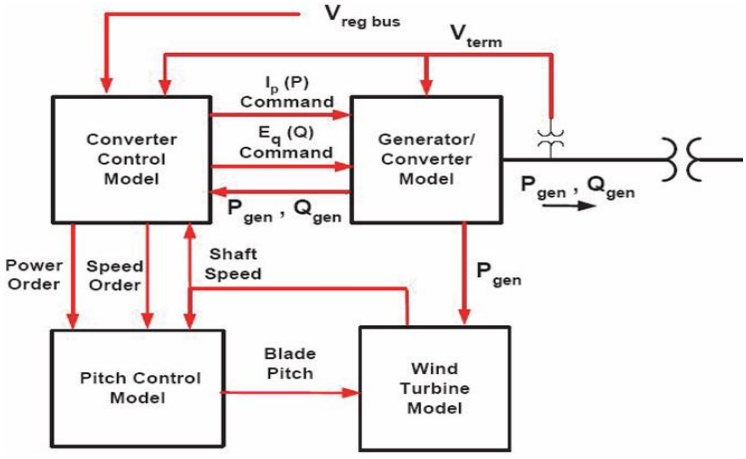

Figure 2-25. Control block of WTG3 in PSS/E [34]

Generator/Converter Model:

Unlike the conventional generator model, the rotor mechanical states are neglected here which are presented in the turbine model. The generator is equivalent to a current source which provides the required active and reactive power into the grid. The control signals are related to the reactive power control signal E_{comd} and the active power control signal I_{comd} coming from the electrical converter control.

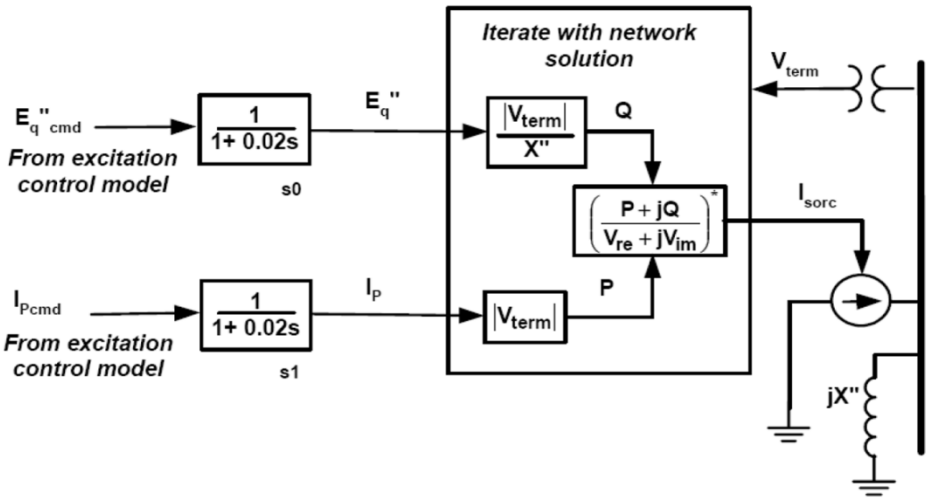

Figure 2-26. WTG3 model [30]

Electrical Converter Control Model:

The electrical converter control model contains two major control loops: the reactive power Q_{ord} control loop and the active power P_{ord} control loop. Figure 2.27 shows the general control strategy.

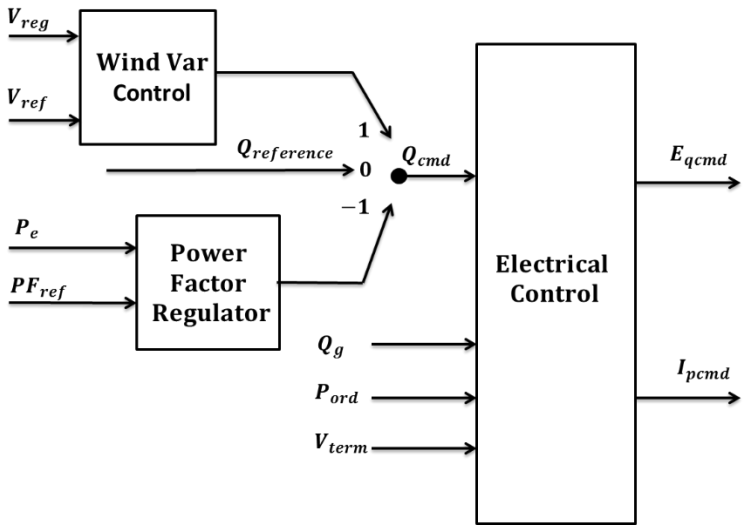

Figure 2-27. WT3 Electrical converter control Strategy

Active Power Control:

Type 2 of the speed control method is utilized as mentioned in 2.5. The rotor speed reference ω_{rref} is calculated from the $P_e - \omega_r$ look up table. The error signal $\Delta\omega$ is generated by comparing ω_{rref} with the measured value ω_r. Then, the $\Delta\omega$ is sent into a PI controller which makes the electrical power order signal P_{order}. The current command I_{pcmd} is finally calculated by dividing the P_{order} by the measured terminal voltage V_{term} and sent to the generator/converter control model. The control scheme is shown in Figure 2.28:

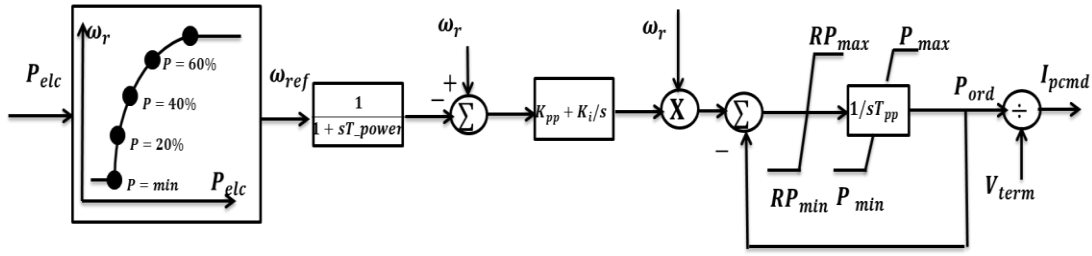

Figure 2-28. Active Power Control in WT3E [34]

Reactive Power Control:

The control methods used in regulating the reactive power of the wind farms in load flow studies are divided into three different terms by changing the flag switch signal $varflg$ in PSS/E:

- If the switch position is -1, the reactive power should be regulated by a pre-set power factor from load flow.
- If the switch position is 0, the reactive power is regulated with a constant value which should be equal to the value defined in load flow;
- If the switch position is set to 1, the control system should monitor a specified bus voltage by comparing its measured value with the reference voltage. The error signal is sent to a PI controller to calculate the reactive power order Q_{cmd}.

The terminal voltage is controlled by the flag switch signal $vltflg$: if the $vltflg$ is set to1, the terminal voltage control is activated. The measured terminal voltage is compared with the reference voltage V_{ref} to create the voltage error signal V_{err}. The error is then used to calculate the voltage command E_{qcmd} as an input for

the generator/converter control. If the $vltflg$ is set to 0, the error between Q_{cmd} and Q_{gen} is compared to create the reactive power command E_{qcmd}. Figure 2.29 shows the control structure of the reactive power control in WT3E. Usually it is recommended that $varflg$ and $vatflg$ should be set to 1 in WT3 model.

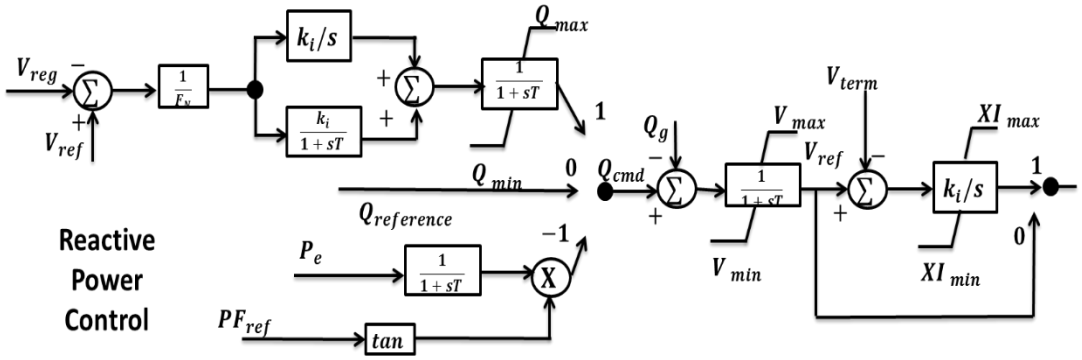

Figure 2-29. Reactive power control in WT3E [34]

Wind Turbine Control:

The rotor mechanical model is similar to the model introduced in previous section. The model used in PSS/E is a two-mass rotor model. It is also possible to change the two-mass rotor model into one-mass rotor model by setting the turbine inertia fraction H_{tfrac} into 0. The relationship between turbine inertia H_t, generator inertia H_g and H_{tfrac} can be expressed as:

$$H_t = H \times H_{tfrac} \tag{2.62}$$

$$H_g = H - H_t \tag{2.63}$$

Pitch Control:

The structure of pitch angle control model is same as the model mentioned above. In dynamic studies, there are two different conditions of the initialization of the pitch control model: 1) the initial electrical power (from the load flow) is less than rated value; 2) the initial electrical power is equal to rated value. Assume that there is no loss in the power transfer [30], $P_m = P_e$ and the rotor speed ω_r is set to $\omega_{ref} = 1.2$ p.u. The maximum power coefficient C_p is used to calculate the required wind speed $v_w$to produce P_m with the pitch angle θ equal to the minimum value θ_{min}. If P_m is less than the rated value (P_{max}), the result of calculated wind speed is used to be the initial value. If P_m reaches its rated value and at the same time the user-input

wind speed v_w is greater than the calculated wind speed value under the condition of $\theta = \theta_{min}$, the initial wind speed is equal to the user-input value while the initial pitch angle value will be increased to produce the rated power.

2.6.3 General control processes of DFIG in PSS/E

The entire control system of the WT3 DFIG model built-in PSS/E is shown in Figure2.30. The explanations of how the control systems work are introduced below:

1) The initial condition of the aerodynamic power extracted from the wind is calculated based on the load flow results. The amount of power needed for the P_{aero} is determined by active power P_{gen} setting in the *.raw* file.

2) P_e and P_m are used to calculate the machine swing equation, for a two-mass model, it is expressed as equations (2.42-2.43). If the H_{frac} is set to zero, the model becomes single mass model.

3) The rotor speed ω_r is compared with the rotor speed reference ω_{ref} value corresponding to the electrical power P_e versus rotor speed ω_{ref} MPT curve. The rotor speed error ω_{err} is sent to both the pitch angle control and rotor side speed control.

4) The rotor speed error ω_{err} is sent to a PI controller in order to make the active power P_{order} signal. The P_{order} signal is then sent to both the pitch angle control and rotor side converter control.

5) In pitch angle control model, P_{order} is compared with the power reference signal (usually the maximum power value P_{max} of the wind turbine is used) for the purpose of calculating the power error signal P_{err}. Both P_{err} and ω_{err} signals are sent to a PI controller to calculate the pitch angle control command signal θ_{cmd}. The pitch angle θ and rotor speed ω_r are used for the calculation of wind power aerodynamic.

6) In rotor side converter control, P_{order} is divided by the measured terminal voltage V_{term} for the purpose of creating the active power current command I_{pcmd}.

7) Usually in PSS/E, it is recommended that $vltflg$ and $varflg$ are set to 1 to enable the control ability relates to the voltage regulation in WTG3 model. The reactive power command Q_{cmd} is compared with the measured reactive power Q_g of the generator to get the voltage reference V_{ref} signal. This signal is further

transferred into the reactive power voltage command E_{qcmd} to the generator/converter control model.

8) Both the active power I_{pcmd} command and reactive power I_{pcmd} command are sent to the generator control model to calculate the final power output through an algebraic calculation.

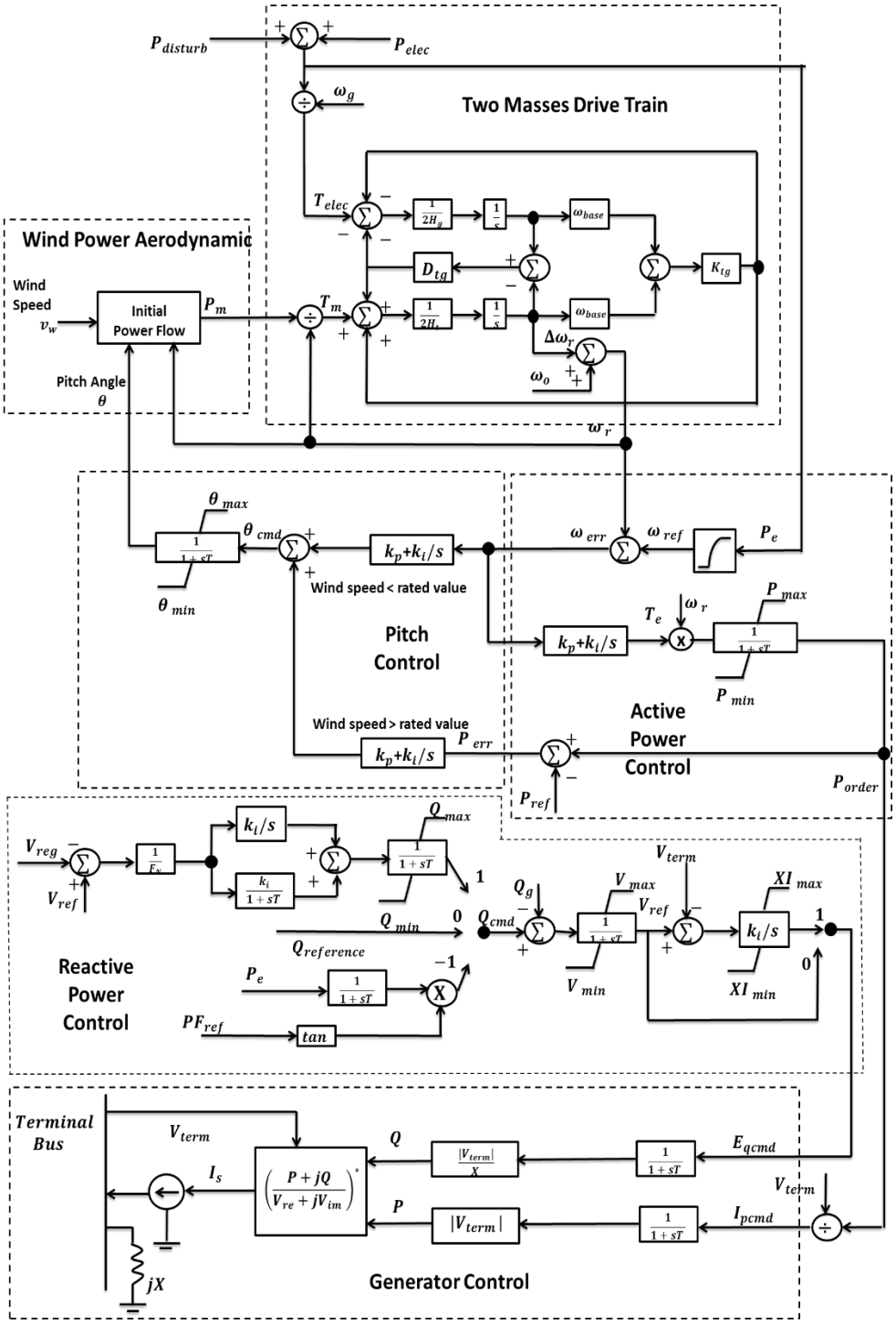

Figure 2-30. DFIG model control strategies built-in PSS/E

2.7 Summary

In this chapter, the fundamental knowledge in power system are introduced for the purpose of providing a better understand in analysing the future power system performance. The grid codes of different countries are illustrated which give the requirements of the generators to provide frequency response capability during the frequency disturbances. The most important elements relate to the power system stability analysis are introduced such as: the swing equations, speed-droop control, loss of main protection, reactive power compensation and equal area criterion.

In addition, the background knowledge of the wind turbine is also introduced. The control theories of the DFIG model are described in detail which include: aerodynamic control, optimal power characteristic, turbine control, rotor side converter control, grid side converter control and pitch angle control. Furthermore, the GE WTG3 DFIG model is introduced as well. The explanations of the structures of this model with its corresponding control systems are mentioned. The DFIG model is decoupled from the grid frequency due to the back-to-back voltage source converter connection. Therefore, it can provide no or very little inertia response during the network disturbances.

References

[1] G. M. Masters, "*Renewable and Efficient Electric Power Systems*", IEEE John Wiley & Sons, Inc, Hoboken, New Jersey, Canada, 2004

[2] I. Erlich, F. Shewarega, "Insert impact of large-scale wind power generation on the dynamic behaviour of interconnected systems," *Bulk Power System Dynamics and Control - VII. Revitalizing Operational Reliability*, iREP Symposium , Charleston, SC, 19-24 Aug. 2007, pp.1-7

[3] J.G. Slootweg, W.L. Kling, "The Impact of Large Scale Wind Power Generation on Power System Oscillations", *Electric Power Systems Research*, Vol. 67, no. 3, 2003, pp. 9-20

[4] Tennet, "*Germany Grid Code*", Dec. 2012. http://www.tennet.eu/de/en/customers/grid-customers/grid-connection-regulations.html

[5] I. Erlich, U. Bachmann, "Grid code requirements concerning connection and operation of wind turbines in Germany," IEEE *Power Engineering Society General Meeting*, San Francisco, USA, 12-16 June 2005, pp.1253-1257

[6] ENERGINET DK, "*Regulation for grid connection*", Denmark, https://www.energinet.dk/EN/El/Forskrifter/Technicalregulations/Sider/Regulations-for-grid-connection

[7] National Grid, "*The Grid Code*", 10 June 2014, http://www2.nationalgrid.com/UK/Industry-information/Electricity-codes/Grid-code/The-Grid-code/

[8] National Grid, "*GC022-Frequency Response*", Workgroup Report, Jan 2013

[9] J. D. Glover, Mulukutla S. Sarma, Thomas J. Overbye, *"Power System Analysis and Design*", Thomson Press, Stamford, USA, 2008, Fourth Edition

[10] P. Kundur, "*Power System Stability and Control*", McGraw-Hill, Inc. NY, 1993

[11] A. Dysko, Graeme M. Burt, S. Galloway, *et al.*, "UK distribution system protection issues," *Generation, Transmission & Distribution, IET* , vol.1, no.4, July 2007, pp.679-687

[12] O. Anaya-Lara, N. Jenkins, J. Ekanayake, *et al.*, "*Wind Energy Generation Modelling and Control*", John Wiley & Sons, Ltd. Great Britain, 2009

[13] W. Bin, L. Yongqiang, Z. Navid, *et al.*, "*Power Conversion and Control of Wind Energy Systems*", John Wiley & Sons, Inc, Hoboken, NJ, USA August 2011

[14] M. Eremia, M. Shahidehpour, "*Wind Power Generation*", John Wiley & Sons, Inc, Hoboken, NJ, USA, 2013

[15] X. Lie, Y. Liangzhong, C. Sasse, "Comparison of Using SVC and STATCOM for Wind Farm Integration," *PowerCon International Conference on Power System Technology*, Chongqing, China, 22-26 Oct. 2006, pp.1-7

[16] L. Holdsworth, X. Wu, J. B. Ekanayake, *et al.*, "Comparison of fixed speed and doubly-fed induction wind turbines during power system disturbances", *IEE Proceedings: Generation, Transmission and Distribution*, vol.150, no.3, May 2003, pp.343–352

[17] Lab-Volt Ltd, *"Principles of Doubly-Fed Induction Generators (DFIG)"*, Canada, 2001

[18] Ng. Artle, J. Fletcher, Y. Jin, "*Paths to Sustainable Energy*", In Tech Press, 2010

[19] J.B. Ekanayake, L. Holdsworth, W. XueGuang, *et al.*, "Dynamic modeling of doubly fed induction generator wind turbines," *Power Systems, IEEE Transactions on* , vol.18, no.2, May 2003, pp.803-809

[20] B. Fox, D. Flynn, L. Bryans, *et al*., "Wind Power Integration: Connection and System Operational Aspects", *IET Power and Energy Series 50, Institution of Engineering and Technology*, London, United Kingdom, 2007

[21] A. Perdana, *Dynamic models of wind turbines. A contribution towards the establishment of standardized models of wind turbines for power system stability studies*, Ph.D. Thesis, Chalmers University of Technology, Goteborg, Sweden, 2008

[22] Y. Ming, L. Gengyin, Z. Ming, *et al.*, "Modeling of the Wind Turbine with a Permanent Magnet Synchronous Generator for Integration," *Power Engineering Society General Meeting*, Tampa, FL, 24-28 June 2007, pp.1-6

[23] A. D. Hansen, J. Clemens, P. Sorensen, *et al.*, "*Dynamic wind turbine models in power system simulation tool DigSILENT*", Riso National Laboratory and Aalborg University, Dec. 2003

[24] M. Kayikci, J.V. Milanović, "Dynamic Contribution of DFIG-Based Wind Plants to System Frequency Disturbances," *Power Systems, IEEE Transactions on* , vol.24, no.2, May 2009, pp.859-867

[25] A. Tapia, G. Tapia, J. Ostolaza, *et al.*, "Modeling and control of a wind turbine driven doubly fed induction generator," *IEEE Transactions on Energy Conversion*, vol. 18, no. 2, Jun. 2003, pp.194-204

[26] L. Shuhui, T.A. Haskew, K.A. Williams, *et al.*, "Control of DFIG Wind Turbine With Direct-Current Vector Control Configuration," *Sustainable Energy, IEEE Transactions on* , vol.3, no.1, Jan. 2012, pp.1-11

[27] I. Erlich, J. Kretschmann, S. Mueller-Engelhardt, *et al*., "Modeling of wind turbines based on doubly-fed induction generators for power system stability studies," *Power and Energy Society General Meeting*, Pittsburgh, PA, 20-24 July 2008 pp.1-8

[28] R.G.de Almeida, J.A. Peas Lopes, "Participation of Doubly Fed Induction Wind Generators in System Frequency Regulation," *Power Systems, IEEE Transactions on* , vol.22, no.3, Aug. 2007, pp.944-950

[29] N.W Miller, J.J. Sanchez-Gasca, W.W. Price, *et al*., "Dynamic modeling of GE 1.5 and 3.6 MW wind turbine-generators for stability simulations," IEEE, *Power Engineering Society General Meeting*, Toronto, Canada, 13-17 July 2003, pp.1977-1983

[30] Nicholas W. Miller, William W. Price, Juan J. Sanchez-Gasca, "Dynamic Modeling of GE 1.5 and 3.6 Wind Turbine -Generators", *GE-Power Systems Energy Consulting, General Electric International*, Inc. Version 3, 2003

[31] Slavomir Seman, "*Transient Performance Analysis of Wind-power Induction Generators*", PhD Thesis, Helsinki University of Technology, 2006

[32] M.V. Nunes, J.A.P. Lopes, U.H. Bezerra, *et al*., "Influence of the variable speed wind generators in transient stability margin of the conventional generators integrated in electrical grids," *IEEE Transactions on Energy Conversion*, vol.19, no. 4, Dec. 2004, pp.692-701

[33] C. Kara, W.Miller Nicholas, J.J. Sanchez-Gasca, "Modelling of GE Wind Turbine-Generators for Grid Studies", *General Electric International, Inc*. Version 4, 2008

[34] *PSS/ETM Program Application Guide, Volumes I and II*, Power Technologies International

CHAPTER 3: LARGE-SCALE EQUIVALENT POWER SYSTEM MODELLING

3.1 Introduction

It is expected that significant differences in dynamic frequency responses between DFIG and synchronous generators will create a number of new challenges in the future, especially if the penetration levels of the wind energy become relatively high. Hence, it is important to assess system performance offline ahead of the anticipated changes. For this purpose, an accurate and validated dynamic model is needed.

Usually, the system dynamic stability analyses are performed in a way of time domain simulations. To achieve this, power system dynamics are described as a set of nonlinear differential equations [1]. Nowadays, however, due to the rapid development of power systems, the equations become more and more complex. This greatly increases the difficulties for the computer to perform numerical calculations of large power systems, even though processing power of modern computers is continually improving. Another important issue is related to the limitations of the commercially marketed power system analysis packages. For example: the application of Real Time Digital Simulator (RTDS) and Electromagnetic Transients Program for DC application (EMTDC) is normally limited by their largest number of nodes and capacity [2]. Therefore, it is often necessary to reduce the size of the system in order to simplify network calculations, save investigation time, as well as to make the results easier to interpret.

The methods used in reducing the size of the network are referred to as power system equivalencing. In general, the core concept of system equivalencing is to divide the whole system into two parts: internal sub-system and external sub-system. All system data within the internal sub-system should be retained. The response of this part of the system is of direct interest. On the other hand, the external sub-system is the part which has little or no impact on internal sub-system's oscillation performance and can be simplified or eliminated [3]. Thus, the dynamic power system equivalencing is the method which reduces the model's order of the external sub-system for the purpose of reducing the calculation burden and data storage on the

computer. It is important to notice that the equivalent model should always maintain the dynamic characteristics of the original model.

In this chapter, a general background of the methodologies developed in 1980s for dynamic network equivalencing is first presented (section 3.2). Several disadvantages and limitations of using these methods are then discussed. Section 3.3 describes an alternative new method developed as part of this thesis for the purpose of deriving an equivalent power system model. In section 3.4, the application of the proposed method is described systematically by modelling the UK power system as an example. Moreover, parameter adjustment is also introduced for the purpose of investigating a variety of future system scenarios. The summary is presented in section 3.5.

3.2 Background of equivalencing methodologies developed in 80s

3.2.1 Background of network equivalents

In 1980s, many dynamic equivalent methods were developed. It was first pointed out by Ward. The idea was to eliminate all generator and load nodes within the external sub-system or equivalent them into several selected generator nodes [4-5]. Later, various techniques were developed in order to identify the groups of generators which could be represented as one aggregated generator. Basically there are two main approaches: 1) modal method, and 2) coherency method.

3.2.2 Modal method

The equivalencing is realised by using the linear state matrix model instead of non-linear model in modal method. The modes which are not easily affected by the disturbances can be eliminated as mentioned in [6].

The behaviour of dynamic power system is usually described by its linearized state-space model (3.1) [7]. The detailed explanation of how to calculate this state-space model is included in chapter 4. Based on the characteristic of matrix **A**, the eigenvalues of matrix **A** demonstrate the system dynamic behaviours. The non-dominant modes can be removed while the modes which make significant contributions to system dynamic performance must be retained as shown in (3.1).

$$\begin{cases} \Delta\dot{x} = \mathbf{A}\Delta x + \mathbf{B}\Delta u \\ \Delta y = \mathbf{C}\Delta x + \mathbf{D}\Delta u \end{cases}$$

$$\begin{bmatrix} \mathbf{A} & \mathbf{B} \\ \mathbf{C} & \mathbf{D} \end{bmatrix} = \begin{bmatrix} \begin{bmatrix} \mathbf{A_1} & 0 \\ 0 & \mathbf{A_2} \end{bmatrix} & \begin{bmatrix} \mathbf{B_1} \\ \mathbf{B_2} \end{bmatrix} \\ [\mathbf{C_1} \quad \mathbf{C_2}] & [\mathbf{D}] \end{bmatrix} \tag{3.1}$$

where $\mathbf{A_1}$ contains the retained modes of matrix **A** and $\mathbf{A_2}$ contains the non-dominant modes of matrix **A**. A number of techniques have been developed for the purpose of identifying the non-dominant modes. For example:

- The modal truncation [8-9] method. This method investigates the pole locations of the matrix **A**. The modes which have the fast decaying characteristic (far away from the origin as shown in eigenvalue plot) are eliminated. A clear definition of fast decaying poles is needed which requires prior knowledge of the external sub-system and its oscillatory performance.
- The selective modal analysis method [10-11]. It identifies the modes which make negligible contribution to the output variables *y* by way of analysing the participation factors.

The modal method can provide a good insight into the oscillatory performance of the system under small disturbance conditions [12]. However, the obtained equivalent results cannot be directly imported/exported into most standard simulation programs as the modal method is typically based on the linearization of the external sub-system. Data conversion is always needed in order to receive and verify the results [3]. In addition, the linear method cannot reflect the complex dynamic system performance during major disturbances such as critical faults. The resulting dynamic equivalents cannot always ensure acceptable performance during large disturbances [3, 6, 12]. Hence, the coherency method is developed.

3.2.3 Coherency method

This method utilizes the coherency concept for the purpose of identifying the coherent group of generators which can be further replaced by one aggregated generator [13-15]. The steps involved in the coherency-based method are listed below:

1) Identify the coherent group of generators.

2) Aggregate each group of generators into one or several equivalent models.

3) Reduce the network by way of aggregating the generator buses into one or several equivalent buses and eliminating the load buses.

The characteristics of the coherent groups of generators according to [13-15] are listed below:

- The classical generator model can be used to represent the aggregated synchronous generator (generator emf behind its transient reactance which is assumed to be constant)
- The coherent groups of generators are independent of the size of disturbance, for example: the behaviour of coherent groups of generators is not changed much if the critical fault clearance time is increased.
- The coherent groups of generators are independent of the amount of detail in the generating units' models. In other words, the generator control devices such as the turbine and excitation system have similar impact on system frequency responses (e.g. swing curves). Hence, they can be aggregated into one device.

3.2.4 Determination of coherent groups of generators

The equivalent network will only give an accurate result during disturbances if the equivalent groups of generators are effectively coherent. Hence, the identification of the coherent groups of generators is the crucial task in coherency method. The coherency recognition is achieved by testing the generators' swing performance during major disturbances. Figure 3.1 shows an example of investigating rotor angle response of three generators [17]. It could be noticed that the rotor angle of generator *i* and generator *j* had almost the same oscillation performance where generator *k* show totally different rotor angle variation. Thus, conclusion could be made that the generator ***i, j*** were coherent and generator *k* was not coherent with the other two.

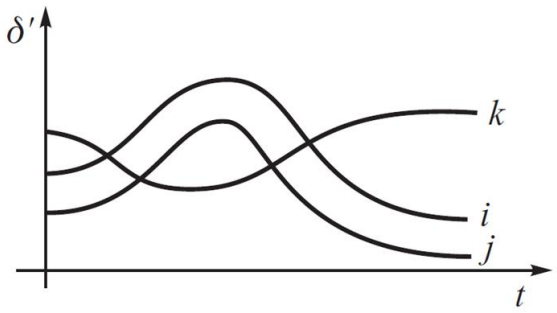

Figure 3-1. Example of coherency analysis for three generators [17]

One group of generators can be defined as coherent if each generator in this group oscillates with the same angular speed or their terminal bus voltages have a constant complex ratio [1, 13]. If generator i and j in group *G* are said to be coherent, the ratio between two terminal bus voltages can be expressed as (3.2):

$$\frac{\bar{V}_i(t)}{\bar{V}_j(t)} = \frac{V_i}{V_j} e^{j[\delta_i(t)-\delta_j(t)]} = \vartheta_i, \;\; i,j \in \{G\} \tag{3.2}$$

As assumed earlier, the voltage magnitudes in the classical generator model are constant. The coherency criteria can be further simplified into (3.3):

$$\delta_i(t) - \delta_j(t) = \delta_i(0) - \delta_j(0) = \delta_{ij}, \;\; i,j \in \{G\} \tag{3.3}$$

where $\delta_i(0)$ and $\delta_j(0)$ are the initial values of rotor angle.

Equation (3.3) represents the exact coherent condition which in reality rarely happens. Usually the criterion is replaced by comparing the difference between rotor angles with a small error region $\varepsilon_{\Delta\theta}$:

$$\Delta\delta_i(t) - \Delta\delta_j(t) < \varepsilon_{\Delta\theta}, \;\; i,j \in \{G\} \tag{3.4}$$

The disadvantage of this method is that the numerical calculation for comparing rotor angles between generators takes high computation effort. Hence, efforts were taken to improve the calculation efficiency as mentioned in [13, 15-18].

3.2.5 Aggregation of generating units

Once the coherent groups of generators have been identified, each group of generators is aggregated into one equivalent model. The classical aggregation method treats the rotors of coherent generators as if they rotate on one common rigid shaft [17]. The inertia time constant H_a and mechanical power P_m of the aggregated generator from *n* generators can be calculated by (3.5-3.6):

$$P_{ae} = \sum_{i\epsilon\{G\}} P_{ie}\ ;\ P_{am} = \sum_{i\epsilon\{G\}} P_{im} \tag{3.5}$$

$$\sum_{i\epsilon\{G\}} M_i \frac{d\omega}{dt} = \sum_{i\epsilon\{G\}} P_{im} - \sum_{i\epsilon\{G\}} P_{ie} - \sum_{i\epsilon\{G\}} D_i = M_a \frac{d\omega}{dt} \tag{3.6}$$

where $M_a = 2H_a$, P_{ae}, P_{am} denote the equivalent inertia constant, electrical and mechanical power of group of generators *{G}* [19]. In most works, the equivalent generator is treated as classical model and its associated control devices of the coherent group of generators are omitted or the most dominant (largest unit) is used. More detailed calculation of the aggregation can be realised by the time domain structure preservation approach [20-21] where the equivalent parameters of generators are calculated through the coefficient matrices in order to preserve the physical characteristics of generating units. In addition, method based on trajectory sensitivity theory was proposed by Chow [14] to perform the aggregation of excitation systems' parameters.

3.3 Network Reduction Methodology

The methods used to construct equivalents of the selected sub-system of the network are referred to as network reduction [4]. There are three main methods proposed by Ward; Dimo and Zhukov. In general, the network reduction includes two main tasks: 1) to replace the coherent groups of generators with equivalent units and eliminate the load nodes; 2) to calculate the equivalent transmission circuits which should maintain the balanced steady state power flow conditions.

3.3.1 Ward method

Ward Method is the simplest network reduction method. In most cases, the nodes need to be retained are defined in group *{R}*, and nodes which can be eliminated are referred to as group *{E}*. The basic concept of this method is to maintain the current and voltage flow at the retained nodes unchanged [4, 17]. The electrical transmission network nodal equation is described as:

$$\begin{bmatrix} I_R \\ I_E \end{bmatrix} = \begin{bmatrix} Y_{RR}\ Y_{RE} \\ Y_{ER}\ Y_{EE} \end{bmatrix} \times \begin{bmatrix} V_R \\ V_E \end{bmatrix} \tag{3.7}$$

The voltage and current at eliminated groups of nodes can be swapped by using the partial inversion:

$$\begin{bmatrix} I_R \\ V_E \end{bmatrix} = \begin{bmatrix} Y_R & K_I \\ K_V & Y_{EE}^{-1} \end{bmatrix} \times \begin{bmatrix} V_R \\ I_E \end{bmatrix} \quad (3.8)$$

$$Y_R = Y_{RR} - Y_{RE}Y_{EE}^{-1}Y_{ER},\ K_I = Y_{RE}Y_{EE}^{-1}, K_V = -Y_{ER}^{-1}Y_{EE}^{-1} \quad (3.9)$$

By this linear matrix algebra, the nodal currents at the retained nodes can be represented by:

$$I_R = Y_R V_R + K_I I_E = Y_R V_R + \Delta I_R \quad (3.10)$$

Thus, the relationship between the voltage and current at the retained nodes can be described as two terms: 1) the equivalent admittance matrix Y_R which consists of the retained nodes and equivalent branches connecting them. The matrix Y_R is called the transfer admittance matrix; 2) the second term of equation (3.10) K_I passes the equivalent currents from the eliminated nodes to the retained nodes. These equivalent currents are normally translated into real and reactive power loads at the retained buses [17, 23]. The matrix K_I is referred to as the distribution matrix. The characteristics of Ward elimination and its extended methods can be summarised as follows:

- In order to improve the accuracy of the reduced network, the extended Ward equivalent is developed by way of introducing additional shunt admittance $Y_{Ei} = S_i^*/V_i^2$ to the diagonal elements of Y_{EE} to replace the power injection from eliminated nodes. Thus, the nodal injections from equivalent currents $\Delta I_R = 0$. However, the additional shunt branches may contain large conduction corresponding to the real power injections. This results in a poor *X/R* ratio causing convergence troubles in computing load flow calculations.
- The Ward-PV method proposed by Machowski in [4] improves the dynamic performance of the reduced network by making all the generator nodes retained while all load nodes are eliminated. The PV relates to all the generator nodes in the external system.

However, the Ward based methods may create additional connections. This can be explained by analysing the elimination step (3.11): assume the node *k* is going to be eliminated, the matrix Y_R becomes:

$$Y_R = Y_{RR} - Y_{RE}Y_{EE}^{-1}Y_{ER} = Y_{RR} - \frac{1}{Y_{kk}}\begin{bmatrix} \vdots \\ \cdots Y_{ik}Y_{kj} \cdots \\ \vdots \\ j \end{bmatrix} i \quad (3.11)$$

where Y_{ik} and Y_{kj} represent the mutual admittance between node *i* and the eliminated node *k*. If node *i* is connected with node *k* then it is referred to as its neighbour, $Y_{ik} \neq 0$. If $Y_{ik} = 0$, the node *i* is not the neighbour of node *k*. Hence, the difference between the original transfer matrix element Y_{ij}^{old} of Y_{RR} and the equivalent transfer matrix element Y_{ij}^{new} of Y_R can be represented as:

$$Y_{ij}^{new} = Y_{ij}^{old} - \frac{Y_{ik}Y_{kj}}{Y_{kk}}, i \neq k, j \neq k \quad (3.12)$$

As a result, the reduced network might create additional connections between the neighbours because the admittances in the new transfer matrix Y_R were changed as shown in Figure 3.2 [17].

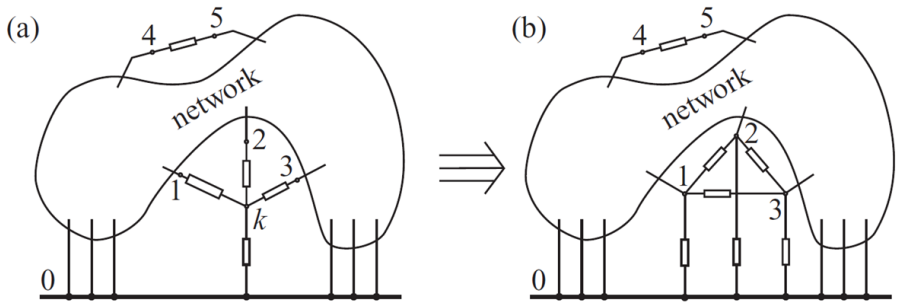

Figure 3-2. Ward Equivalent: a) original system (node *k* need to be eliminated). b) equivalent system after node *k* elimination [17]

3.3.2 Dimo's method

The difference between Dimo's method and Ward method is that it replaces the external nodes by one equivalent node rather than eliminates them. However, Dimo's method also creates fictitious connections in the reduced network [17].

In order to aggregate a group of nodes into one node, one fictitious bus *f* is defined at the beginning. The nodes need to be aggregated are all connected with this bus by a number of fictitious admittances Y_{fi}. The principle of choosing these admittances is to make the terminal voltage of all the added branches equal. Normally the admittances are made to correspond to nodal injections at the

aggregated nodes. In other words, to make the voltage at the fictitious node *f* equal to zero.

$$Y_{fi} = \frac{S_i^*}{V_i^2} \ , i \ \epsilon \ \{A\} \tag{3.13}$$

However, it is not a good choice to run the system with an equivalent node operating at zero voltage. One negative admittance is always added to create an extra fictitious branch connecting the bus *f* and the aggregated node *a*. The admittance is determined to make the terminal voltage at bus *a* equal to the weighted average voltages of the aggregated nodes:

$$Y_{fa} = -\frac{S_a^*}{V_a^2} \ , S_a = \sum_{i\epsilon\{A\}} S_i \ , V_a = \frac{S_a}{I_a^*} = \frac{\sum_{i\epsilon\{A\}} S_i}{\sum_{i\epsilon\{A\}} (\frac{S_i}{V_i})^*} \tag{3.14}$$

The reduced network is connected to the internal sub-system with the aggregated node *a* at last. The method is usually used in load nodes elimination since the equivalent external sub-system can only confirm the accuracy if the admittances of the fictitious branches unchanged under different operating conditions. In other words, only the load nodes can be represented as constant admittances and with a power-voltage characteristic $S = V^2 Y^*$ unchanged. However, the fictitious branches and the negative admittance created in the equivalent network may also cause convergence problems in load flow studies.

3.3.3 Zhukov method

The method was first developed by Zhukov in 1964. The aggregation is achieved in a way of replacing a group of generators by an equivalent node based on the following two conditions:

1. The current and voltages remain unchanged at the retained nodes.

2. The power injection at the equivalent node is equal to the total power injections at the aggregated nodes.

The equivalent matrix calculated from Zhukov method has one major advantage that it does not change the transfer matrix admittance Y_{RR}. The first condition is achieved if $Y_{RA}V_A$=$Y_{Ra}V_a$:

$$\begin{bmatrix} I_R \\ I_A \end{bmatrix} = \begin{bmatrix} Y_{RR} \ Y_{RA} \\ Y_{AR} \ Y_{AA} \end{bmatrix} \times \begin{bmatrix} V_R \\ V_A \end{bmatrix}, \begin{bmatrix} I_R \\ I_a \end{bmatrix} = \begin{bmatrix} Y_{RR} \ Y_{Ra} \\ Y_{aR} \ Y_{aa} \end{bmatrix} \times \begin{bmatrix} V_R \\ V_a \end{bmatrix} \tag{3.15}$$

$$Y_{RR}V_R + Y_{RA}V_A = Y_{RR}V_R + Y_{Ra}V_a \quad (3.16)$$

If the reduced network needs to be used for other states (different from the initial state), the condition $Y_{Ra} = Y_{RA}\vartheta$ must hold. Hence, the transfer ratio $\vartheta = V_a^{-1}V_A$ should remain constant for all the aggregated generators in this group. This is also the criteria used to determine the groups of coherent generators as mentioned in equation (3.2).

The second condition is satisfied when:

$$V_a I_a^* = V_A^T I_A^* \Longrightarrow V_a Y_{aR}^* V_R^* + V_a Y_{aa}^* V_a^* = V_A^T Y_{AR}^* V_R^* + V_A^T Y_{AA}^* V_A^* \quad (3.17)$$

To substitute the ratio ϑ into equation (4.19):

$$Y_{aR} = \vartheta^{*T} Y_{AR}, Y_{aA} = \vartheta^{*T} Y_{AA}\vartheta \quad (3.18)$$

Finally, the equivalent network can be expressed as:

$$\begin{bmatrix} I_R \\ I_a \end{bmatrix} = \begin{bmatrix} Y_{RR} & Y_{RA}\vartheta \\ \vartheta^{*T} Y_{AR} & \vartheta^{*T} Y_{AA}\vartheta \end{bmatrix} \times \begin{bmatrix} V_R \\ V_a \end{bmatrix} \quad (3.19)$$

Although this method does not introduce fictitious branches compared with Dimo's method, it still introduces fictitious shunt at the retained nodes. Moreover, the process of identifying coherent groups of generators requires high numerical calculation efforts.

3.4 Proposed Novel Methodology

All the methodologies introduced above need the original system data in order to establish either the state-space linear model or the electrical transmission network nodal equation. However, due to the pattern of the power system market has been changed a lot in these decades, the industrial data have become more and more privatization. The significant competitions among the power companies made the information of power system utilities become confidential. Hence, it is impractical to get access to these data for the researchers focused on power system analyses with a practical network. Due to these limitations, most of the works in power system steady-state analyses and transient performance analyses were investigated based on a very simple network where an infinite bus or a voltage source model was usually

assumed to represent the main grid. There is still insufficient amount of research focused on the systematic quantification of the power systems frequency performance based on a real representative and properly validated dynamic model, especially in a large power system.

The installation of the renewable energy will introduce a great number of new challenges for system operators in the future. It is crucial to establish the simulink models and predict the future system performance before applying any renewable scenario. Hence, a new proposed method of establishing the equivalent network is introduced. The processes of the method are mainly divided into four parts:

- **Steady-state transmission network data calculation**: the coherent groups of generators and the retained bus nodes should be identified at first. Then, the transmission-line impedance data of the equivalent network are calculated based on the proposed method.
- **Dynamic parameters setting**: the classical synchronous generators' dynamic data are chosen according to the standard model reference; the small signal analysis and Individual Channel Analysis and Design (ICAD) are both applied for calculating the appropriate parameters of control devices such as: excitation system and power system stabilizer.
- **Parameter adjustment**: to provide an approach to achieve model flexibility in changing different system operating conditions for the purpose of exploring a variety of future system scenarios.
- **Validation**: the work is accomplished by comparing the system frequency response with historic data records from actual events. The comparisons should cover the analyses in both load flow and dynamic frequency performance. The total system inertia constants and speed droop settings are tuned as well.

3.4.1 Background in transmission circuit

In power system steady-state studies, the transmission lines are usually divided into three types: short-length, medium-length and long-length lines [24].

Short-length line: This type of transmission line is usually applied to overhead line less than 80km long. Only the series resistance and reactance are considered as shown in Figure 3.3. The shunt admittance is neglected due to the small distance.

$$z = R + j\omega L,\ \Omega/m;\ \ Z = zl$$
$$y = G + j\omega C,\ s/m;\ \ Y = yl \tag{3.20}$$

where z and y are the series impedance and admittance per unit length of the two port network; l is the length of the transmission line. The relationship between sending end and receiving end of the line can be expressed as:

$$V_s = V_R + ZI_R$$
$$I_s = I_R \tag{3.21}$$

where V_s and I_s represents the sending end voltage and current; V_r and I_r represents the receiving end voltage and current.

Medium-length line: It is also referred to as the π circuit. The lumped shunt capacitance is normally located half at each end of the line. This type of transmission line is applied with a range of 80km to 250km.

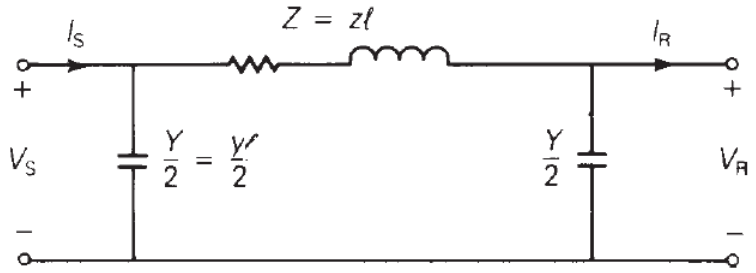

Figure 3-3. **π** circuit –medium length transmission line [24]

$$V_s = V_R + Z(I_R + I_{C2})$$
$$I_s = I_R + I_{C2} + I_{C1} \tag{3.22}$$

where the current on two shunt branches can be expressed as:

$$I_{C1} = \frac{V_S Y}{2},\ I_{C2} = \frac{V_R Y}{2} \tag{3.23}$$

Long length line: This type of circuit normally used if the length is over 250km. The line resistance, reactance and capacitance are no longer lumped but rather uniformly distributed along the line. The voltage and current at any section of length Δx can be represented as:

$$V(x + \Delta x) = V(x) + z(\Delta x)I(x)$$
$$I(x + \Delta x) = I(x) + y(\Delta x)V(x + \Delta x) \tag{3.24}$$

The detailed calculation steps of this type of line can be found in [24]. The voltage at any point of x along the line in terms of receiving end voltage and current can be described as:

$$V(x) = \cosh(\gamma x)\, V_R + Z_c \sinh(\gamma x)\, I_R$$
$$I(x) = \frac{1}{Z_c}\sinh(\gamma x)\, V_R + \cosh(\gamma x)\, I_R \tag{3.25}$$

where the characteristic impedance $Z_c = \sqrt{z/y}\,, \Omega$ and the propagation constant $\gamma = \sqrt{zy},\ \ m^{-1}$.

In most of power system analyses, the π circuit is utilized to represent the transmission circuit since it can not only provide accurate results but also consisted with more simplified structure than long length line.

3.4.2 Determination of the number of equivalent nodes and their locations

To introduce the processes of equivalencing more intuitively, the UK transmission network is considered as an example. The systematic steps of establishing the trustful dynamic equivalent network is demonstrated. The power flow parameters of the reduced network are calculated in this chapter where the dynamic parameters of the generators with their associated control devices are introduced in next chapter.

As mentioned earlier, the key points in modelling the UK network should include following aspects: 1) to determine the number of the retained nodes and their locations; 2) to define the distribution profile of generators and their corresponding types of governors; 3) to define the distribution profile of demand; 4) to calculate the equivalent transmission line impedance; and the most important issue 5) to adjust parameters under different operating conditions.

The UK transmission system is quite a complex power network which includes nearly thousand nodes distributed across the whole country. As mentioned above, in order to reduce the size of the network, the coherent groups of generators should be identified at first. However, it is impractical to establish the reduction model by using any previously developed network reduction method since no detailed original network data are public available. Hence, the coherent groups of generators can only be identified based on the historic system performance records. If a group of generators in one area has significant oscillatory swing against another, it is possible to assume the generators in this area are coherent.

Fortunately, these information are available from the public resources: National Electricity Transmission System Seven Year Statement (NETS SYS). The National

Grid Electricity Transmission plc (NGET) publishes its Seven Year Statement (now it is replaced by Ten Year Statement) every year. The information introduced in the statement is based on data from the users of England and Wales transmission system. It is also cooperated by two Scottish transmission licensees: Scottish Power Transmission Ltd (SPT) and Scottish Hydro Electric Transmission Ltd (SHETL) [25].

The NETS SYS provides a wide range of information including: generation and demand profiles; power transmission weakness; external interconnection with Europe countries; current system's oscillation performance; future plan for transmission circuits' reinforcement and the renewable energy installation scenarios, etc.

In order to understand the system's frequency performance and identify the requirements for transmission line reinforcement, the whole UK transmission system has been divided into 17 study zones based on 17 critical boundaries (11 in England & Wales and 6 in Scotland).

These 17 boundaries are defined since they reflect the historically main weaknesses on the interconnected system. These weaknesses may lead to the need to restrict the power flows across the system. Otherwise, the system may operate at unacceptable conditions. The unacceptable conditions are defined by the Licence Standard include:

- Unacceptable overloading of any primary transmission device.
- Unacceptable voltage conditions which relates to the voltage capability issues and the system instability issues.

There was no significant inter-area oscillation existed inside each study zone. The major inter-area to inter-area oscillations existed between England & Wales and Scotland. Hence, the assumption can be made that these 17 studies zones reflect the major system problems related to both load flow and dynamic stability issues. The generators in each zone are coherent and can be aggregated into one generator.

Unlike the previously introduced network reduction methods, the system is not defined as internal sub-system and external sub-system here. The main purpose in this research is to test the entire system frequency performance during major disturbances rather than a specific internal sub-system. Hence, each study zone was

represented with one node which was close to the major power plant or the main transmission line according to the documents: “GB transmission system with large power stations” and “GB transmission boundaries and SYS study zones [25]” (as shown in Appendices a and b).

In addition, the major transmission lines connecting Scotland and England are consisted by two 400KV parallel AC transmission circuits according to the maps. Hence, three extra nodes are added in study zone 3, 6 and 7 in order to establish the power transfers to adjacent zones as shown in Figure 3.9.

3.4.3 Estabilishing generation and demand profile

Once the equivalent nodes have been determined, each group of generators and demand of the 17 study zones can be aggregated into one unit connecting to the chosen nodes. The next step is to determine the total amount of generation and demand distributed in each study zone.

These information are also accessible from SYS. The detailed effective generation, demand and their total capacity are all listed in the document. Table 3.1-3.2 demonstrate the generation and demand profile in study zone 9 as an example:

Table 3.1. Studied Boundary 9: Generation and Demand Profile [25]

Studied Boundary Generation, Demand and Transfer (MW)								
Boundary	Name	Quantity (MW)	10/11	11/12	12/13	13/14	14/15	15/16
B9	Midlands	Effective Generation	40318	40500	40676	40389	40399	39575
B9	Midlands	Demand	28736	28761	28846	28914	29169	29064
B9	Midlands	Planned Transfer	11582	11739	11829	11475	11230	10512

Table 3.2. Study Zone 9: Subtotals of Capacity by Plant Type [25]

Subtotals of Capacity by Plant Type and SYS Study Zone, 2010/11								
Plant Type	CCGT	CHP	Large Coal	Nuclear AGR	Nuclear Magnox	Pumped Storage	Wind Offshore	Total
Z9	2934	365	1987	2408	960	2004	182	10840

In order to further simplify the equivalent network, the generation types are all considered as the classical synchronous generator and their associated turbine as steam turbine. The detailed power flow data of all study zones are included in Appendices c and d.

3.4.4 Calculation of equivalent transmission line parameters

The lengths of the transmission lines between each study zone are mostly in the range of medium-length, so the π circuit is used. The equivalent transmission line impedance calculation is achieved if the following assumptions are made: it is assumed that the voltage magnitudes and angles at each end of the line (V_1, V_2 and θ_1, θ_2) as well as the power transfer from bus 1 to 2 (P and Q) are known.

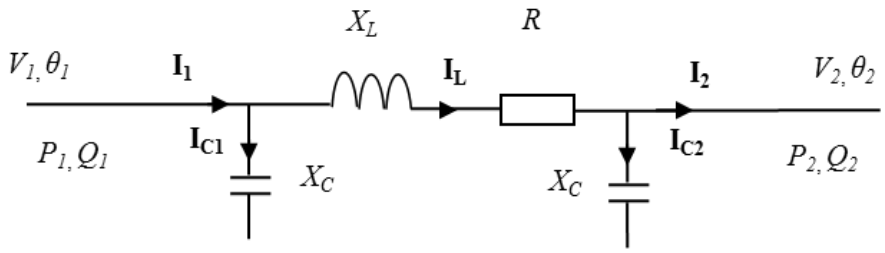

Figure 3-4. Two nodes transmission circuit [26]

With these assumptions it is possible to calculate the line parameters R, X_L and X_C by solving the equations (3.26):

$$\begin{cases} \mathbf{V_1} = \mathbf{V_2} + \mathbf{I_L}\,(R + jX_L) \\ \mathbf{I_L} = \mathbf{I_1} - \mathbf{I_{C1}},\ \mathbf{I_L} = \mathbf{I_2} + \mathbf{I_{C2}} \\ \mathbf{I_1} = \frac{\mathbf{S_1}}{\mathbf{V_1}},\ \mathbf{I_2} = \frac{\mathbf{S_2}}{\mathbf{V_2}}, \mathbf{I_{C1}} = \frac{\mathbf{V_1}}{jX_C},\ \boldsymbol{I_{C2}} = \frac{\mathbf{V_2}}{jX_C} \end{cases} \tag{3.26}$$

However, table 3.1 and 3.2 only provide the total amount of generation and demand distributed in each sub-system. The detail power flow results such as power transfer between zones are not mentioned. Thus efforts must be made to explore the voltage magnitudes and angles at each node as well as their power transfer to its adjacent nodes. These parameters can be obtained from the "Power Flow Diagrams" where the detailed system power flow results are superimposed on the diagrams. The processes of calculating the equivalent transmission line parameters between zone 1 and zone 4 is illustrated as follow:

- The nodes close to the major power plant or main transmission line are found on the map as shown in Figure 3.5-3.6

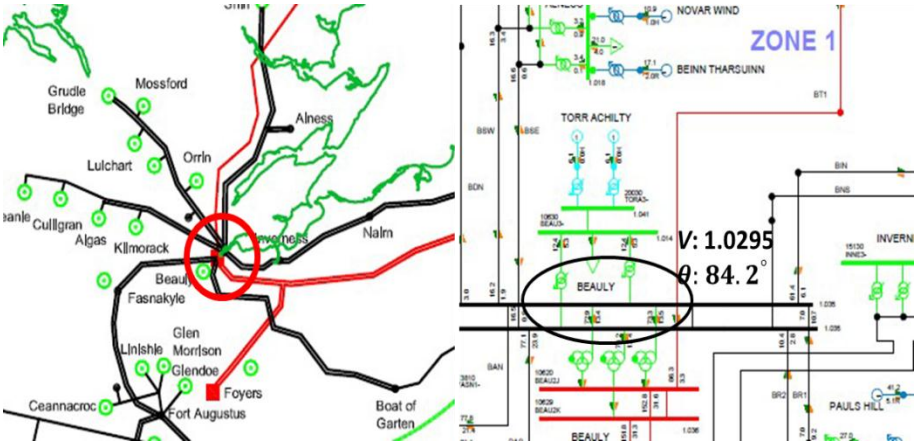

Figure 3-5. Voltage magnitude and angle of node at Zone 1

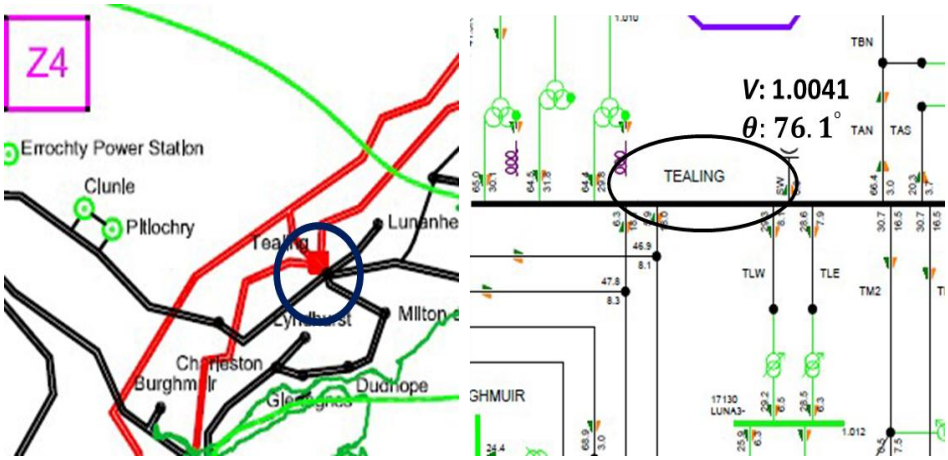

Figure 3-6. Voltage magnitude and angle of node at Zone 4

- Node BEAULY and TEALING are chosen to represent the aggregated node at study zone 1 and zone 4. The voltage magnitudes and angles at BEAULY and TEALING are selected as the aggregated node voltage variables.

- The transmission line connecting zone 1 and zone 4 which crosses the boundary B1 is found on the map. Figure 3.7 demonstrates how to identify the power transfer (both sending end and receiving end active power and reactive power) between zone 1 and zone 4. The total power transfers between zones are summed up and the equivalent transmission line parameters are calculated

by solving the set of equations 3.26. The data used for calculating the line parameters are listed in Table 3.3.

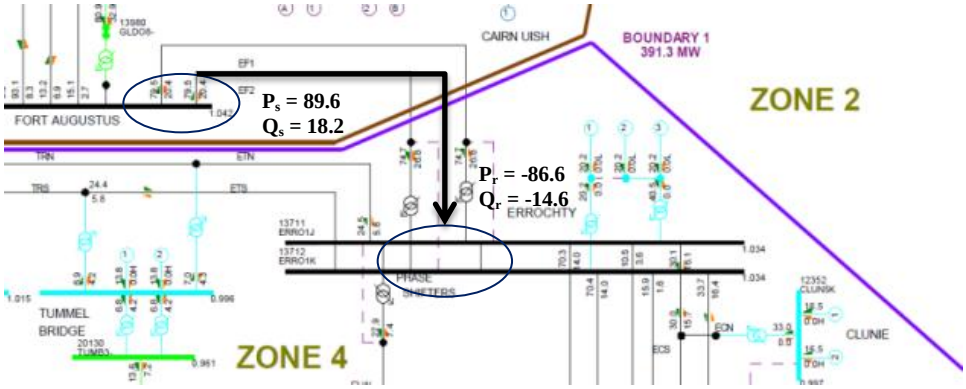

Figure 3-7. Identify power flow between zone 1 and zone 4

Table 3.3. Power Transfer between Study Zone 1 and 4

Node	Name	Voltage (kV)	Voltage (pu)	Angle (Deg)	Active Power(MW)	Reactive Power(MVar)
1	Beauly	400	1.0295	84.2	151.7	-7
4	Tealing	400	1.0041	76.1	-150.4	-13.4

In order to perform the required calculation in a more efficient manner, one software environment has been designed based on Matlab Graphical User Interface (GUI). A transmission line calculator is designed to calculate all parameters of the π-circuits. The example screenshot of the program is presented in Figure 3.8. It contains several functionalities:

- The entire buses voltage magnitude and angle information with their power transfer to adjacent nodes can be either loaded from a pre-formatted Excel spread sheet or typed manually. The calculation of all the equivalent transmission lines can be finished automatically by single button click.
- The variables corresponding to each connection can be chosen and able to be modified at any time. The single calculation function is possible for any specific transmission line parameters modification.
- Save the results in an Excel file format automatically which is suitable for data importing to the PSS/E software.

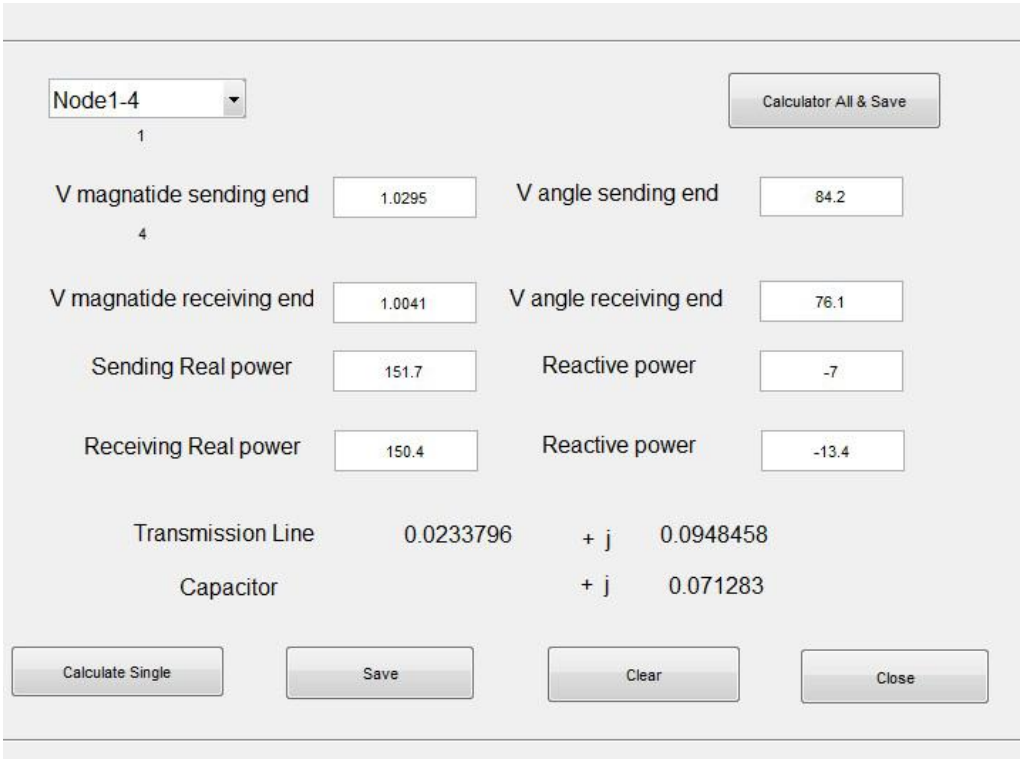

Figure 3-8. Transmission line parameters calculator

- The resulting line parameters R, X_L and X_C between zone 1 and 4 are finally calculated as shown in Table 3.4:

Table 3.4 Transmission line parameters between Study Zone 1 and 4

From Node	Name	To Node	Name	R (pu)	X_L (pu)	X_C (pu)
1	Beauly	4	Tealing	0.0234	0.0944	0.071

However, one unusual transmission line (with negative resistance) is observed which connecting the study zone 13 and 14. This is probably due to the network density inside the zone 14 (London) is relatively high since it is the largest power consuming area in the country. Hence, large differs of the voltage angles among the nodes can be found inside this zone. An extra node (node 21) closes to the boundary 14 is then added. The final UK equivalent power system is modelled as one 21-bus system as shown in Figure 3.9. The full data of transmission line parameters are presented in Appendices e and f.

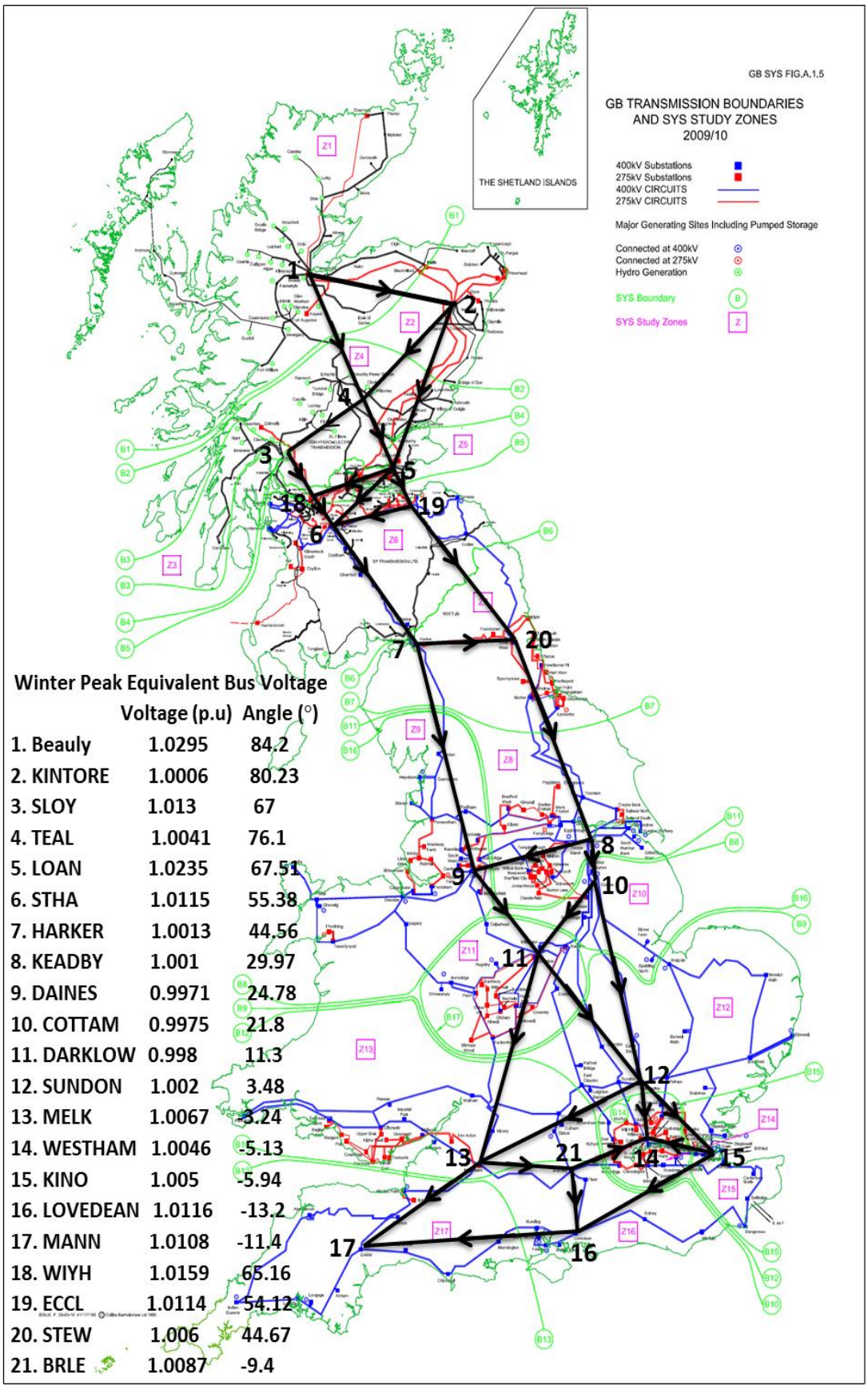

Figure 3-9. 21-buses equivalent UK transmission system

3.4.5 Modal flexibility in changing the operating conditions

The calculated equivalent network is based on the winter peak demand operating conditions. Method is needed to modify the system parameters under different operating conditions so that the model can be used for exploring a variety of future system scenarios. The procedure can be described as follows:

The historical demand data with each half hour of the day is recorded on "New Electricity Trading Arrangements, Balancing Mechanism Reporting System (BMRS) [27]". This is an online reports website used by the National Grid Operator as a means of balancing power flows in UK. It provides both real time and historic data records to support achieving the Balancing Mechanism which is one of the key aspects of the New Electricity Trading Arrangements (NETA). NETA was introduced to England and Wales in 2001 for the purpose of providing a competition market environment while maintaining a secure electricity system. The system operator provides the balancing services in accordance with the grid code to secure the electricity supply by providing the offers to sell or buy energy from the participants. It is a trustful data resource website.

Demand: The historical demand data with each half hour of the day were recorded on BMRS as shown in Figure 3.10. Thus, the demand on a specific day and time (referred to as Historical Demand) can be used to scale down all existing loads in the model with one common ratio: Historical Demand/Winter peak Demand.

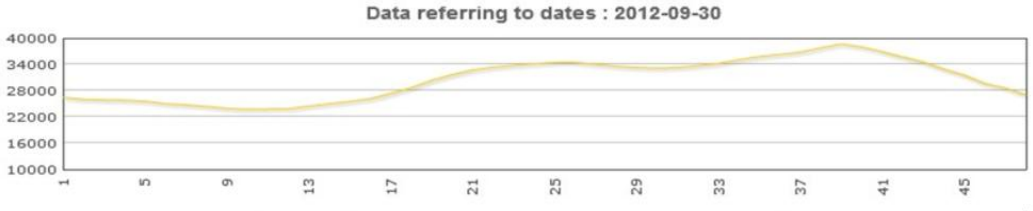

DATE	S/P	INDO Publish Time	INDO
2012-09-30	1	2012-09-29 23:30:00	24977.000
2012-09-30	2	2012-09-30 00:00:00	24112.000
2012-09-30	3	2012-09-30 00:30:00	23966.000
2012-09-30	4	2012-09-30 01:00:00	23930.000
2012-09-30	5	2012-09-30 01:30:00	23409.000
2012-09-30	6	2012-09-30 02:00:00	22692.000
2012-09-30	7	2012-09-30 02:30:00	22296.000
2012-09-30	8	2012-09-30 03:00:00	21942.000
2012-09-30	9	2012-09-30 03:30:00	21533.000
2012-09-30	10	2012-09-30 04:00:00	21212.000

Figure 3-10. Historic half hour demand example [27]

Generation: The data changing for the generation is relatively more complicated than demand adjustment. The total amount of generation capacity distributed in each study zone was not presented. The concept relates to cost benefits is utilized to achieve the generation data adjustment.

In April 2010, Britain issued a new 'deterministic' standard which invited the industry's consultation [28]. The standard believes that a cost-benefit analysis should be used in network investment and dispatching. According to this approach, large coal and CCGT plants are dispatched according to the Dark and Spark Spread as shown in Figure 3.11.

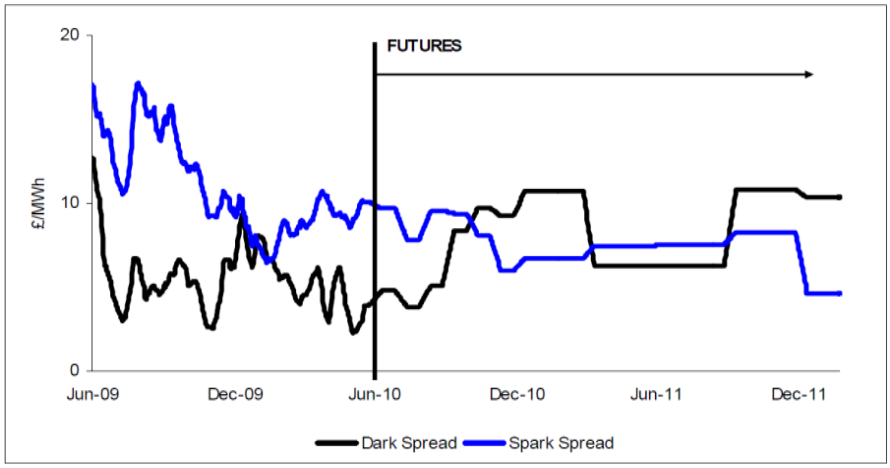

a) Power Generation Economy Years 2009-2011

b) Power Generation Economy Years 2012-2014

Figure 3-11. Spark and Dark spread [29]

The ‘spark spread’ is the difference between the cost for CCGT to generate 1MWh energy and the price for that energy can be sold. The ‘dark spread’ is used for Coal plant in the same way [29]. It can be seen that in early years (before 2009), CCGT plants made more profits due to the low gas price compared with the coal fired power plants. After that, the situation changed with the coal fired generation became more attractive of the two in 2010. In later years (after 2011), the spark spread curve was replaced by the relative dark and spark spreads as shown in 3.11b. The data demonstrated on the curve indicates that the coal plant will be strongly favoured over gas plant in the following years.

According to these spark spread curves, the assumptions can be made that before 2010, the CCGT plants in each zone will be dispatched before the coal plant. In other words, all CCGT plants are set online in each zone while the rest amount of generation are equally distributed among each zone (similar to the method that were used in calculating demand with one ratio). All nuclear power plants are dispatched at all the times expect there are some particular issues happened on that day. After 2011, the coal plants take the priority to operate first.

The principles outlined above are used in the model to split the total amount of generation between coal, CCGT and nuclear technology in each study zone. The applications of this method are introduced in chapter 5 for the purpose of the validation of the established system.

3.5 Summary

In this chapter the necessity of why an accurate dynamic equivalent network is needed is first explained. Then, the system network equivalencing methods referred to: modal method and coherency based method are introduced. The modal method can provide good notification about the various modes of oscillations exist in the system. However, the equivalence is based on linearizing the non-linear differential equations. It contains two major disadvantages related to the poor ability to reflect the complex dynamic system performance during major disturbances and need of data converting to import/export the equivalent results into simulation programs. The coherency methods use the concept of coherent groups of generators. The elimination of the buses is achieved by the network reduction methods.

There were three network reduction method developed in 1980s: Dimo's method, Ward method and Zhukov's method. Ward method is the simplest reduction method however it may create additional branches. Moreover, the equivalent system cannot reflect the dynamic performance of the external subsystem since all external nodes are eliminated. Dimo's method is usually used in load nodes reduction. A number of fictitious admittance may be introduced which are not welcomed for the most of power flow calculations. Zhukov's method maintains the characteristic of the electrical transmission network nodal equation. However, it may still create fictitious shunt branches and take high numerical calculation efforts on identifying the coherent groups of generators.

Due to the limitations and difficulties in using these methods, one new methodology is proposed. The method is able to establish the equivalent network based on the limited public available information and can be applied to any kind of network equivalencing. The equivalent UK transmission network is demonstrated as an example to explain the processes of the method. One novel equivalent transmission line calculating method is also mentioned. At last, an approach to achieve model flexibility in changing the system operating conditions is also presented based on the BMRS.

References

[1] E.J.S. Pires de Souza, A.M. Leite da Silva, "An efficient methodology for coherency-based dynamic equivalents," *Generation, Transmission and Distribution, IEE Proceedings*, vol.139, no.5, Sep 1992, pp.371-382

[2] X. Lei, D. Povh, O. Ruhle, "Industrial approaches for dynamic equivalents of large power systems," *IEEE Power Engineering Society Winter Meeting,* , NY, USA, 2002, pp.1036-1042

[3] F. de Oliveira Resende, "*Contributions for MicroGrids Dynamic Modelling and Operation*," PhD thesis, Porto University, Porto – Portugal, 2007

[4] J. Machowski, A. Cichy, F. Gubina, *et al*., "External subsystem equivalent model for steady-state and dynamic security assessment, "*Power Systems, IEEE Transactions on* , vol.3, no.4, Nov 1988, pp.1456-1463

[5] J. B. Ward, "Equivalent circuits for power-flow studies," *Electrical Engineering* , vol.68, no.9, Sept. 1949, pp.794

[6] U.D. Annakkage, N. K C Nair, Y. Liang, *et al*., "Dynamic System Equivalents: A Survey of Available Techniques," *Power Delivery, IEEE Transactions on* , vol.27, no.1, Jan. 2012, pp.411-420

[7] P. Kundur, "*Power System Stability and Control*", McGraw-Hill, Inc. NY, 1993

[8] J.M. Undrill, J. A. Casazza, E.M. Gulachenski, *et al*., "Electromechanical Equivalent for Use in Power System Stability Studies," *Power Apparatus and Systems, IEEE Transactions on* , vol.PAS-90, no.5, Sept. 1971, pp.2060-2071

[9] J.M. Undrill, A.E. Turner, "Construction of Power System Electromechanical Equivalents by Modal Analysis," *Power Apparatus and Systems, IEEE Transactions on* , vol.PAS-90, no.5, Sept. 1971, pp.2049-2059,

[10] I.J. Perez-Arriaga, G.C. Verghese, F.C. Schweppe, "Selective Modal Analysis with Applications to Electric Power Systems, Part I: Heuristic Introduction," *Power Engineering Review, IEEE* , vol.PER-2, no.9, Sept. 1982, pp.29-30

[11] G.C. Verghese, I.J. Perez-Arriaga, F.C. Schweppe, "Selective Modal Analysis with Applications to Electric Power Systems, Part II: The Dynamic Stability Problem," *Power Engineering Review, IEEE* , vol.PER-2, no.9, Sept. 1982, pp.30-31

[12] S. Geeves, "A modal-coherency technique for deriving dynamic equivalents," *Power Systems, IEEE Transactions on* , vol.3, no.1, Feb 1988, pp.44-51

[13] R. Podmore, "Identification of Coherent Generators for Dynamic Equivalents," *Power Apparatus and Systems, IEEE Transactions on* , vol.PAS-97, no.4, July 1978, pp.1344-1354

[14] R.J. Galarza, J.H. Chow, W.W. Price, *et al.*, "Aggregation of exciter models for constructing power system dynamic equivalents," *Power Systems, IEEE Transactions on* , vol.13, no.3, Aug 1998, pp.782-788

[15] L. Wang, M. Klein, S. Yirga, *et al*., "Dynamic reduction of large power systems for stability studies," *Power Systems, IEEE Transactions on* , vol.12, no.2, May 1997, pp.889-895

[16] N.M. Peterson, W.F. Tinney, D.W. Bree, , "Iterative Linear AC Power Flow Solution for Fast Approximate Outage Studies," *Power Apparatus and Systems, IEEE Transactions on* , vol.PAS-91, no.5, Sept. 1972, pp.2048-2056

[17] J. Machowski, J.W. Bialek, J.R. Bumby, *Power System Dynamics and Stability*. John Wiley & Sons Ltd, Banfins Lane, Chichester, 1997

[18] J. R. Winkelman, J.H. Chow, B. C. Bowler, *et al*., "An Analysis of Interarea Dynamics of Multi-Machine Systems," *Power Apparatus and Systems, IEEE Transactions on* , vol.PAS-100, no.2, Feb. 1981, pp.754-763

[19] J.P. Yang, G.H. Cheng, Z. Xu, "Dynamic Reduction of Large Power System in PSS/E," *IEEE/PES Transmission and Distribution Conference and Exhibition: Asia and Pacific*, Dalian, China, Aug. 2005, pp.1-4

[20] M.L. Ourari, L-A. Dessaint, V.Q. Do, "Generating units aggregation for dynamic equivalent of large power systems," *Power Engineering Society General Meeting*, Denver, Co, June 2004, pp.1535-1541

[21] A.A.M. Zin, B.C. Kok, M.W. Mustafa, *et al*., "Time domain dynamic aggregation of generating unit based on structure preserving approach," *Power Engineering Conference*, 2003. Proceedings. National, 15-16 Dec. 2003, pp.154-160

[22] *PSS/ETM Program Application Guide*, Volumes I and II, Power Technologies International

[23] J. Garinger; William D. Stevenson. "*Power System Analysis*," McGraw-Hill, Inc. NY, 1994

[24] J. D. Glover, Mulukutla S. Sarma, Thomas J. Overbye, "*Power System Analysis and Design*." Thomson Press, Stamford, USA, 2008, Fourth Edition

[25] National Grid, "*Seven Year Statement*", November 2012, http://www.nationalgrid.com/uk/Electricity/SYS/CURRENT

[26] J. Xia, A. Dyśko, "UK transmission system modelling and validation for dynamic studies," *Innovative Smart Grid Technologies Europe (ISGT EUROPE)*, 4th IEEE/PES , Copenhagen, Denmark, 6-9 Oct.2013, pp.1-5

[27] New Electricity Trading Arrangements (neta), *Balancing Mechanism Reporting System* (BMRS), http://www.bmreports.com

[28] SP Transmission, Scottish and Southern Energy and National Grid, "*Review of Required Boundary Transfer Capability with Significant Volumes of Intermittent Generation*", Ref. GSR009, June 2010

[29] National Grid, "*Winter Consultation Report* 2010/11", July 2011

CHAPTER 4: EQUIVALENT SYSTEM MODELLING: DYNAMIC DATA CALCULATION

4.1 Introduction

A novel network reduction method was proposed in chapter 3. The calculation of the power flow data of the UK transmission system was introduced which included: the determination of generations and demand profile in each study zone; chosen of the aggregated nodes of the system; and the calculation of equivalent transmission line parameters. For the purpose of identifying the system frequency responses under future high penetration levels of wind farm conditions, systematic processes of dynamic equivalencing based on small signal analysis and frequency response methods are introduced in this chapter.

With the developments of the continuing growth in interconnections, new technologies and controllers were utilized in the system. A number of new power system stability issues occurred. The definition of stability is "the ability of an electric power system, for a given initial operating condition, to regain a state of operating equilibrium after being subjected to a physical disturbance, with most system variables bounded so that practically the entire system remains intact."[1] Usually, the reliability and security of the system were investigated by stability analyses referred to: transient stability and dynamic stability.

Dynamic stability is also related to small signal stability which concerned the ability of system to maintain synchronism during small disturbance. In current power system, the small disturbance based stability problems is usually associated with the insufficient damping of oscillations. The power system oscillations can be either local or global.

The local oscillation modes are associated with the oscillation of a single generator against a group of generators. It won't be discussed in this research since all the groups of generators in each study zone were assumed coherent.

The global oscillations involve a group of generators in one area swing against a group of generators in another area. In UK, the major global oscillations existed in UK power system between Scotland and England & Wales were mentioned by National Grid in report [2] according to the historical system frequency performance

data records. In today's power system, power system stabilizers (PSS) are widely used to achieve satisfied system oscillation stability.

Transient stability is the ability of system to maintain synchronism following a severe disturbance, for example loss of large generation plants or a three-phase fault on a transmission line. The primary responses of the machines during a transient are mainly depended on their stored kinetic energy in the rotating masses (inertia constant *H*). The new steady-state frequency is largely depended on the speed-droop characteristics of the turbine-governors.

Therefore, the appropriate dynamic parameters of the synchronous generators with their associated control systems such as excitation system, turbine-governors and power system stabilizers (PSS) are tuned to have a similar dynamic performance of the established model compared to the actual system based on the dynamic and transient stability analyses. The determination of the dynamic parameters of UK equivalent system is presented to explain the procedures of the proposed method.

In section 4.2, the original dynamic model of UK equivalent system is developed without AVR and PSS attached to the generators. The dynamic parameters of the synchronous generators are determined. Section 4.3 gives a brief introduction about small-signal stability analysis method. The characteristics of eigenvalue, eigenvectors and participation factor are also included. The frequency control methods and Individual Channel Analysis and Design (ICAD) method are introduced in section 4.4. Section 4.5 and 4.6 demonstrate the systematic steps of designing the AVR and PSS respectively. The influences of these control devices on system frequency performance during major disturbances are presented. Conclusion is made in section 4.7.

4.2 Equivalent System Dynamic Model Development

The components which may affect the electrical and mechanical output of the machines need to be determined in this stage. The components include: network load flow data which has already been described in chapter 3; the dynamic data of the equivalent system units (generator units and dynamic model of load, etc) must be tuned to have a similar dynamic performance compared to the actual system.

4.2.1 Generator

The classical generator models are assumed to represent the aggregated synchronous generator. PSS/E program contains a strong models library for simulation studies [3]. The typical round rotor generator model (GENROU) is used. Its parameters are obtained from manufacturer data sheets and standard parameters from [4-6]. These data include generator inertia constant *H*; d-axis transient time constant T'_{d0}; sub-transient time constant T''_{d0}; q-axis sub-transient time constant T''_{q0}; d-axis synchronous reactance X_d; transient reactance X'_d; sub-transient reactance X''_d; q-axis synchronous reactance $X_q$and sub-transient reactance X''_q as shown in Table 4.1. The typical synchronous generator parameters with different MVA rating are listed to meet the different generation profiles in each study zone.

Table 4.1. Generator parameters with different MVA rating [6]

MVA	300	1400	2000	6000
T'_{d0}(s)	8.5	5	5	7.6
T''_{d0}(s)	0.03	0.053	0.06	0.09
T''_{q0}(s)	0.9	0.123	0.09	0.2
H(s)	3.84	4.5	4.5	5
X_d(pu)	2.72	0.85	0.88	0.9
X_q(pu)	2.6	0.7	0.69	0.68
X'_d(pu)	0.36	0.3	0.3	0.3
X''_d(pu)	0.26	0.2	0.2	0.25
X''_q(pu)	0.26	0.2	0.2	0.25

4.2.2 Turbine governor

According to the grid code [7] and "Frequency Response Report" [8], not all of the generating plants need to provide the primary frequency response due to the economy and security concern. Only a certain numbers of power stations responding automatically to provide a primary response of 10% of its capacity in 10 seconds to keep the system stable during major disturbances and other power stations respond manually. To implement this principle, in simulation studies, in each study zone the generators are separated into two groups: The first group of generators (amounting to 90% of total capacity) is not equipped with any turbine governor (i.e. no turbine response following a disturbance), and the second group (amounting to 10% of total capacity) with the steam turbine models (TGOV1). Their parameters are listed in

Table 4.2 based on IEEE Standard [9]. T_1 is the governor time constant; T_2/T_3 represents the fraction of turbine power that is developed by high-pressure turbine; T_3 corresponds to the reheater time constant.

Table 4.2. Steam turbine parameters

R	T_1 (s)	V_{max} (pu)	V_{min}(pu)	T_2 (s)	T_3 (s)	D_t
0.02	0.3	2	-2	5	20	0

4.2.3 Other components

The loads are converted from a constant MVA loads into 100% constant active power and reactive power. In other words, all loads are assumed as frequency independent in order to simplify the model. Usually the determination of parameters and transfer functions of control devices is a challenged task. Hence, the small signal analysis and frequency response methods are used in determining the equivalent parameters of the control devices.

4.3 Small Signal Analysis

4.3.1 Linearzied system equations

It is not easy and convenient to assess the stability issues for a non-linear system such as power system. Hence, methodologies have been developed to solve the stability problems by the way of converting the non-linear system equations into linearized equations [10]. Small signal analysis is one of the most widely used methods based the assumption that the power system operating states will not be appreciably different compare to its initial state if the system is perturbed by a small perturbation [11]. The small perturbations can be any physical quantities such as change of rotor speed $\Delta\delta$, change of voltage ΔV or change of electric power ΔP, etc.

The dynamic descriptions of the system can be expressed as *n* first-order nonlinear differential equations (4.1-4.2) [4, 11]:

$$\dot{x}_i = f_i(x_1, x_2, \cdots x_n; u_1, u_2, \cdots u_r; t) \;\; i = 1,2 \cdots n \qquad (4.1)$$

$$y = g_k(x_1, x_2, \cdots x_n; u_1, u_2, \cdots u_r; t) \;\; k = 1,2 \cdots m \qquad (4.2)$$

where *n* is the order of the system and x_i is related to the system state variables.

State variables represent the minimum amount of information that can be used to describe the system behaviour. The choice of state variables is not unique. For example, the synchronous generators are usually represented by fifth-order model, third-order model (neglecting stator flux transient) or first-order model (further omission of the rotor flux transient). $\dot{x}_i$ is referred to as the derivative of state variable x_i with respect to time t; u are the inputs of the system and y are the outputs of the system. Applying the assumption that $\dot{x}_i$ is time irrelevant under a small perturbation, the dynamic performance of the system can be further simplified into (4.3-4.4):

$$\dot{x}_i = f_i(x,u) \;\; i = 1,2 \cdots n \tag{4.3}$$

$$y = g_k(x,u) \;\; k = 1,2 \cdots m \tag{4.4}$$

Therefore, the system can be linearized to investigate the dynamic response if the perturbations are small [5]. The nonlinear equations $f_i(x,u)$ can be expressed in terms of Taylor's series expansion while the second and higher order parts of the partial derivatives of f are neglected as shown in (4.5):

$$\begin{aligned} \dot{x}_i &= \dot{x}_{i0} + \Delta\dot{x}_i = f_i[(x_0 + \Delta x), (u_0 + \Delta u)] \\ &= \dot{x}_{i0} + \frac{\partial f_i}{\partial x_1}\Delta x_1 + \cdots \frac{\partial f_i}{\partial x_n}\Delta x_n \\ &\quad + \frac{\partial f_i}{\partial u_1}\Delta u_1 + \cdots \frac{\partial f_i}{\partial u_r}\Delta u_r \end{aligned} \tag{4.5}$$

where x_0 is the equilibrium points where all derivatives of state variables are equal to zero simultaneously. Hence, $\dot{x}_{i0}$ is equal to zero, the change of state variables can be further expressed as (4.6), same as the output expression (4.7):

$$\Delta\dot{x}_i = \frac{\partial f_i}{\partial x_1}\Delta x_1 + \cdots \frac{\partial f_i}{\partial x_n}\Delta x_n + \frac{\partial f_i}{\partial u_1}\Delta u_1 + \cdots \frac{\partial f_i}{\partial u_r}\Delta u_r \tag{4.6}$$

$$\Delta y_i = \frac{\partial g_i}{\partial x_1}\Delta x_1 + \cdots \frac{\partial g_i}{\partial x_n}\Delta x_n + \frac{\partial g_i}{\partial u_1}\Delta u_1 + \cdots \frac{\partial g_i}{\partial u_r}\Delta u_r \tag{4.7}$$

Applying equation (4.6-4.7) for all state variables in the vector *x* and *y*, the dynamic power system linearized equations can be determined as (4.8):

$$\begin{aligned} \Delta\dot{x} &= \mathbf{A}\Delta x + \mathbf{B}\Delta u \\ \Delta y &= \mathbf{C}\Delta x + \mathbf{D}\Delta u \end{aligned} \tag{4.8}$$

$$\mathbf{A} = \begin{bmatrix} \frac{\partial f_1}{\partial x_1} & \cdots & \frac{\partial f_1}{\partial x_n} \\ \vdots & \ddots & \vdots \\ \frac{\partial f_n}{\partial x_1} & \cdots & \frac{\partial f_n}{\partial x_n} \end{bmatrix} \mathbf{B} = \begin{bmatrix} \frac{\partial f_1}{\partial u_1} & \cdots & \frac{\partial f_1}{\partial u_r} \\ \vdots & \ddots & \vdots \\ \frac{\partial f_n}{\partial u_1} & \cdots & \frac{\partial f_n}{\partial u_r} \end{bmatrix}$$
$$\mathbf{C} = \begin{bmatrix} \frac{\partial g_1}{\partial x_1} & \cdots & \frac{\partial g_1}{\partial x_n} \\ \vdots & \ddots & \vdots \\ \frac{\partial g_m}{\partial x_1} & \cdots & \frac{\partial g_m}{\partial x_n} \end{bmatrix} \mathbf{D} = \begin{bmatrix} \frac{\partial g_1}{\partial u_1} & \cdots & \frac{\partial g_1}{\partial u_r} \\ \vdots & \ddots & \vdots \\ \frac{\partial g_m}{\partial u_1} & \cdots & \frac{\partial g_m}{\partial u_r} \end{bmatrix} \quad (4.9)$$

The matrix **A**, **B**, **C** and **D** contain all the derivatives of the functions in f and g which relate to the state variables x, input variables u and output variables y. Equations (4.8) can be further transferred into the frequency domain by Laplace transforms:

$$\begin{aligned} s\Delta x(s) - \Delta x(0) &= \mathbf{A}\Delta x(s) + \mathbf{B}\Delta u(s) \\ \Delta y(s) &= \mathbf{C}\Delta x(s) + \mathbf{D}\Delta u(s) \end{aligned} \quad (4.10)$$

Hence, the stability of the system can be observed from the matrix **A**. However the matrix **A** is a combination of the rate of change of each state variable where the cross-coupling exists between them. In order to eliminate the cross-coupling and analyse the system stability in a more effective way, several quantities has been developed referred to eigenvalues, eigenvectors and participation factor.

4.3.2 Characteristics of eigenvalues, eigenvectors and participation factor

The eigenvalues and eigenvectors are calculated by solving the followed equations:

$$(\mathbf{A} - \lambda I) = 0 \implies \det(\mathbf{A} - \lambda I) = 0 \quad (4.11)$$

$$\mathbf{A}\Phi_i = \Phi_i\lambda_i\,,\ \psi_i\mathbf{A} = \lambda_i\,\psi_i \quad (4.12)$$

The vector Φ_i is a *n*-column vector which is referred to as the right eigenvector and vector ψ_i is a *n*-row vector which is referred to as the left eigenvector. The right eigenvectors identifies the activity of state variables x_k in the ith mode and the left eigenvectors weights the contribution of this activity of state variables x_k to the ith mode. However, the elements of eigenvectors are dependent on the units and scaled by the state variables. Normally, the participation factor P is utilized to identify the relationship between the state variables x_k and modes i th. P is calculated by

multiplying the elements of the left and right eigenvectors which makes it dimensionless.

Once the linearized equations are transferred into time domain equations, the final relation between the change of state variables x_i and eigenvalues can be expressed as:

$$\Delta x_i(t) = \Phi_{i1}\psi_1\Delta x(0)e^{\lambda_1 t} + \cdots \Phi_{in}\psi_n\Delta x(0)e^{\lambda_n t} \tag{4.13}$$

According to equation (4.13), the stability of the system can be determined by its eigenvalues with the characteristics as follows:

1. If the eigenvalue is real, it represents to a non-oscillatory mode. The components $e^{\lambda_i t}$ correspond to the conclusion: a negative real eigenvalue results a decaying performance while a positive real value represents an instable mode of the system.
2. If the eigenvalue is complex for example: $\lambda = \sigma \pm j\omega$. The real part of the eigenvalue gives the same characteristics as rule 1. The imaginary part of the eigenvalues gives the frequency of oscillation $f = \omega/2\pi$(Hz). The damping ratio $\zeta = -\sigma/\sqrt{\sigma^2 + \omega^2}$ is used to identify the amount of decay of the amplitude of the oscillation in $t = 1/|\sigma|$ seconds.

An example of how to calculate the state-space equations of the synchronous generator is demonstrated as follow:

The simplest first-order synchronous generator is assumed by neglecting the effects of all resistances. The dynamic performance of this model is only related to its swing equation. The linearized equation can be calculated as:

$$\begin{aligned} \frac{d\Delta\omega_r}{dt} &= \frac{1}{2H}(\Delta T_m - \Delta T_e - K_D\Delta\omega_r) \\ \frac{d\Delta\delta}{dt} &= \omega_0\Delta\omega_r \end{aligned} \tag{4.14}$$

In per unit, the air-gap torque is equal to the air-gap power. Therefore $T_e = \frac{E'V_B}{X_T}\sin\delta$. The state-matrix form of the first-order synchronous generators is:

$$\begin{bmatrix} \dot{\Delta\omega_r} \\ \dot{\Delta\delta} \end{bmatrix} = \begin{bmatrix} -\frac{K_D}{2H} & -\frac{K_S}{2H} \\ \omega_0 & 0 \end{bmatrix}\begin{bmatrix} \Delta\omega_r \\ \Delta\delta \end{bmatrix} + \begin{bmatrix} \frac{1}{2H} \\ 0 \end{bmatrix}\Delta T_m \tag{4.15}$$

where the derivative of T_e is equal to $K_s = \frac{E'V_B}{X_T}\cos\delta_0$; E' is the voltage behind X'_d ; V_B is the bus voltage; X_T is the equivalent reactance between machine and bus. Therefore, the state-matrix form can be obtained:

Rearranging the equation and transfer it into Laplace *s*-domain, the system eigenvalue can be calculated from (4.16):

$$s^2 + \frac{K_D}{2H}s + \frac{K_s\omega_0}{2H} = 0 \implies s^2 + 2\zeta\omega_n s + \omega_n^2 = 0 \qquad (4.16)$$

The system oscillation frequency $\omega_n = \sqrt{K_s\frac{\omega_0}{2H}}$ and the damping ratio $\xi = \frac{1}{2}\frac{K_D}{\sqrt{K_s 2H\omega_0}}$ can be obtained which indicate that the increase of K_s may increase the frequency of oscillation and decrease the damping ratio; the increase of K_D increases the damping ability of the system.

The synchronous generator (GENROU) used in this research is the sixth-order generator. The small signal analysis of this type of modelling approach was mentioned in [5, 12-13] which indicated that it could provide a good dynamic representation of synchronous generator in dynamic studies.

4.4 Frequency Response Analysis

The frequency response methods have several advantages over the eigenvalue analysis [6, 14-17]: they are not restricted to analysis the system within its natural oscillatory frequency; the methods are able to investigate coupling effect between controllers at nonoscillatory modes; they have the abilities in identifying the parameters of control devices for enhancing the system stability and security. Therefore, the frequency response methods are always used for the purpose of providing wider frequencies of interest in power system stability analysis

The frequency response methods use the transfer functions to describe the specific input/output relations. The transfer functions of the system can be derived from (4.10):

$$G(s) = \frac{\Delta y(s)}{\Delta u(s)} = \mathbf{C}(sI - \mathbf{A})^{-1}\mathbf{B} + \mathbf{D} \qquad (4.17)$$

where **A**, **B**, **C** and **D** are the matrix in state space linear equation; **D** is usually zero for most physical systems. The frequency response is achieved by replacing the Laplace variable 's' into frequency variable '$j\omega$' within the frequency ranges of interest [16].

4.4.1 Bode-Nyquiest plot frequency control

The classical frequency response methods related to the Bode-Nyquist analysis have achieved great success in industrial engineering [6, 16, 18]. The dynamic characteristics of the system can be directly read from the graphical plots between the selected inputs and outputs.

Nyquist plot method: Usually the system transfer function (4.17) is rearranged and expressed as the relations between its zeros and poles:

$$G(s) = \frac{\Delta y(s)}{\Delta u(s)} = \frac{b_m(s-z_1)(s-z_2)\cdots(s-z_m)}{a_n(s-p_1)(s-p_2)\cdots(s-p_n)} \tag{4.18}$$

The quantities $z_1, z_2 \cdots z_m$ are referred to as zeros of the transfer function while $p_1, p_2 \cdots p_n$ are defined as the poles of the transfer function. The poles and zeros are usually plotted in the *s*-plane. The poles of transfer function are equal to the eigenvalues of the matrix **A**. The zeros and poles are two important quantities in identifying the system dynamic stability problems.

The difficulty in plotting a complex function $G(s)$ with a complex variable s on a single set of coordinates is overcome by the mapping process in Nyquist plot analysis [19]. For example, if $G(s) = s + 1$, the point $s_0 = 1 + j2$ is mapped into the point $G(s_0) = 1 + j2 + 1 = 2 + j2$ on the $G(s)$-plane.

The frequency domain Nyquist plot is achieved by substituting $j\omega$ for *s*. The resulting $G(j\omega)$ is a complex function of the variable ω. Therefore, the transfer function $G(j\omega)$ can be plotted in two dimensions with ω as a parameter and expressed as:

$$\begin{gathered} G(j\omega) = |G(j\omega)| \cos\phi(\omega) + j|G(jw)| \sin\phi(\omega) \\ G(j\omega) = R(\omega) + jI(\omega) \end{gathered} \tag{4.19}$$

Nyquist stability criterion: Assumed the two blocks feedback control system as Figure 4.1:

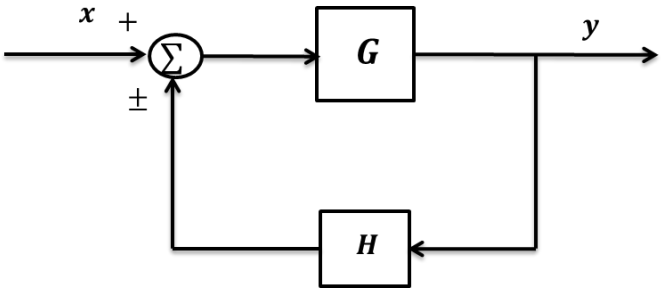

Figure 4-1. Feedback control system [19]

Defines $G(s)H(s)$ as the open-loop transfer function and $F(s) = 1 + G(s)H(s)$ as the denominator of the closed-loop system transfer function. The zeros of $F(s)$ are the closed-loop poles (eigenvalue) of the system. According to the characteristics of eigenvalue of the matrix **A**, the system is stable only if there is no zero of $F(s)$ in the right-half-*s*-plane (RHP).

If each point in the *s*-plane is mapped into the point in the $F(s)$-plane, the stability assessment of the Nyquist analysis can be determined with several definitions as followed [19]:

- All points to the right of a contour which is traversed in a prescribed direction are defined as enclosed by it.
- The clockwise direction is defined as the positive direction.
- A positive encirclements of the origin in the $F(s)$-plane is defined as if the line drawn from the origin to a point on the curve rotates 360^0 in a clockwise direction. Counterclockwise direction corresponds to a negative encirclement.
- The total number of clockwise encirclements N in $F(s)$-plane equals to the number of zeros Z minus the number of poles P of $F(s)$ enclosed by the *s*-plane contour.
- The characteristics of the system can be further simplified by the way of investigating the contour in $G(s)H(s)$-plane by shift the origin of coordinates to the point (-1, 0).

Therefore, it is simple and straightforward to analyse the stability of the system from the Nyquist plot by checking the number of counterclockwise encirclements of the point (-1, 0) in the $G(s)H(s)$-plane. The closed-loop system is stable only if

equation (4.20) is met: the number of counterclockwise encirclements of (-1, 0) point in the $G(s)H(s)$-plane is equal to the number of poles of $G(s)H(s)$ in the RHP.

$$-N = P \geq 0 \tag{4.20}$$

The relative frequency stability is measured in the way of "Gain Margin (GM)" and "Phase Margin (PM)" [20] as shown in Figure 4.2: The GM and PM in Nyquist analysis are defined as:

- **Gain Margin**: The value $k_g = |G(j\omega)H(j\omega)|$ at the phase crossover frequency. (Phase crossover frequency is the frequency with respect to $arc(G(j\omega_{PM})H(j\omega_{PM}))= -180^{\circ}$)
- **Phase Margin**: The angle of degree $\gamma_{PM} = 180^{\circ} + arc(G(j\omega_c)H(j\omega_c))$ at the gain crossover frequency. (Gain crossover frequency $\omega_c$is the frequency which $|G(j\omega_c)H(j\omega_c)| = 1$)

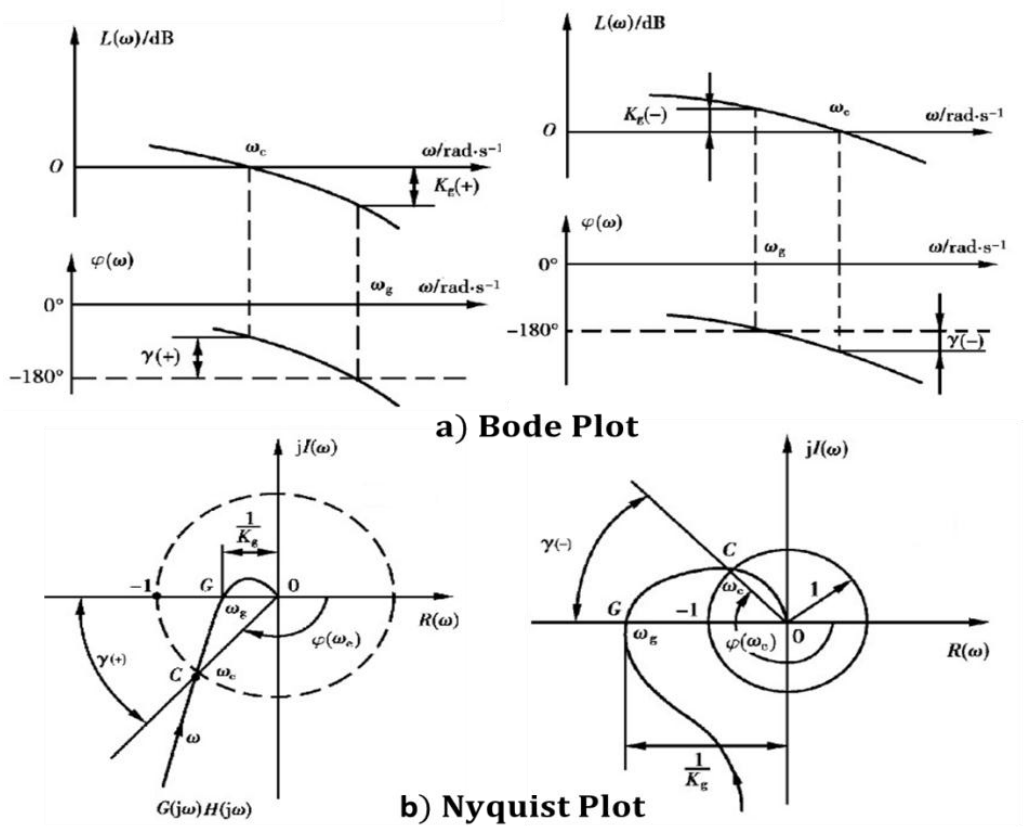

Figure 4-2. Gain Margin and Phase Margin [20]

Based on the Nyquist criterion, the system is stable if the GM k_g is less than 1 and PM $\gamma_{PM} > 0$ to ensure no encirclement at (-1, 0) exists.

Bode plot method: the method plots the complex function $G(s)$ of the real and imaginary parts as a function of frequency in two 2-D graphs: the magnitude of $G(j\omega)$ and the phase angle of $G(j\omega)$. Equation (4.19) can be expressed in terms of polar equation:

$$G(j\omega) = |G(j\omega)|e^{j\phi(\omega)} \tag{4.21}$$

The logarithmic scales are used in Bode plots because they can simplify the calculation of the magnitude and phase angle. For the purpose of reflecting more information with a wider range of frequencies, the logarithmic scale: $\log_{10}\omega$ is introduced to the ω-axes. The magnitude of the open-loop transfer function $G(j\omega)H(j\omega)$ is equal to the sum of decibel (*db*) magnitude of a number of individual terms where *db* is defined as (4.22):

$$db = 20\log_{10}|G(j\omega)| \tag{4.22}$$

The typical Bode plots of continuous-time frequency response functions and their asymptotic approximations are introduced in [19-20]. The major advantage of the Bode method is that the processes of designing a feedback control system are relatively simple by shaping the asymptotic Bode plots based on the control requirements with several common compensations. For example: gain compensation, lead compensation and lag compensation, etc.

The **Bode stability criterion** is defined through its relative stability indicators GM and PM:

- **Gain Margin**: Number of decibels that $k_g(db) = |20\log_{10} 1/|G(j\omega_{PM})H(j\omega_{PM})||$ is below 0*db* at the phase crossover frequency.
- **Phase Margin**: Number of degree $\gamma = arc(G(j\omega_c)H(j\omega_c))$ is above than -180° at the gain crossover frequency.

The corresponding criterion applied in Bode method is: the GM $k_g(db)$ must below the 0*db* (where$|G(j\omega)H(j\omega)| = 1$) and PM $\gamma_{PM} < -180^{\circ}$.

4.4.2 Individual Channel Analysis and Design (ICAD)

In power system control, it is not difficult to design a single loop controller by using the well-established control design methods as mentioned above. However, the most of practical power networks are more complicated which contain more than one

input and output referred to as the multivariable systems. In [14, 21-23], the difficulties in designing the control system for a multivariable system were mentioned. The cross-coupling between control loops is one of the major obstacles in designing the feedback controllers. Hence, the challenge is to find out a way which can provide an appropriate framework for interpreting the multivariable systems in a more transparent way.

The Individual Channel Analysis and Design (ICAD) method was developed by W.E. Leithead and J. O'Reilly in 1990s. The hearts of the method is to decompose the multi-input and multi-output systems into several individual single-input and single-output channels. Hence, the classical deign Bode-Nyquist methods can be applied in each individual channel.

The application of ICAD in multivariable systems is introduced by using the simplest multivariable 2×2 problem as example:

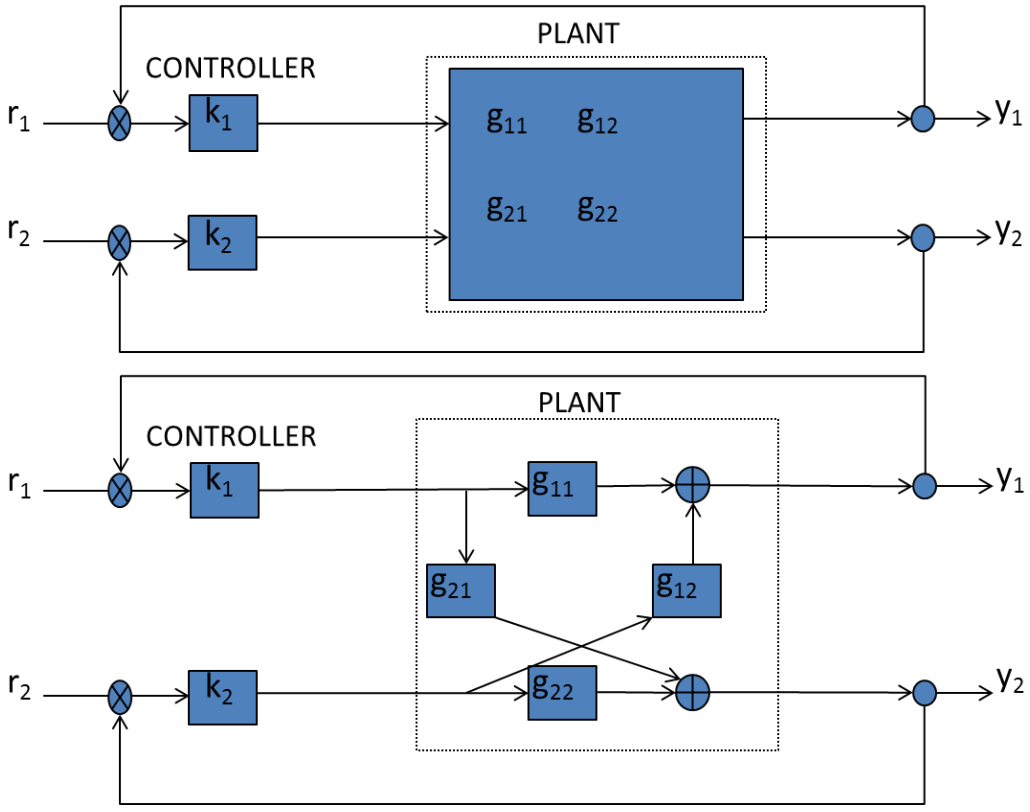

Figure 4-3. 2-input and 2-output control problem with diagonal feedback

$$G(s) = \begin{bmatrix} g_{11} & g_{12} \\ g_{21} & g_{22} \end{bmatrix} \quad K(s) = \begin{bmatrix} k_{11} & 0 \\ 0 & k_{22} \end{bmatrix} \tag{4.23}$$

where $G(s)$ is the system transfer function; g_{ij} are the elements of the $G(s)$; $K(s)$ is the controller matrix. It can be obtained out that the relation between input signal r_i and output signal y_1 is via two paths: one is directly through $g_{11}(s)$ and the other is through another input signal r_2 via the bottom loop $g_{12}(s)$. It is possible to redraw these blocks and transfer each pair of input and output as one channel as its forward pass between reference r_i and output y_i combined with an additive cross-reference disturbance signal d_i as obtained in Figure 4.4:

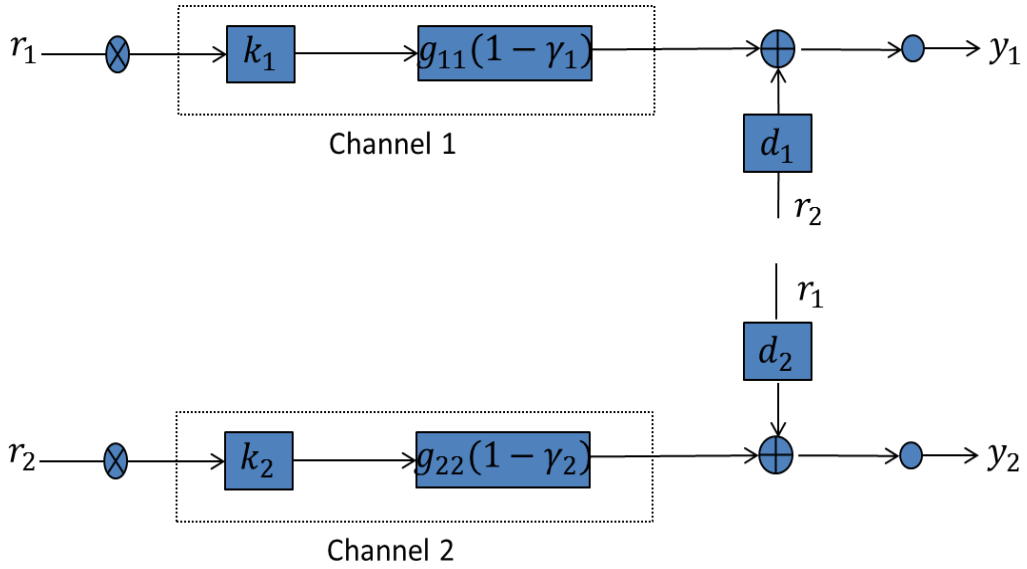

Figure 4-4. Individual channel 1 and channel 2

The forward transfer function in Figure 4.4 are:

$$C_1 = k_1 g_{11}(1-\gamma_1) = k_1 g_{11}(1 - g_{12}g_{22}^{-1}H_2 g_{21}g_{11}^{-1}) \tag{4.24}$$

$$d_1 = g_{12}g_{22}^{-1}H_2 \quad H_2 = \frac{k_2 g_{22}}{1+k_2 g_{22}} \tag{4.25}$$

$$C_2 = k_2 g_{22}(1-\gamma_2) = k_2 g_{22}(1 - g_{21}g_{11}^{-1}H_1 g_{12}g_{22}^{-1}) \tag{4.26}$$

$$d_2 = g_{21}g_{11}^{-1}H_1 \quad H_2 = \frac{k_1 g_{11}}{1+k_1 g_{11}} \tag{4.27}$$

It is important to mention that ICAD is not the single-loop design method. The disturbance loops d_i and the multivariable structure function $\gamma(s)$ preserve the loop interactions which were assumed small and neglected in earlier method.

However, the disturbance loops d_i of $C_i(s)$ is dependent on controller $k_j(s)$ of channel $C_j(s)$, where $i \neq j$. In order to over this obstacle, the following assumption is made:

The closed-loop bandwidth of channel C_1 is significantly smaller than the bandwidth of channel C_2.The bandwidth of a system is "the ranges of frequencies of how well the system responds to variations in the input signal" [19]. Usually the gain crossover frequency ω_c is a good approximation of the bandwidth for a closed-loop system. The Bode magnitude plot of channel 1 and channel 2 are drawn in Figure 4.5. Since the controller gain of K_2 is relatively high, the bandwidth ω_{h2} of the sub control system H_2 will always larger than the bandwidth ω_1 of channel 1. Hence, the uncertainty in H_2 is maintained in C_1 over the frequency range $(0, \omega_1)$. For any frequency higher than ω_1, the influence from H_2 is unimportant in channel 1 due to the rapid roll-off the gain in channel 1.

In the processes of feedback design, the controller K_1 is normally designed at first with the gain of K_2 relatively high. Then the controller K_2 is designed on the basis of designed K_1 for a 2×2 system. These procedures can be easily extended into $m \times m$ systems as demonstrated in [21, 24].

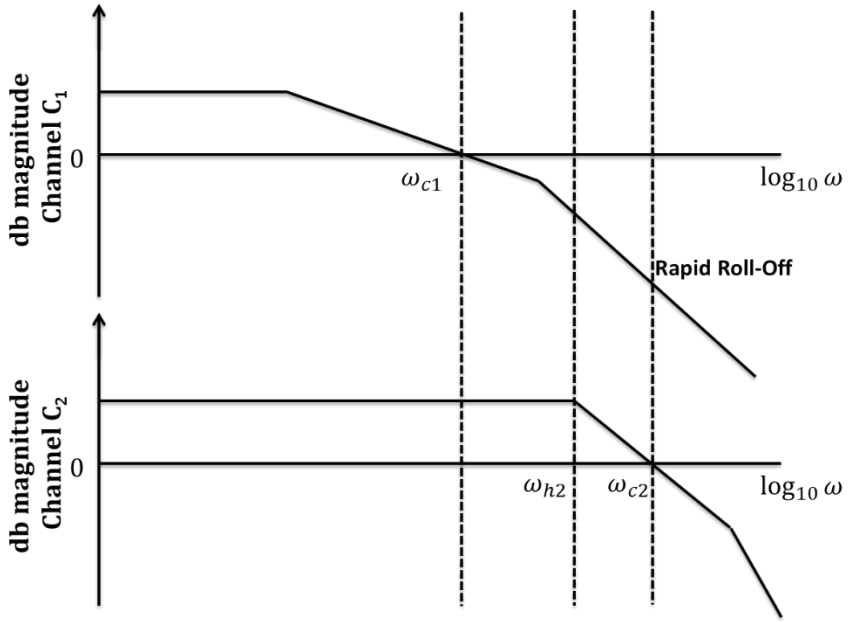

Figure 4-5. Bode magnitude plot for open-loop channel 1 and channel 2 [21]

4.5 Automatic Voltage Regulator (AVR) Design

AVR and PSS are the two major control devices used in the power system industries. Lots of works have been focused on finding the effective ways to apply AVR and PSS in power system stability issues.

Under heavy/light load conditions, the synchronous generator may need to inject/absorb the reactive power into the network due to the reactive power changed in the loads and transmission networks. This task is usually accomplished by the AVR. The function of AVR is to provide voltage regulation to maintain the terminal voltage of the synchronous generator to its reference value by a control loop: where its input and output are defined as the terminal voltage reference V_{ref} and terminal voltage output ΔE_T.

4.5.1 System performance with no AVR attached

The equivalent UK dynamic system was assessed by using the small signal analysis. The eigenvalues of the state matrix were calculated with a small perturbation (0.01). The modes which had the dominant influence on system damping and stability performances were investigated.

The eigenvalues of system with no AVR and PSS attached to the generators were presented in Table 4.3. It could be obtained that most of the eigenvalues had negative real parts which indicating a stable mode except one unstable eigenvalue λ_{29} . In addition, there were two lightly damped modes $\lambda_{25,26}$ $\lambda_{27,28}$ which had poor damping ratio below 0.1.

Table 4.3. Eigenvalue of equivalent system with no AVR

	Eigenvalue	Damping Ratio	Oscillation Frequency (rad/s)
$\lambda_{1,2}$	$-8.561e^{-1} \pm 9.612i$	$1.043e^{-1}$	9.650
$\lambda_{3,4}$	$-1.036 \pm 9.412i$	$1.095e^{-1}$	9.469
$\lambda_{5,6}$	$-1.695 \pm 9.333i$	$1.787e^{-1}$	9.485
$\lambda_{7,8}$	$-1.519 \pm 9.327i$	$1.607e^{-1}$	9.450
$\lambda_{9,10}$	$-1.470 \pm 8.912i$	$1.628e^{-1}$	9.033
$\lambda_{11,12}$	$-1.490 \pm 8.778i$	$1.674e^{-1}$	8.904

$\lambda_{13,14}$	$-1.441 \pm 8.504i$	$1.670e^{-1}$	8.625
$\lambda_{15,16}$	$-1.342 \pm 8.518i$	$1.556e^{-1}$	8.624
$\lambda_{17,18}$	$-1.204 \pm 8.472i$	$1.407e^{-1}$	8.557
$\lambda_{19,20}$	$-1.171 \pm 8.156i$	$1.421e^{-1}$	8.240
$\lambda_{21,22}$	$-1.224e^{-1} \pm 8.106i$	$1.493e^{-1}$	8.198
$\lambda_{23,24}$	$-7.187e^{-1} \pm 7.051i$	$1.014e^{-1}$	7.088
$\lambda_{25,26}$	$-5.048e^{-1} \pm 6.186i$	$8.135e^{-2}$	6.206
$\lambda_{27,28}$	$-2.662e^{-1} \pm 4.212i$	$6.308e^{-2}$	4.221
λ_{29}	$3.204e^{-1}$	$-1e^{0}$	$3.204e^{-1}$

4.5.2 Influences of AVR on oscillation stability

In order to enhance the system transient stability, the automatic voltage regulators (AVR) were attached to all generators. Usually, high-gain fast response AVR [14] is selected to assist the power system in maintaining synchronism during disturbances. The excitation system channel was defined as the transmission between terminal voltage reference V_f and terminal field voltage ΔE_{FD}. The SEXS model in PSS/E [3] was used to represent the AVR. The transfer function of AVR was:

$$AVR(s) = \frac{30}{1+0.05s} \tag{4.28}$$

The eigenvalues plot of the system with/without AVR attached was demonstrated in Figure 4.6. The eigenvalues of the system with all generators equipped with AVR were listed in Table 4.4. It could be identified that with the activity of AVR, the unstable real mode moved to the left-hand-plan. However, the high-gain AVR may have a detrimental effect on the oscillation stability of the system [14, 17, 25]. An analysis of possible interarea modes with AVRs attached to all generators presented in Table 4.4 revealed the presence of an unstable interarea mode at frequency 4.392rad/s as well as two lightly damped interarea modes.

Table 4.4. Eigenvalue of equivalent system with AVR

	Eigenvalue	Damping Ratio	Oscillation Frequency (rad/s)
$\lambda_{1,2}$	$-8.316e^{-1} \pm 9.592i$	$1.038e^{-1}$	9.628
$\lambda_{3,4}$	$-1.015 \pm 9.391i$	$1.074e^{-1}$	9.446
$\lambda_{5,6}$	$-1.675 \pm 9.331i$	$1.767e^{-1}$	9.480
$\lambda_{7,8}$	$-1.536 \pm 9.301i$	$1.624e^{-1}$	9.457
$\lambda_{9,10}$	$-1.461 \pm 8.910i$	$1.618e^{-1}$	9.029
$\lambda_{11,12}$	$-1.513 \pm 8.796i$	$1.695e^{-1}$	8.925
$\lambda_{13,14}$	$-1.486 \pm 8.538i$	$1.712e^{-1}$	8.666
$\lambda_{15,16}$	$-1.163 \pm 8.162i$	$1.410e^{-1}$	8.244
$\lambda_{17,18}$	$-1.197 \pm 8.118i$	$1.459e^{-1}$	8.206
$\lambda_{19,20}$	$-1.320 \pm 8.515i$	$1.532e^{-1}$	8.616
$\lambda_{21,22}$	$-1.234 \pm 8.483i$	$1.440e^{-1}$	8.573
$\lambda_{23,24}$	$-6.831e^{-1} \pm 7.248i$	$1.202e^{-1}$	7.280
$\lambda_{25,26}$	$-6.191e^{-1} \pm 7.058i$	$8.738e^{-2}$	7.085
$\lambda_{27,28}$	$-4.296e^{-1} \pm 6.200i$	$6.913e^{-2}$	6.214
$\lambda_{29,30}$	$+7.109e^{-2} \pm 4.391i$	$-1.619e^{-2}$	4.392

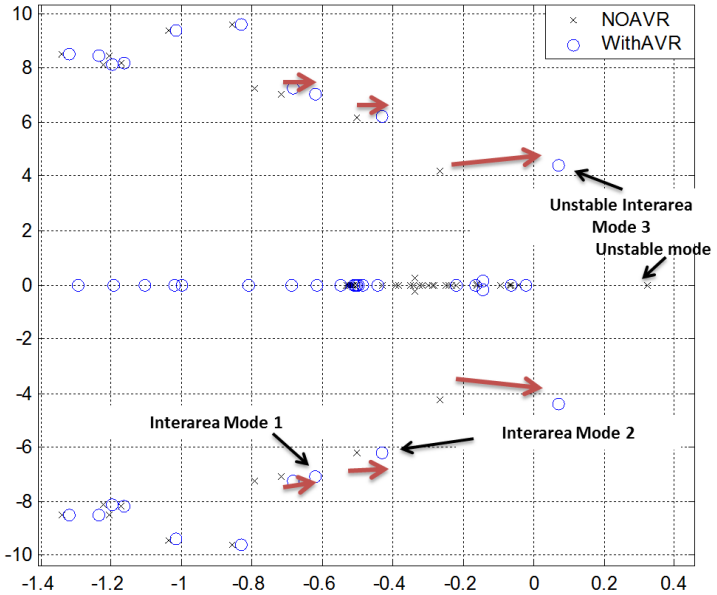

Figure 4-6. Equivalent system eigenvalue-plot: with & without AVR

Indeed, it was pointed out in the UK Ten Year Statement [26] that "several power system stabilisers (PSS) should be installed between generators in England and Wales and Scotland for the purpose of oscillation stabilization." Hence, further eigenvalue-eigenvector analysis of these interarea modes with their corresponding participation factors indicated that there were three major oscillation modes in UK system as shown

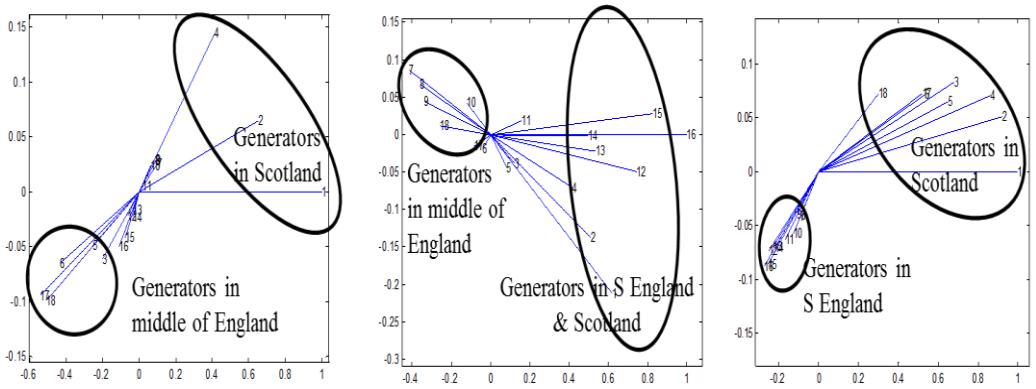

a) Mode 1 b) Mode 2 c) Mode 3

Figure 4-7. Oscillation modes between Scotland and England & Wales

- Mode 1, the generators in Scotland swinging against generators in the middle of the England;
- Mode 2, the generators in Scotland & South of the England swing against those generators in the middle of England;
- Mode 3 indicates oscillation between generators in Scotland and generators in the South of England.

These oscillation performances could be a good validation of dynamic performance of the equivalent of the system. Furthermore, the participation factors as shown in Table 4.5 indicated that generators $G_1, G_2, G_4, G_5, G_6, G_7, G_8, G_{12}, G_{17}, G_{18}$ (attached to corresponding nodes in Figure 3.9) have the dominant effects on the interarea modes. Therefore, any attempt to stablise the dynamic system or improve the damping performance of the interarea oscillatory modes by way of installation of PSS must be realised through these particular generators.

Table 4.5. Participation factor of machine state $\boldsymbol{\omega}$ related to interarea modes

State ω	G_1	G_2	G_3	G_4	G_5	G_6	G_7	G_8	G_9
Mode1	**1.000**	**0.574**	0.012	0.133	0.191	0.328	0.130	0.065	0.045
Mode 2	0.149	0.134	0.001	0.044	0.009	0.002	**0.770**	**0.354**	0.190
Mode 3	**0.751**	**0.957**	0.087	**0.399**	**1.000**	**0.448**	0.122	0.072	0.065
	G_{10}	G_{11}	G_{12}	G_{13}	G_{14}	G_{15}	G_{16}	G_{17}	G_{18}
Mode1	0.013	0.001	0.024	0.001	0.003	0.011	0.018	**0.594**	**0.659**
Mode 2	0.018	0.026	**1.000**	0.090	0.131	0.332	0.432	0.006	0.066
Mode 3	0.061	0.101	**0.365**	0.051	0.084	0.107	0.110	**0.484**	0.239

4.6 Power System Stabiliser (PSS) Design

According to the above results, the power system stabilizer should be attached for the purpose of stabilizing the oscillatory modes. The function of PSS is to add damping to the generator rotor oscillations through an auxiliary signal to the voltage input of AVR [4]. The auxiliary signal can be the generator power, frequency or generator speed. The typical control function of the PSS used in this thesis is based on equation 4.29 [27]:

$$PSS(s) = K_s \frac{T_W}{1+T_W s} \frac{1+T_1 s}{1+T_2 s} \frac{1+T_3 s}{1+T_4 s} \tag{4.29}$$

It contains one washout filter with its time constant T_W in order to make the transition caused by the changes in input more smooth; two lead-lag compensators to introduce phase advance or phase lag to stable the RHP poles based on the stability requirements.

4.6.1 Choose locations for PSS

Since the reduced UK dynamic network has more than twenty buses with totally eighteen generators throughout the country. It is impossible to attach the PSSs to each generator bus. The particular locations where the PSSs should be installed must be considered at first. The eigenvectors with their participation factors indicated that the generator $G_1, G_2, G_4, G_5, G_6, G_7, G_8, G_{12}, G_{17}, G_{18}$ might be the good locations to be equipped with stabilizers.

The open-loop PSS channel was defined as the response between AVR input deviation and generator speed deviation $\Delta\omega_i$ .The Bode plot of open-loop PSS channels of all generators without PSS were demonstrated in Figure 4.8:

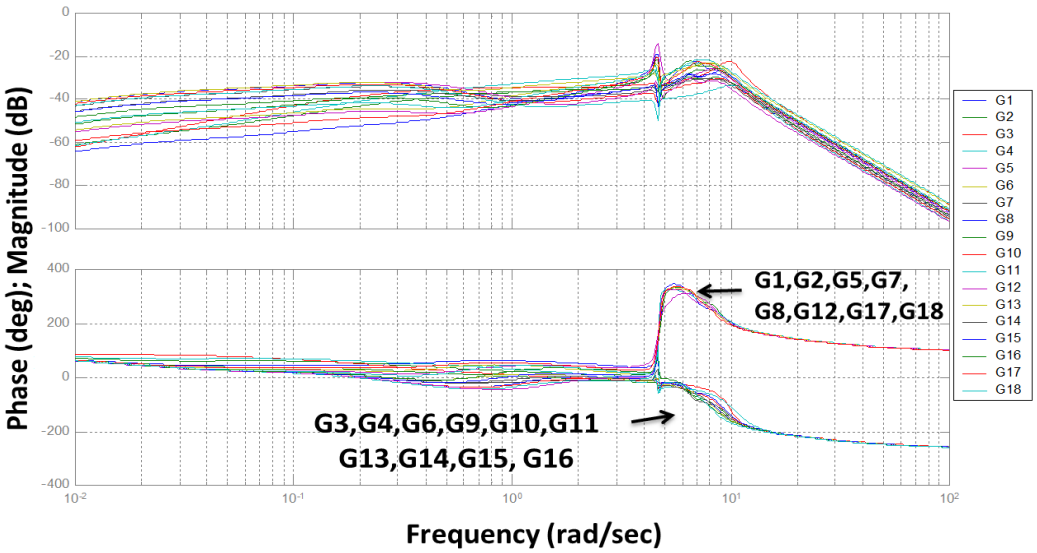

Figure 4-8. Open-loop channels (speed $\Delta\boldsymbol{\omega}$/voltage reference) without PSS

It could be seen that the channel $C_1, C_2, C_5, C_7, C_8, C_{12}, C_{17}, C_{18}$ correspond to the unstable oscillation modes (on the Bode plot characteristic in the PSS channel the magnitude peak is accompanied by a step-up in phase [15] at the frequency 4.392rad/s). Hence, it is possible to stable the unstable interarea mode by attaching PSSs to these generators [15, 25]. This Bode characteristic also helps minimise the number of PSSs needed, an important economical consideration.

Once the locations were determined, an 8-input and 8-output multivariable-system were created. The processes of designing PSS were based on ICAD method to overcome the coupling effect existed between controllers. The step-by-step multimachine Nyquist-Bode PSS design methodology of [25] was applied.

4.6.2 Equilvalent model behaviour with/without PSS

The STAB1 model in PSS/E [3] was used to represent the PSS. The model's control block is presented in Appendix j. The structure of designing the PSS_1 is shown in Figure 4.9 with the PSS_1 channel opened while all other channels closed:

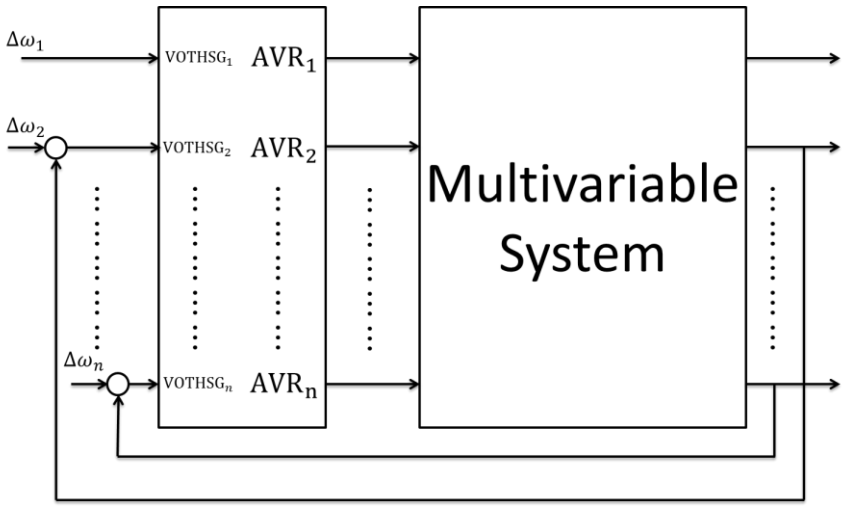

Figure 4-9. Open-loop channel of $\boldsymbol{PSS_1}$ with other PSS channels closed

The Bode characteristic of C_1 was shown in Table 4.6. The two significant magnitude peaks corresponded to two major interarea modes: the unstable oscillation mode at frequency 4.392(rad/s) and the lightly damped oscillation mode at frequency 7.085(rad/s). The stabilisation of the unstable interarea oscillation mode is achieved by raising the two significant magnitude gain peaks value above 0*db*. If the interarea mode is stable, the higher the gain peak value is above 0*db*, the better the system damping by PSS [14]. Hence, PSS_1 was designed for the purpose of raising the gain at 4.392(rad/s) and 7.085(rad/s) above 0*db*.

Table 4.6. Bode-Nyquist plot of open loop PSS channel 1

The transfer function of $PSS_1 = 0.95\ \frac{s}{s+1}\ \frac{15s+1}{s+1}\ \frac{0.3s+1}{0.1s+1}$
Bode Diagram of PSS_1
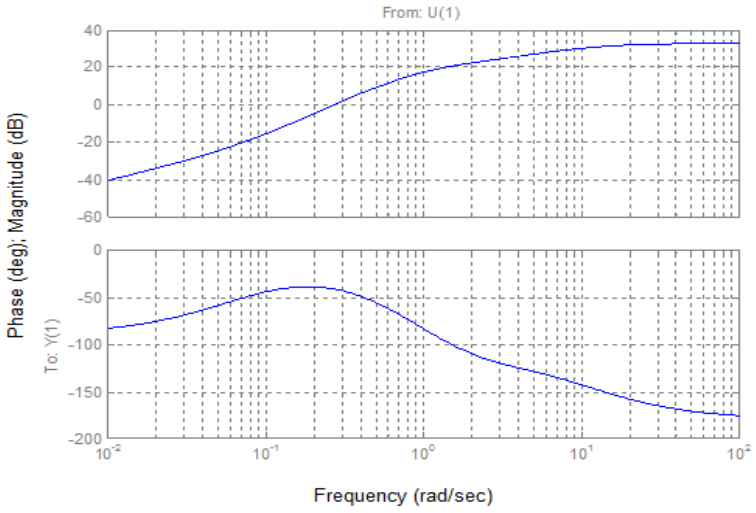

Bode Diagram of $C_1$with/without PSS

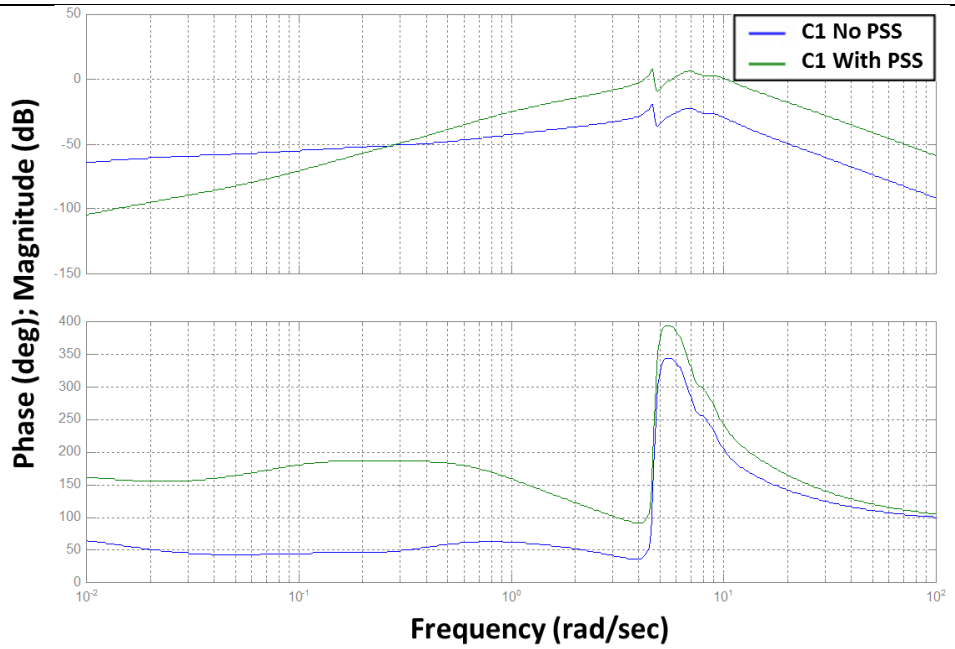

Nyquist Diagram of $C_1$with/without PSS

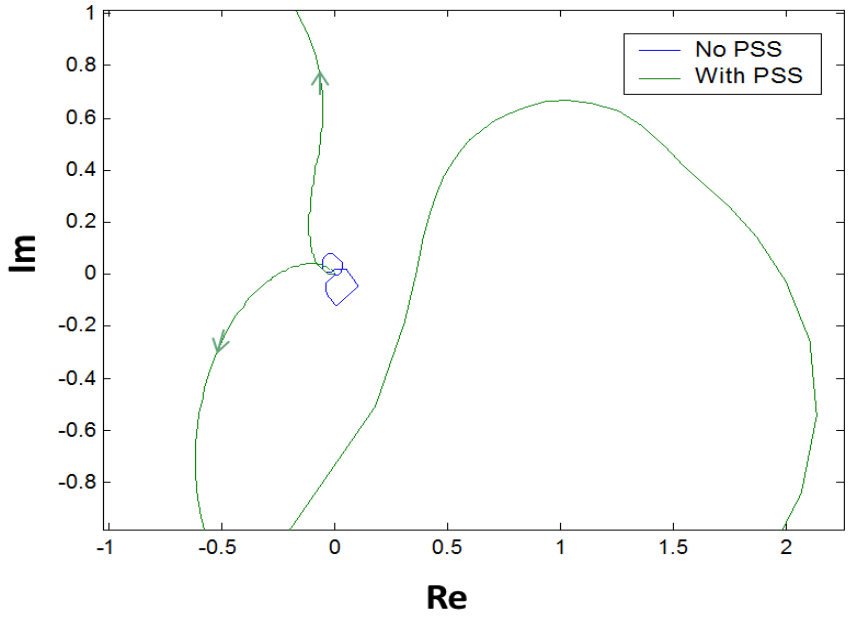

The transfer functions of other PSS channels were designed as shown in Table 4.7. The Bode-Nyquist plots of the open loop PSS channels with and without PSS were demonstrated in Table 4.8.

Table 4.7. Transfer functions of PSS channel 2-8

Channel 2	$P_2 = 1.65 \frac{s}{s+1} \frac{10s+1}{s+1} \frac{0.3s+1}{0.02s+1}$
Channel 3	$P_3 = 1.8 \frac{s}{s+1} \frac{10s+1}{0.8s+1} \frac{0.3s+1}{0.16s+1}$
Channel 4	$P_4 = 2.4 \frac{s}{s+1} \frac{10s+1}{0.6s+1} \frac{0.3s+1}{0.2s+1}$
Channel 5	$P_5 = 1.8 \frac{s}{s+1} \frac{10s+1}{s+1} \frac{0.3s+1}{0.2s+1}$
Channel 6	$P_6 = 1.6 \frac{s}{s+1} \frac{30s+1}{0.8s+1} \frac{0.3s+1}{0.1s+1}$
Channel 7	$P_7 = 2 \frac{s}{s+1} \frac{10s+1}{0.5s+1} \frac{0.3s+1}{0.2s+1}$
Channel 8	$P_8 = 2 \frac{s}{s+1} \frac{10s+1}{0.7s+1} \frac{0.3s+1}{0.15s+1}$

Table 4.8. Frequency Characteristics of system with/without PSS

	Bode Diagram of PSS_i
*C*2	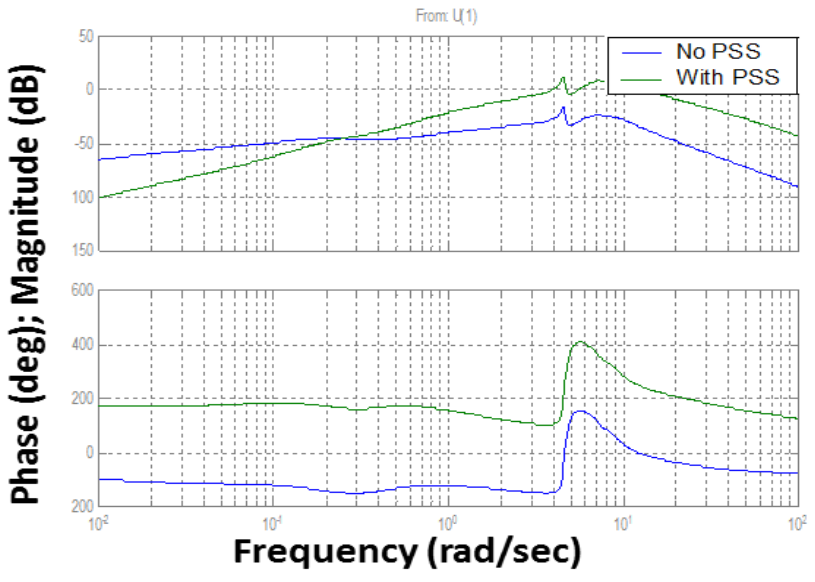

*C*3	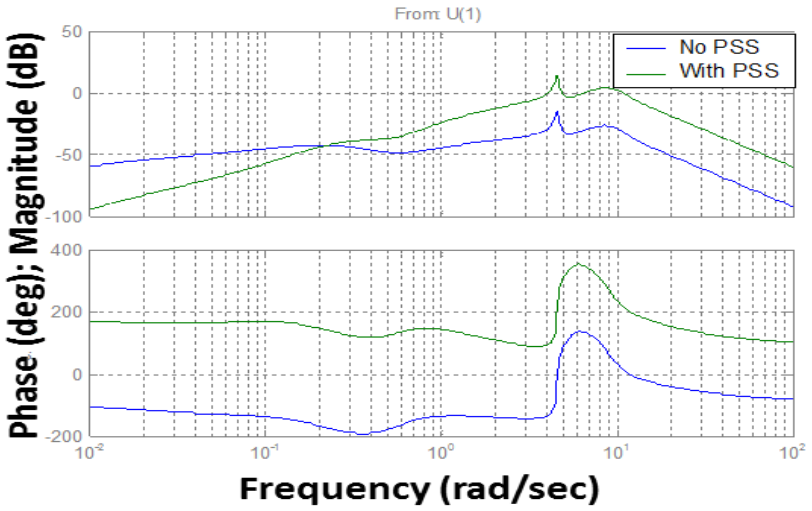 From: U(1) No PSS With PSS Phase (deg); Magnitude (dB) Frequency (rad/sec)
*C*4	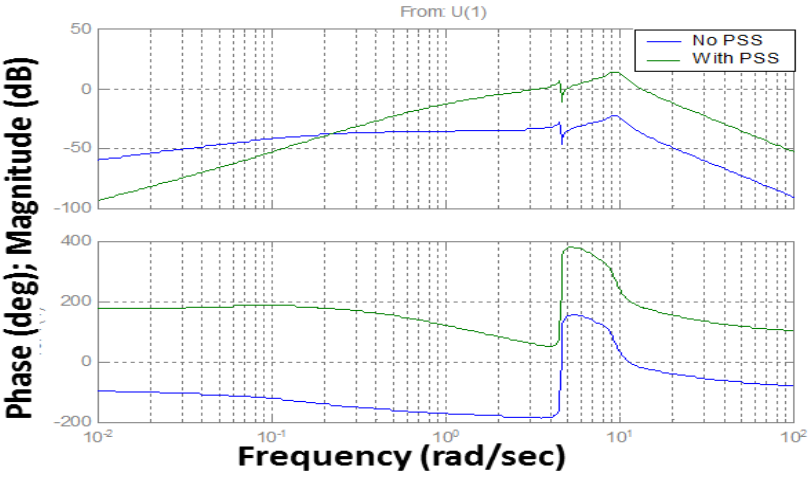 From: U(1) No PSS With PSS Phase (deg); Magnitude (dB) Frequency (rad/sec)
*C*5	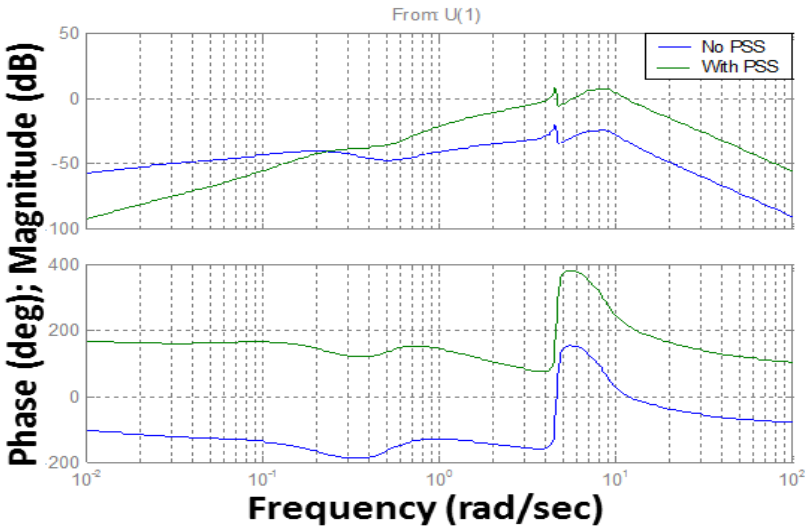 From: U(1) No PSS With PSS Phase (deg); Magnitude (dB) Frequency (rad/sec)

*C*6	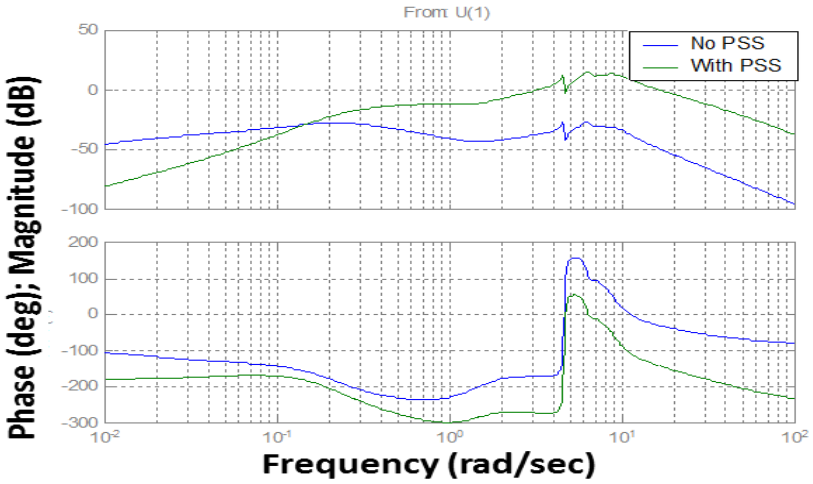 From: U(1) No PSS With PSS Phase (deg); Magnitude (dB) Frequency (rad/sec)
*C*7	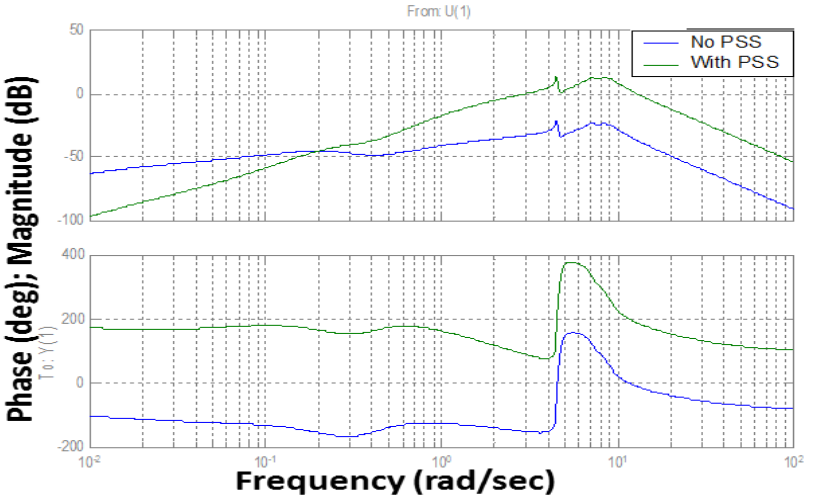 From: U(1) No PSS With PSS Phase (deg); Magnitude (dB) To: Y(1) Frequency (rad/sec)
*C*8	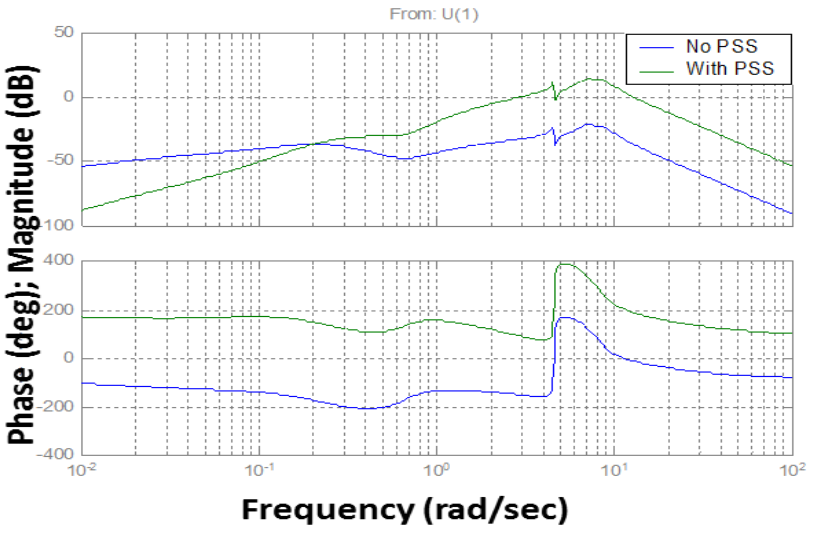 From: U(1) No PSS With PSS Phase (deg); Magnitude (dB) Frequency (rad/sec)

	Nyquist Diagram of PSS_i
*C*2	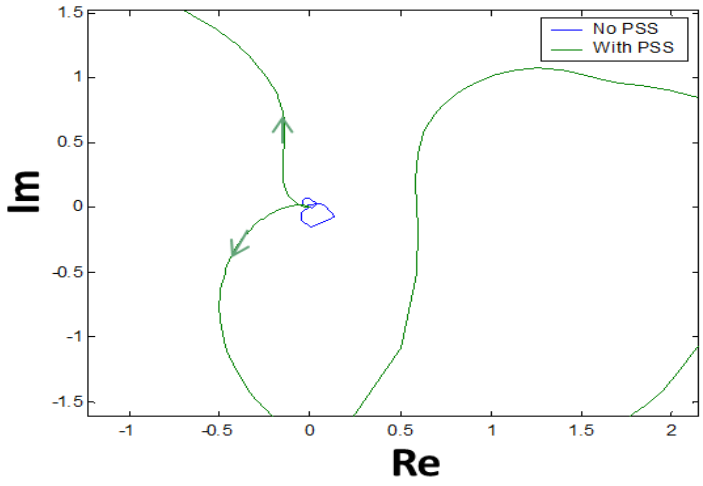
*C*3	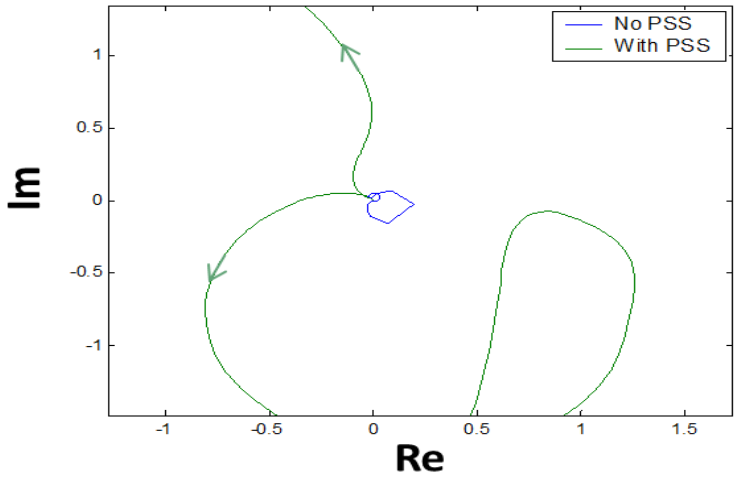
*C*4	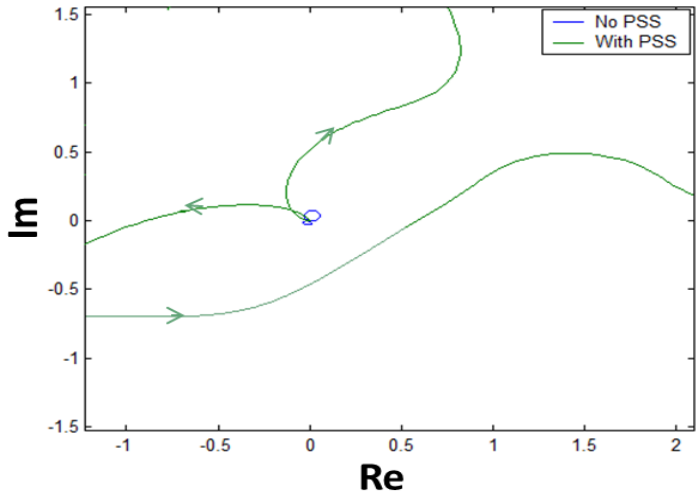

*C*5	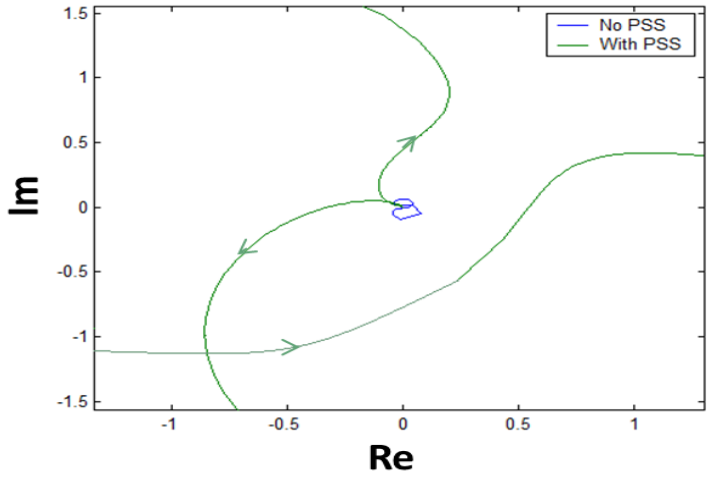 No PSS With PSS Im Re 1.5 1 0.5 0 -0.5 -1 -1.5 -1 -0.5 0 0.5 1
*C*6	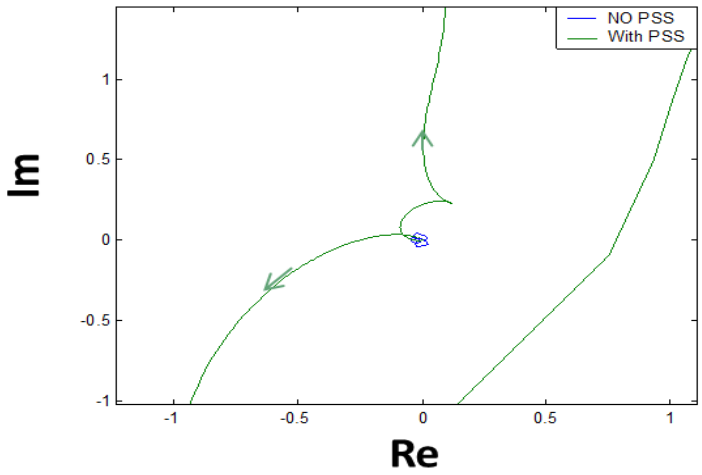 NO PSS With PSS Im Re 1 0.5 0 -0.5 -1 -1 -0.5 0 0.5 1
*C*7	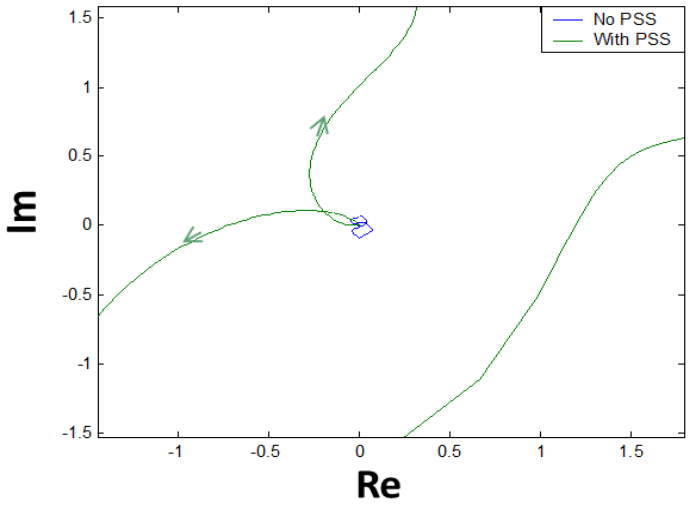 No PSS With PSS Im Re 1.5 1 0.5 0 -0.5 -1 -1.5 -1 -0.5 0 0.5 1 1.5

*C*8	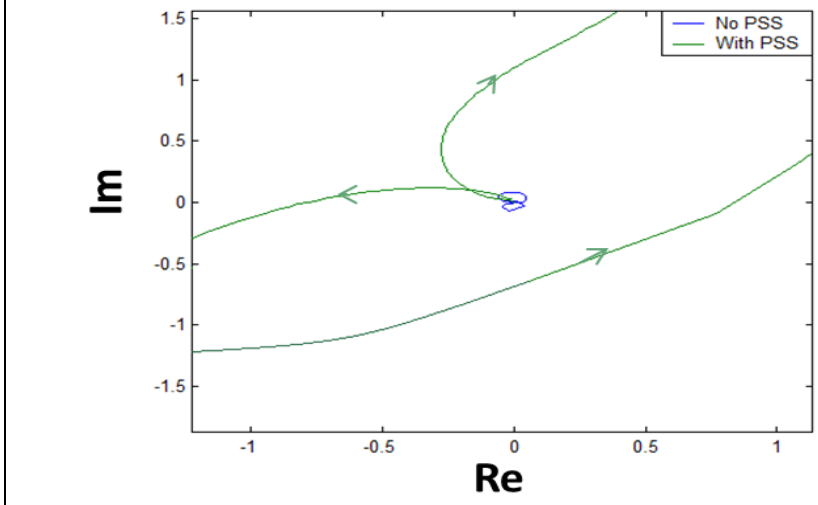

When all eight PSSs were attached to the relevant generators, the unstable interarea oscillation mode (magnitude peak accompanied by a step-up in phase) at frequency 4.392 rad/s was stabilised with damping ratio increased from -0.0162 to 0.156. Also, the stable interarea oscillation modes at frequency 7.085 rad/s were further damped with damping ratio increasing from 0.0874 to 0.1537.

4.6.3 System transient performance with PSS attached

One final confirmation of the stability robustness with the assist of PSSs was achieved by a time domain simulation. The response of generator G_5's terminal voltage V_5 to a 100ms phase-ground fault at bus 11 was tested with the system with/without PSS attached to generators. The result is shown in Figure 4.10:

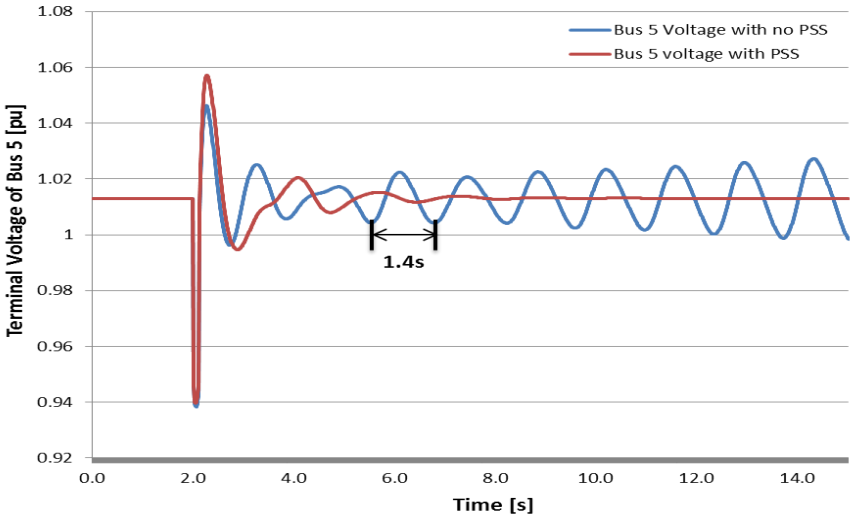

Figure 4-10. Terminal voltage response of Bus 5 to 100ms fault at Bus 11

The transient stability of the equivalent dynamic system was achieved with the help of the eight designed PSSs. The major unstable oscillation mode at the frequency 0.7Hz (1.4s) in the system as it shown in Figure 4.10 was significantly improved.

4.6.4 Systematic approaches in dynamic system equivalencing

The general approaches in dynamic parameters equivalencing can be summarised in a following step by step procedure:

1) The classical generator model is used to represent the aggregated synchronous generator where its dynamic parameters are obtained from manufacturer data sheets and standard parameters based on the different MVA ratings.
2) The loads are modelled as either frequency independent or frequency dependent. The frequency independent loads can be represented as constant active and reactive power at buses. The relation between system frequency and active power demand of the loads can be modelled with the assumption that the percentage frequency deviation results in proportional percentage change in active power demand [28].
3) Analysis of the eigenvalues is performed on the system without any control devices added. Based on this analysis, the parameters of AVRs are tuned according to the small signal analysis which ensures system transient stability.
4) The presence of the interarea oscillation modes in the system with AVRs equipped to the generators is identified. If one or more unstable oscillation modes exist, PSSs are needed to provide damping. The determination of appropriate PSSs locations is achieved by the analysing eigenvalue-eigenvectors with their corresponding participation factors.
5) Finally, the design procedure for tuning PSS parameters is performed based on ICAD method which can be summarised as follows:
    a. Sequentially, define an open-loop PSS channel for generator G_i as PSS_i, and set the gains of other PSS_j channels to a high value, where $j > i$.

b. Design the PSS_i by way of raising the gain above 0db around the interarea mode frequency with rapid gain roll off at lower and higher frequencies.
c. Repeat the process a. and b. for all generators with PSSs.

4.7 Summary

Systematic approaches in dynamic data tuning of an equivalent system are described and applied into the equivalent UK system. The dynamic stability of the system is analysed based on the small signal analysis method which indicates that the system has unstable real mode and lightly damped interarea modes. With the assessments of the eigenvalue-eigenvector plots, the dynamic equivalent system with no controllers attached present that there are three major oscillation performances between the generators in Scotland, England (middle) and England (South) & Wales.

The Bode-Nyquist plot methods are usefully applied to multimachine power systems to provide a wider range of frequencies of interest in power system stability analyses. Meanwhile, the ICAD method is also applied for the purpose of providing an appropriate framework for interpreting the multivariable systems in a more transparent way. Therefore, the coupling problems between controllers can be transferred into the problems among several single-input and single-out channels.

With the AVRs attached to all generators, the transient stability performance are improved but at the expense of robust oscillation stability. The corresponding eigenvectors and participation factors indicate that the generators $G_1, G_2, G_5, G_7, G_8, G_{12}, G_{17}, G_{18}$ are appropriate locations to attach the PSSs. The dynamic equivalent UK system can achieve robust stability when all eight PSSs are attached to the relevant generators. The damping ratio of the unstable interarea oscillation mode at frequency 4.392 $\mathrm{rad/s}$ is increased from -0.0162 to 0.156. A time domain simulation study is demonstrated to confirm the results.

References

[1] P. Kundur, J. Paserba, V. Ajjarapu, *et al*., "Definition and classification of power system stability IEEE/CIGRE joint task force on stability terms and definitions,"*Power Systems, IEEE Transactions on* , vol.19, no.3, Aug. 2004, pp.1387-1401

[2] Department for Business Enterprise& Regulatory Reform, "*Generic stability analysis of the GB electricity transmission system in the long term report*", National Grid, 2008.

[3] *PSS/ETM Program Application Guide*, Volumes I and II, Power Technologies International

[4] P. Kundur, "*Power System Stability and Control*", McGraw-Hill, Inc. NY, 1993

[5] J.G.Slootweg, J. Persson, A.M. van Voorden, *et al*., "A study of the eigenvalue analysis capabilities of power system dynamic simulation software", *14th Power System Computation Conference*, Sevilla, 24-28 June 2002, pp.1-3

[6] N. Martins and L. T. G. Lima, "Eigenvalue and frequency domain analysis of small-signal electromechanical stability problems*," IEEE Special Publication on Eigenanalysis and Frequency Domain Methods for System Dynamic Performance*, 1989, pp. 17-33

[7] National Grid, "*Grid code Report*", November 2011, pp.11-61

[8] National Grid, "*GC022 Frequency Response*", Workgroup Report, January 2013, pp.13-09

[9] I.C. Report, "Dynamic Models for Steam and Hydro Turbines in Power System Studies," *Power Apparatus and Systems, IEEE Transactions on*, vol.92, no.6, 1973, pp.1904-1915

[10] O. Samuelsson, S. Lindahl, "Discussion of "Definition and classification of power system stability"," *Power Systems, IEEE Transactions on* , vol.21, no.1, Feb. 2006, pp.446

[11] P.M.Anderson, A.A. Fouad, "*Power System Control and Stability*", John Wiley & Sons, Inc., Hoboken, NJ, 2003

[12] M. Gibbard, D. Vowles, "*Simplified 14 Generator model of the SE Australian power system*", PhD thesis, University of Adelaide, South Australia, June 2010

[13] X. F. Wang, "*Modern Power Systems Analysis*", Chapter 8, Small-signal stability analysis of power system, McGraw-Hill, Delhi, 2008, third edition

[14] G. J W Dudgeon, W.E. Leithead, A. Dysko, *et al*., "The Effective Role of AVR and PSS in Power Systems: Frequency Response Analysis," *Power Systems, IEEE Transactions on* , vol.22, no.4, Nov. 2007, pp.1986-1994

[15] I. Kamwa, R. Grondin, Y. Hebert, "Wide-area measurement based stabilizing control of large power systems-a decentralized/hierarchical approach," *Power Systems, IEEE Transactions on* , vol.16, no.1, Feb 2001, pp.136-153

[16] N. Martins, "Efficient Eigenvalue and Frequency Response Methods Applied to Power System Small-Signal Stability Studies," *Power Systems, IEEE Transactions on* , vol.1, no.1, Feb. 1986, pp.217-224

[17] G.E. Boukarim, S. Wang, J.H. Chow, *et al*., "A comparison of classical, robust, and decentralized control designs for multiple power system stabilizers," *Power Systems, IEEE Transactions on* , vol.15, no.4, Nov 2000, pp.1287-1292

[18] K.E. Bollinger, R. Winsor, A. Campbell, "Frequency Response Methods for Tuning Stabilizers to Damp out Tie-Line Power Oscillations: Theory and Field-Test Results," *Power Apparatus and Systems, IEEE Transactions on* , vol.PAS-98, no.5, Sept. 1979, pp.1509-1515

[19] Jospeh J. Distefano, Allen R. Stubberud, Ivan J. Williams, "*Feedback and control systems book*", McGraw-Hill Press, USA, 1990, second edition

[20] Z. Qing, F. Huacheng, "*Automatic Theory*", ChongQing University Press, ChongQing, China, 2001

[21] J. O'Reilly, W. E. Leithead, "Multivariable control by 'individual channel design", *International Journal of Control*, vol. 54, no.6, 1991, pp.1-46

[22] J. O'Reilly, W. E. Leithead, "m-input m-output feedback control by individual channel design", *International Journal of Control*, vol. 56, no. 6, 1992, 1347-1397

[23] G. J W Dudgeon, W.E. Leithead, J. O'Reilly, *et al*., "Prospects for the decentralised control of small-scale power networks with embedded

generation," IEEE *Power Engineering Society Winter Meeting*, Singapore, Jan. 2000, pp.1399-1404

[24] J. O'Reilly, W. E. Leithead, "Performance issues in the individual channel design of 2-input 2-output system", *International Journal of Control*, vol. 54, no. 1, 1991, pp.47-82

[25] A. Dysko, W.E. Leithead, J. O'Reilly, "Enhanced Power System Stability by Coordinated PSS Design," *Power Systems, IEEE Transactions on*, vol.25, no.1, Feb. 2010, pp.413-422

[26] National Grid, "*Seven Year Statement*", November 2012, http://www.nationalgrid.com/uk/Electricity/SYS/CURRENT

[27] E.V. Larsen, D. A. Swann, "Applying Power System Stabilizers Part I: Part II, Part III," *Power Apparatus and Systems, IEEE Transactions on* , vol. 100, no.6, June 1981, pp.3017-3024

[28] M.Y. Akhtar, "Frequency-dependent dynamic, representation of induction-motor loads," *Electrical Engineers, Proceedings of the Institution of* , vol.115, no.6, June 1968, pp.802-812

CHAPTER 5: PROPOSED EQUIVALENT METHOD VALIDATION AND MODELLING FUTURE SCENARIOS IN UK SYSTEM

5.1 Introduction

Several network reduction methodologies have been introduced in previous chapters. Due to the limitation of lacking available original network data, it is impractical to use these methods to create an equivalent network which can represent a real system. Thus, a novel proposed method is introduced. The detail processes of how to establish the UK equivalent power system have been explained in the previous two chapters. However, it is valuable and necessary to validate this model in order to prove the proposed method has good accuracy in both the power flow studies and dynamic frequency responses.

The validation of the equivalent model is based on the historical system frequency response data records under real system events for example: sudden loss of generation which causes significant frequency deviation in the system [1-3]. Therefore, a useful source of information is one of the most important elements of validation. Phasor Measurement Unit (PMU) can be a trustful data resource. PMU is "A device or a function in a multifuncation device that produces synchronized phasor, frequency, and rate of change of frequency (RoCoF) estimates from voltage and/or current signals and a time synchronizing signal" [4]. PMUs measure the phasor information which includes magnitude, phase angle and frequency from the electrical sine waves in real time. PMU data are measured at widely locations in power system. The measured voltage or current are synchronized by a common time stamp based on the clock-synchronization technique such as global positioning system (GPS). Due to that reason, the synchronized comparison of two quantities is possible. PMUs are usually used to assess the power system performance in real time [4-5].

Once the equivalent model is validated, it is necessary to update the system to reflect the probable future system performance under high penetration levels of wind. Based on the UK National Grid Electricity Ten Year Statement (ETYS), the increasing penetration levels of the wind farms (DFIG) may pose a number of new challenges in the future due to its inertia-less performance. The challenges are related

to different distribution scenarios of the wind plants; different penetration levels of DFIG; lack of reactive power support which is limited by the MVAr capacity of the wind generators, etc [3, 6]. Therefore an appropriate modelling of future scenarios in UK power system is needed.

In this chapter, the established UK dynamic equivalent network is validated and subsequently extended to represent future system scenarios with high penetration of wind farms; Section 5.2 compares the proposed method to the Ward method based on well-known IEEE 14 Bus System; In section 5.3, two different real network events are repeated in simulation in order to validate the model; In section 5.4, the future wind energy establishing plans by the year 2020 are described. The model is extended to represent a future UK transmission system according to the UK Gone Green scenario; Section 5.5 gives the conclusion.

5.2 Comparision of Proposed Methodology With Ward Method

5.2.1 IEEE 14 Buses System

The Ward method needs the full original system data in order to establish the electrical transmission network nodal equation for network equivalencing. It is impractical to compare the proposed method against the Ward method based on the UK equivalent network. Hence, another system is needed which its full original data should be easily accessed. The IEEE 14 Bus System is the well-known power system, the full network data can be found in [7].

The internal subsystem and external subsystem need to be defined based on the Ward method at the beginning. Therefore, Bus 1 and Bus 2 were chosen as the internal subsystem since two major power plants were located at these two buses. The rest 12 buses were defined as the external buses. They were further divided into 4 areas as shown in Figure 5.1. The system power flow data was also shown in Figure 5.1.

In A2, A3 and A5, the buses which were directly connected with generators were retained (Bus 3, Bus 6 and Bus 9) during the network reduction. In area 4, Bus 13 was retained since it had the major power transfers and the largest demand in this study area. All other buses and transmission lines are eliminated. The equivalent

network contains 6 nodes (2 nodes in the internal network **A1 (B1, B2)** and 4 nodes in the external network **A2 (B3), A3 (B6), A4 (B13), A5 (B9)**).

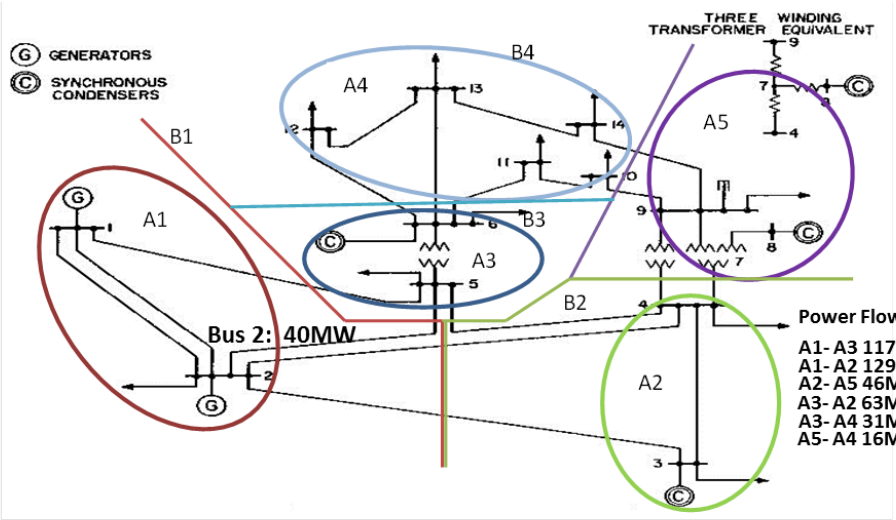

Figure 5-1. IEEE 14 Bus System [7]

5.2.2 Power flow resluts comparision

The Ward method was used to calculate the equivalent network through the built-in Equivalence Network Activity in PSS/E software [8]. The power flow data of IEEE 14 Bus System was imported into the PSS/E and the required internal subsystem and external subsystem are defined based on the above assumption. The diagrams of the equivalent network created by both two methods are shown in Figure 5.2.

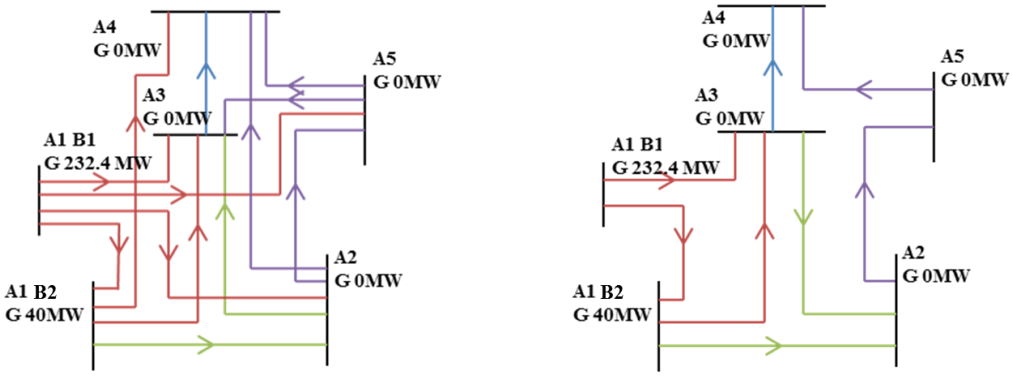

a) Ward method b) Proposed method

Figure 5-2. Equivalent network for IEEE 14 Bus System

The results show that the Ward method tends to create additional "fictitious" connections between zones which were mentioned in chapter 3. This is because the transfer matrix Y_{RR} is changed and additional connections are created to replace the eliminated parts of the network. In contrast, the proposed method is able to retain the original system structure, as well as it can produce a similar power flow result as shown in Table 5.1.

Table 5.1. Power flow result comparison

Power Flow	**A1-A2**	**A1-A3**	**A2-A5**	**A3-A2**	**A3-A4**	**A5-A4**
P(MW) original	129	117	46	63	31	16
Q(MVar) original	-1	-4	-11	-10	10	11
P(MW) proposed	128.9	117.5	44.3	63.8	30.3	16.1
Q(MVar) proposed	1.2	-2.5	-12.7	-8.3	10.8	11.6
Voltage (Retained nodes)	**A1 / B1-1**	**A1 / B1-2**	**A2 / B3**	**A3 / B6**	**A4 / B13**	**A5 / B9**
Magnitude (pu) original	1.06	1.045	1.01	1.0281	1.0199	1.0461
Angle (Degree) original	0	-5	-12.7	-10.4	-15.6	-13.7
Magnitude (pu) proposed	1.06	1.045	1.01	1.0281	1.0191	1.0461
Angle (Degree) proposed	0	-4.99	-12.65	-10.36	-15.5	-13.6

Table 5.1 indicated that the proposed method had a high accuracy compared to the original system data in steady-state studies. The power flows between each zone were well matched.

5.2.3 Dynamic perfromance comparision

For the purpose of analysing the dynamic system performance of both equivalent models, a system major disturbance: loss of one 40 MW generation unit (internal area A1 Bus2) is simulated at 1s. The case is simulated using the original network data and then with both network reduction methods. The results are shown in Figure 5.3. The loss of generation causes the frequency decrease about 0.45 Hz in 3 s as shown in the original frequency response curve (IEEE14). The system frequency trace during the event demonstrates that both methods produce very similar response compare with the original curve. Moreover, the new proposed

method delivers slightly higher accuracy (max error 0.0103) compared to the Ward method (max error 0.0267).

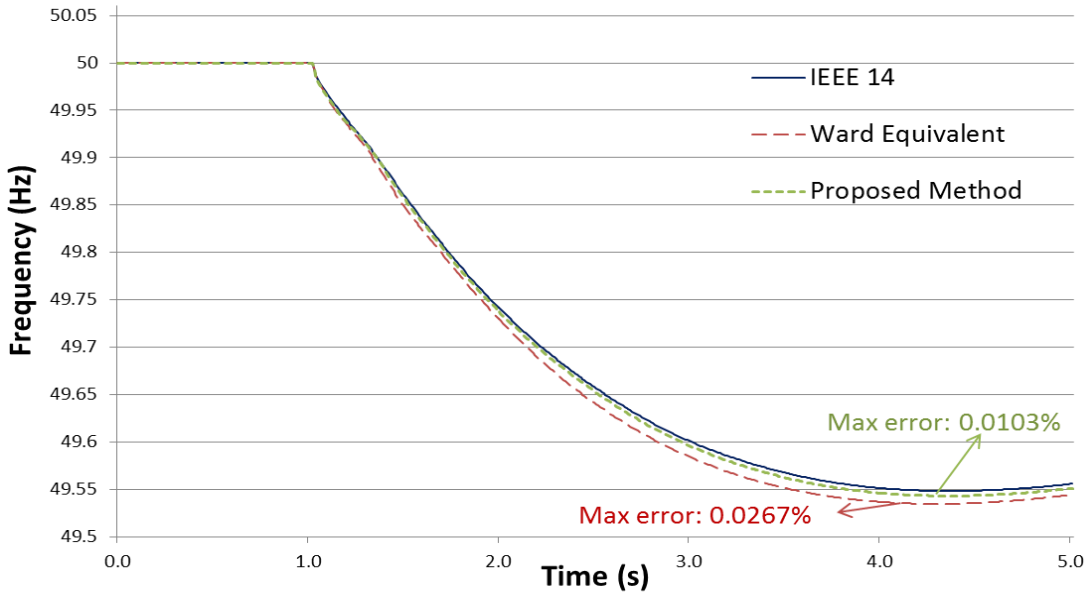

Figure 5-3. Frequency response during loss of generation at bus 2

Hence, conclusions can be made that the proposed method can not only retain the original system structure without adding any fictitious branches but also produce similar dynamic characteristics of frequency response.

5.3 UK Dynamic System Validation

The above test was based on a relatively small network, the transmission system and the distributions of power plants were not very complicated. However, the UK transmission system is very large which contains hundreds of nodes. Therefore, it is necessary to validate whether the proposed method can reflect similar frequency performance compare to the data records under the real system events.

5.3.1 Method used to validate UK system

The validation of the network was achieved by the way of comparing the real system events data records with the simulation results [2]. PMU data records were used as a trustful source of information for the purposes of dynamic model validation. This requires a capture of a significant network event (frequency and voltage phase angle) from a number of locations together with the specifics of disconnected loads, generators or major transmission lines. The event is then

repeated in simulation to validate the model. There are several PMU devices installed in different locations across the UK: Glasgow, Manchester and London. In this thesis, the data collected from these three places were used for the equivalent dynamic system validation.

Steady-state validation: The power flow validation is achieved by analysing the voltage angle shift at different parts of the system, prior to and after the event.

Dynamic validation: The record of the frequency response can be used to validate the inertia and system dynamics. Moreover, it is also possible to validate the potential oscillation performances of the equivalent model through either frequency response curves or voltage phase angle curves.

5.3.2 Validation case 1: loss of HVDC interconnector based on PMU data records

In case 1, an example frequency profile recorded during the recent transmission system event in UK was used for validation purposes. In order to verify the model response, the equivalent network loading was first adjusted to reflect the loading conditions at a particular day and time. The historical demand data as shown in Figure 5.4 was provided from BMRS (32 GW) [9].

The voltage phase angle difference between the three locations was first used for load flow solution validation. Figure 5.5 presents voltage phase angle as recorded from PMU and equivalent network simulation results. The waveforms demonstrated the phase difference between Glasgow to Manchester and Glasgow to London with Glasgow voltage angle as reference.

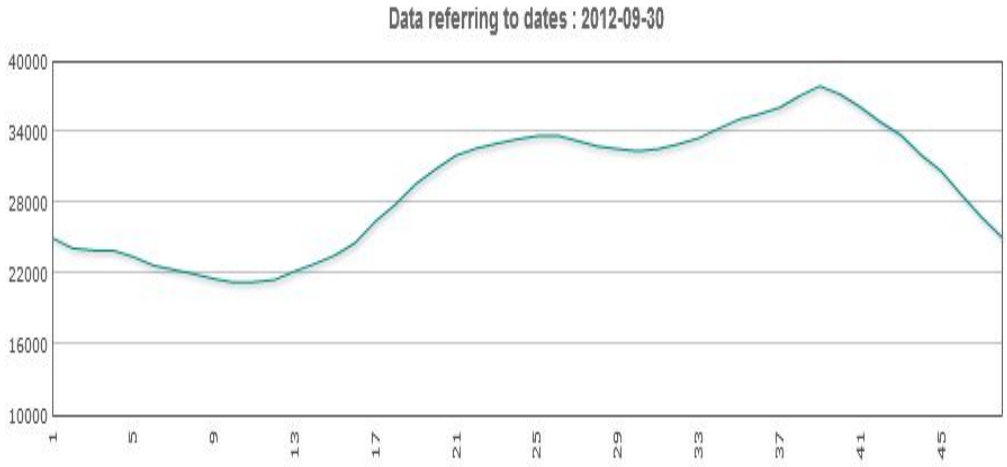

Figure 5-4. Historic demand data during the event [9]

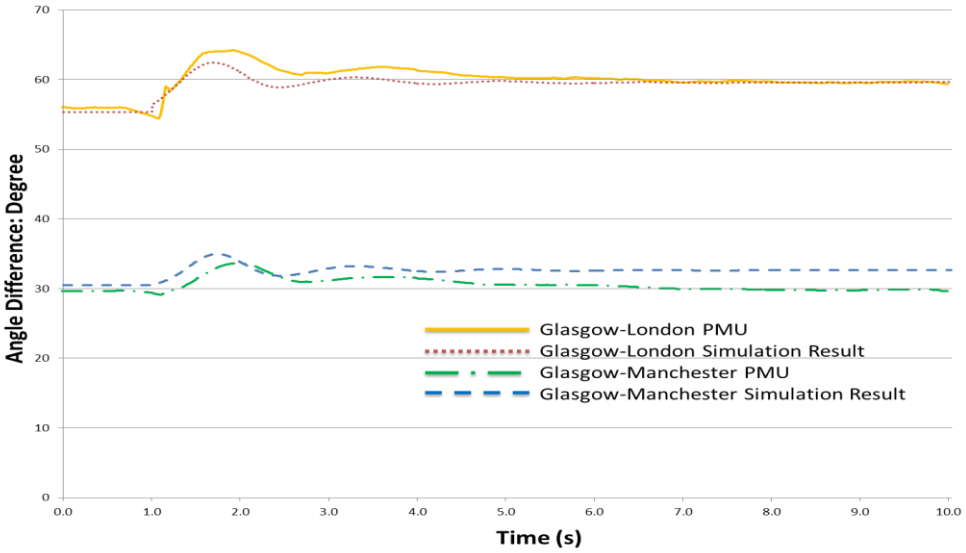

Figure 5-5. Voltage phase angle difference during a major system event PMU recorded data compare with Simulation results

The above results show that the equivalent network had a similar load condition where the pre-fault phase difference were 29.8 ° (PMU data)/ 30.4 ° (simulation results) and post fault phase angle difference 29.9 ⁄32.2 ° between Glasgow and Manchester; pre-fault phase difference 56 ⁄55.7 ° and post fault phase difference 59.9 ⁄59.8 ° between Glasgow and London. Moreover, both responses reflected that one major oscillation (0.58 Hz) existed during the event.

Frequency responses during the initial stage of this event were demonstrated in Figures 5.6 and 5.7. The system primary frequency response was compared. The loss of generation caused frequency drop from 49.96 Hz to 49.62 Hz as shown in PMU data records.

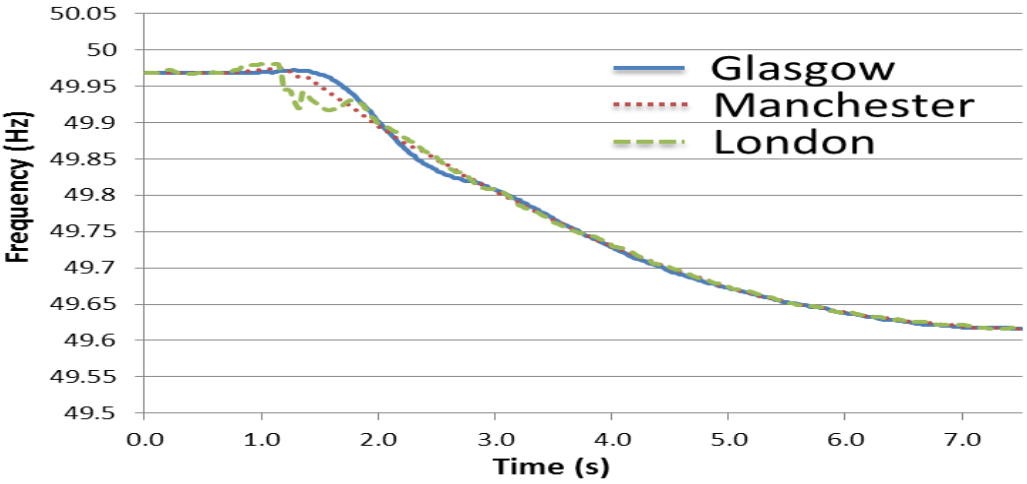

Figure 5-6. Frequency profile during a major system event: PMU recorded data

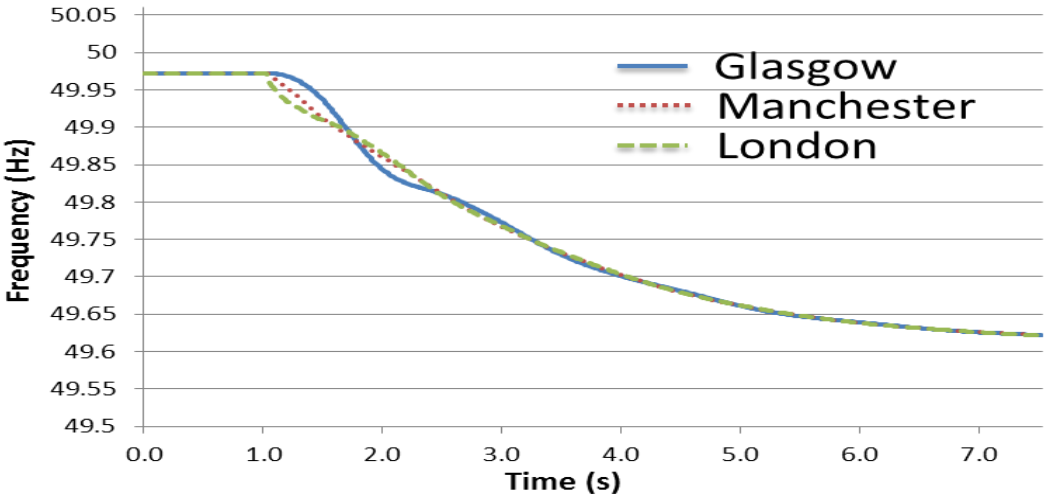

Figure 5-7. Frequency profile during a major system event: equivalent network

The results demonstrated that there was a very good correspondence between the recorded and simulated responses. The simulated results were well matched to PMU recorded data. Also both of the figures showed that there was one significant oscillation existed. A small initial difference in the frequency trace recorded in London can be attributed to the transient nature of the commutation failure involved during this event. However, this is hard to simulate due to lack of detail information near the distributed network close to London.

5.3.3 Validation case 2: May 2008 UK Loss of Generation incident

This case is based on the well-known UK 2008 May loss of generation event. On the day 27th May 2008, there was an unexpected loss of 1582MW of generation within two minutes for unrelated reasons resulted in a large frequency disturbance. The loss of generation lead to the Low Frequency Demand Disconnection (LFDD) issues happened where a large number of demands need to be disconnected from the grid and the largest duration was up to 63 minutes [10].

The loss of generation happened in near two minutes in two stages as follows:

1. First 345 MW generation loss occurred at Longannet power plant (study zone 5), which resulted in frequency drop of about 0.127 Hz in 12 s. This loss of frequency is within National Grid policy where the frequency deviation is less than 0.5 Hz.

2. Secondly, a loss of 1237 MW generation at Sizewell power plant occurred (study zone 12). At the same time, one 132 MW embedded generation losses of

generation occurred results in total 1369 MW loss of generation. This resulted in frequency falling to 49.15 Hz in about 20 s. These losses are significantly exceeds the daily maximum secured loss 1260 MW.

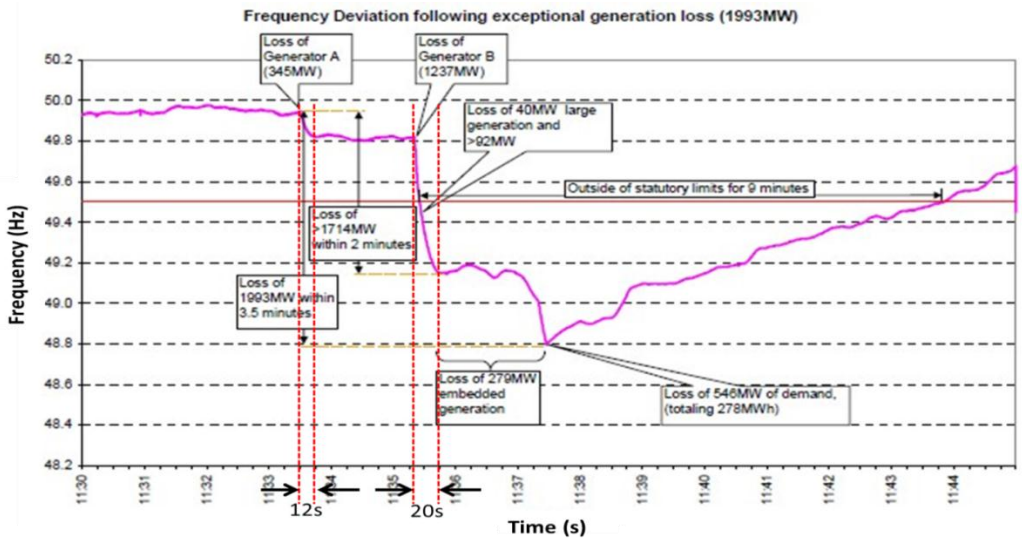

Figure 5-8. Frequency response during generation loss in 2008 [10]

Although it is difficult to simulate the whole process of the event due to lack of information about emergency actions been taken during the whole event, the rate of change of frequency performance directly following each loss of generation can still be used to validate the model dynamic response.

The demand curve for 27th May was forecast as shown in Figure 5.9. The demand during the event happened was 42.2 GW. All the forecast power flows on the day were within acceptable limits. Hence, there is no specific condition need to be considered.

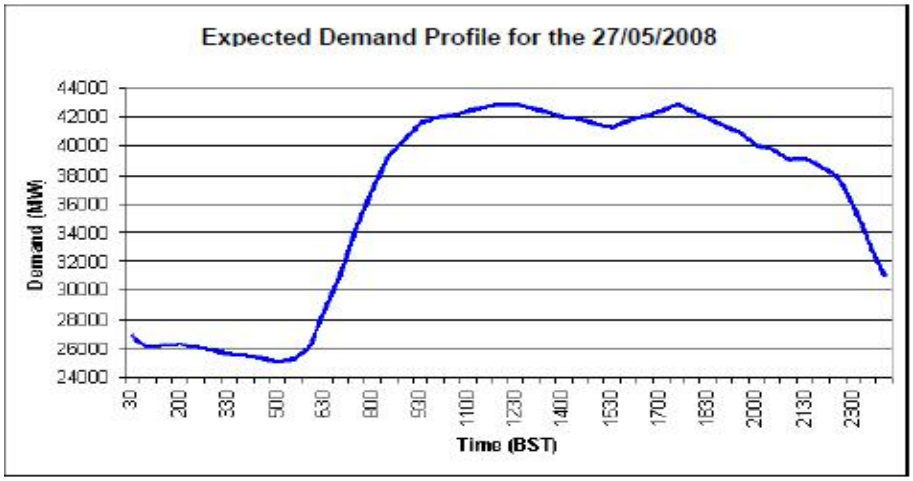

Figure 5-9. Expected demand on May 27th 2008 [10]

The simulated result of these two stages was presented in Figure 5.10.

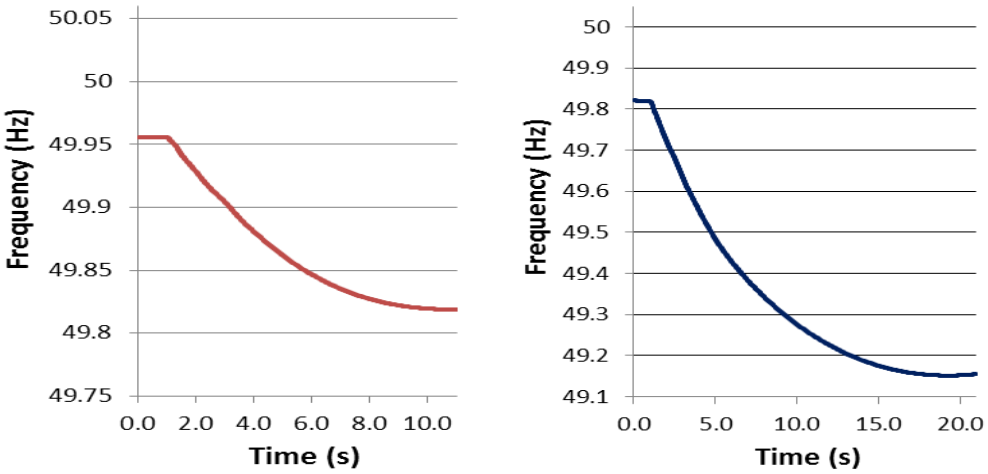

a) First Loss of Generation b) Second Loss of Generation

Figure 5-10. Frequency response during generation loss in 2008: simulated results

The results in Figure 5.10 show that primary frequency drops of both loss of generation occurrences are well matched: the first loss of 345 MW resulted in the frequency drop from 49.95 Hz to 49.82 Hz within 10s and second loss of 1369 MW results in a further frequency drop by 0.65 Hz which made frequency fall down to 49.165 Hz within about 20s. These results proved that the established equivalent UK system was able to reflect the existing system response during the disturbance.

5.4 Description for future network plan

The future offshore developing scenarios should cover a number of cases which represent a wide range (low to high) of the potential outcomes. This will enable the analyses on specific challenges to the system. The UK National Grid: Future Scenarios Consultation outlines a few alternative directions of system development based on the comments received from industrial participants [11]. These scenarios have been termed as: Slow Progression (SG), Gone Green (GG) and Accelerated Growth (AG). The scenarios are significantly different from one another starting from 25GW of installed offshore capacity in SG to 57GW in AG by 2030; each scenario has appropriate generation capacity to meet the requirement of Security of Supply and the existing nuclear power stations are assumed to extend their lives in all scenarios with different durations.

Slow Progression (SG): under this scenario, the growths of clean energy are slow while comparing to the GG and AG cases based on the assumption of lower future energy prices background (particularly gas and carbon). The carbon reduction target is met for the year 2020 but not the indicative target for 2030 [11-12].

Accelerated Growth (AG): This scenario has a fast speed on offshore wind farms installation. All renewable energy targets are met by 2050. However, this scenario is established based on the background of higher carbon prices, significant increase of supply chain and strong government support. It is impractical to realize the task and it has already been removed in the latest published Ten Year Statement 2014 by NG [6].

Gone Green (GG): The Gone Green scenario can also meet the renewable targets in all the cases by 2020, 2030 and 2050 [11-12]. The speed of building wind farms is relatively faster than that in SG. The nuclear power plants are assumed to have the longer working life extension (ten years) compared to SG (five years). Because this scenario is established based on the consideration of a balanced approach with contributions from different generations to meet the carbon reduction target, it is the main strategy used by National Grid to analyses the future system performance. Hence, in this thesis, all the case studies are based on the GG scenario [6].

5.4.1 UK Equivalent model in the year of 2020

The updated 21 bus equivalent transmission network model superimposed on the UK map is shown in Figure 5.11. Additional 9 onshore wind plants are added into zone 1, 2, 3, 4, 5, 6, 9 and 13. The PSS/E DFIG WT3 type model of wind farms are used to represent the onshore wind plants. Since the offshore wind farms are all connected to the grid with the fully converter HVDC connection, they will not have frequency response during the network disturbance. The offshore wind farms are represented as the negative loads where the influence of the fully converter connection are neglected for the purpose of reducing the complexity of the model.

5.4.2 Demand Definition

The peak demand (including the transmission losses) is defined as the forecast transmission peak demand. The small embedded generation is treated as the negative

load for a simplified calculation. The future transmission peak demand provided by the National Grid ETYS is forecasted from the analysing on annual electricity consumption, energy price, embedded generation development and new emerging technology such as heat pumps and electric vehicles development [6, 11]. The winter peak transmission demand under the Gone Green scenario has very slow growth which has no dominant increase due to the low economic growth. The peak demand is increased from 56GW in the year 2012 to 57.7GW by 2020 [6, 12]. The summer minimum demand is defined as 23GW by 2020.

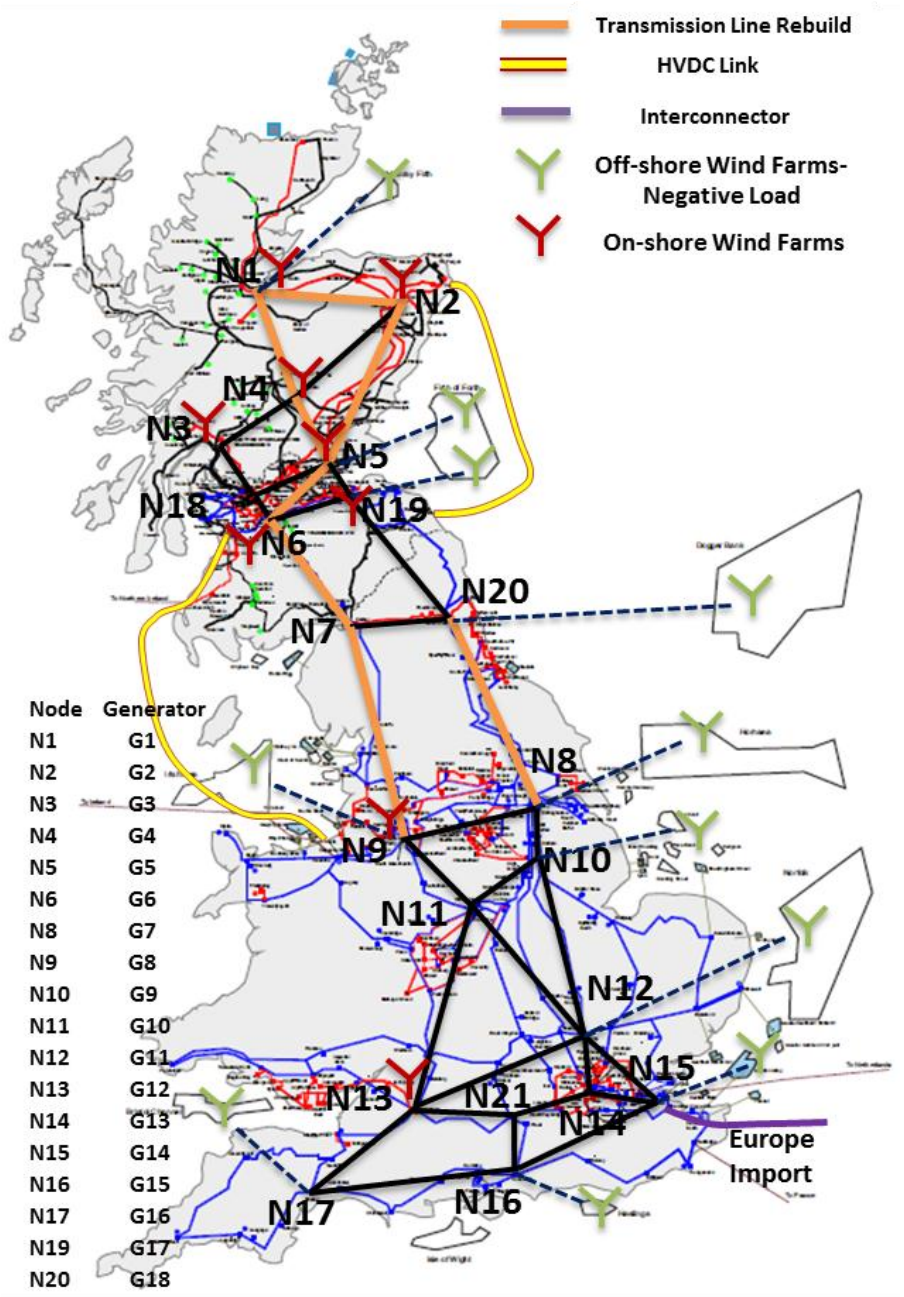

Figure 5-11. Update UK transmission system operating in 2020

5.4.3 Generation Definition

Generation is assumed to meet carbon dioxide emission requirements for all targets by the year 2020, 2030 and 2050 in GG scenario:

- Wind reaches 25GW which needs an increase of 18 GW to 2020;
- Coal plant decreases by 7GW from existing 25GW to 18GW in 2020;
- 3GW increase in Gas/CHP capacity;
- 5GW nuclear capacity increases by 2020.

Table 5.2 lists the generation capacity with different types of plant information for study zone 6 as an example.

Table 5.2. Zone 6 generation profile 2008-2020 [6]

Plant Type	**2008(MW)**	**2012 (MW)**	**2020(MW)**
Nuclear	2334	2334	2334
Coal	716	716	165
Interconnector	360	360	360
Offshore	0	0	3065
Onshore	975	1667	3531
Total	4388	5080	9458

5.4.4 Transmission lines reinforcements

Due to the high penetration levels of wind in Scotland, the power transfer across several boundaries may need reinforcements. Based on the ETYS, following several reinforcements are made:

1. Seven transmission lines are rebuilt connecting study zones 1, 2, 4, 5, 6, 7 and 8. The updated transmission line data (marked in orange in Figure 5.11) reflect these changes by including the information provided by ETYS “Transmission circuit change 2012 to 2021”.
2. All transmission lines previously assumed as single circuits have been replaced with double-circuits.
3. Two new HVDC links are added to the system: 2GW Eastern HVDC link from Peterhead to England and 2.4GW Western HVDC link from Deeside to

Hunterston. The VSCDCT model in PSS/E was used to implement these lines and the detailed parameters are included in the in Appendix i.

5.4.5 Power flow validation of the updated model

The power flow results of the updated UK equivalent model were compared to the forecast results which were demonstrated in ETYS [6]. Figure 5.12 demonstrated the power flow from North to South under GG scenario based on winter peak demand condition. The simulation results between zones were also presented as shown in Figure 5.12. The results show that the real power transferred across the boundary were well-matched where the blue data represented the simulation results and the purple/red data is the prediction data by NG.

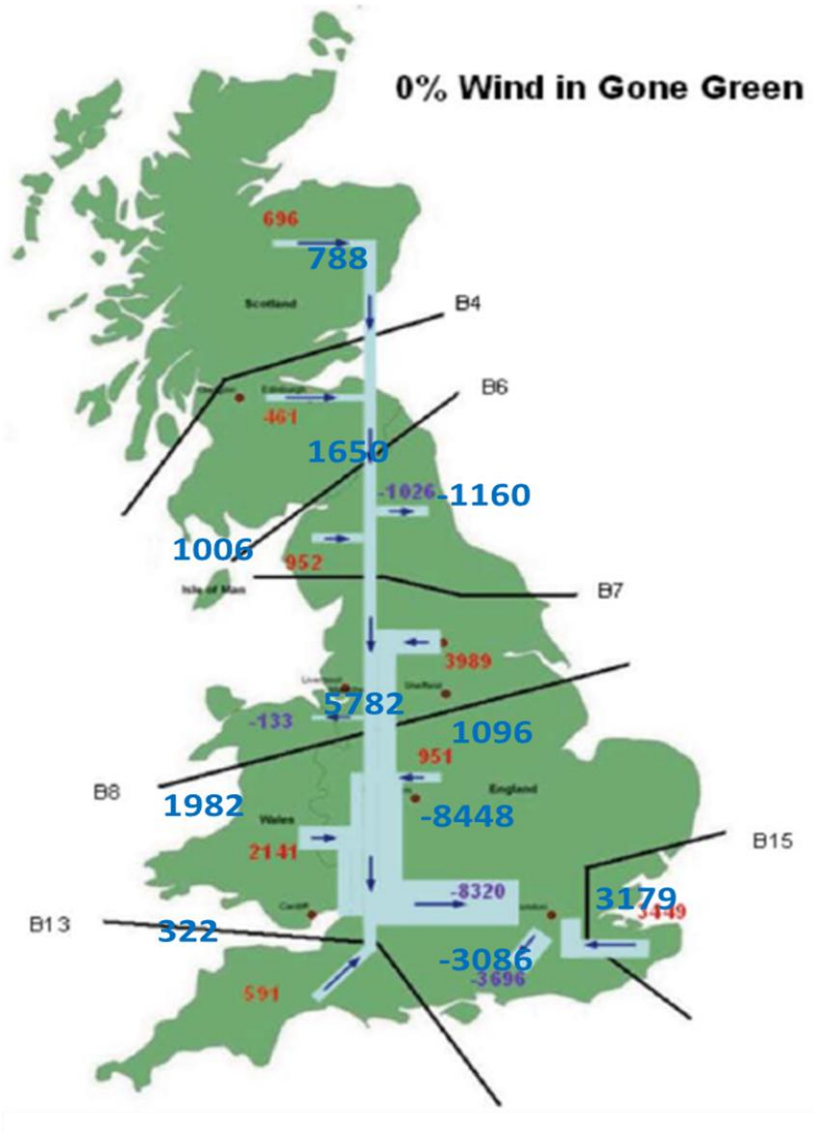

Figure 5-12. Power flow validation: UK Transmission System in 2020 (GG)

5.4.6 Future scenarios with different penetration levels of offshore windfarm

The onshore and offshore wind farms are distributed in different locations throughout the UK. These large power park especially the large offshore wind farms may result the variations in power flow [6]. The high penetration levels of wind plants will change the pattern of the power flow which may enhance or worsen the system transient stability.

Therefore, the penetration levels of wind farms are assumed to increase from 0% to 70% for all the case studies according to ETYS. Furthermore, two different distributions of wind energy resources are considered as shown in Figure 5.13:

- Wind energy is distributed evenly throughout the UK (equal distribution denoted as ED): a large amount of power (5355 MW) may transfer from North to South.

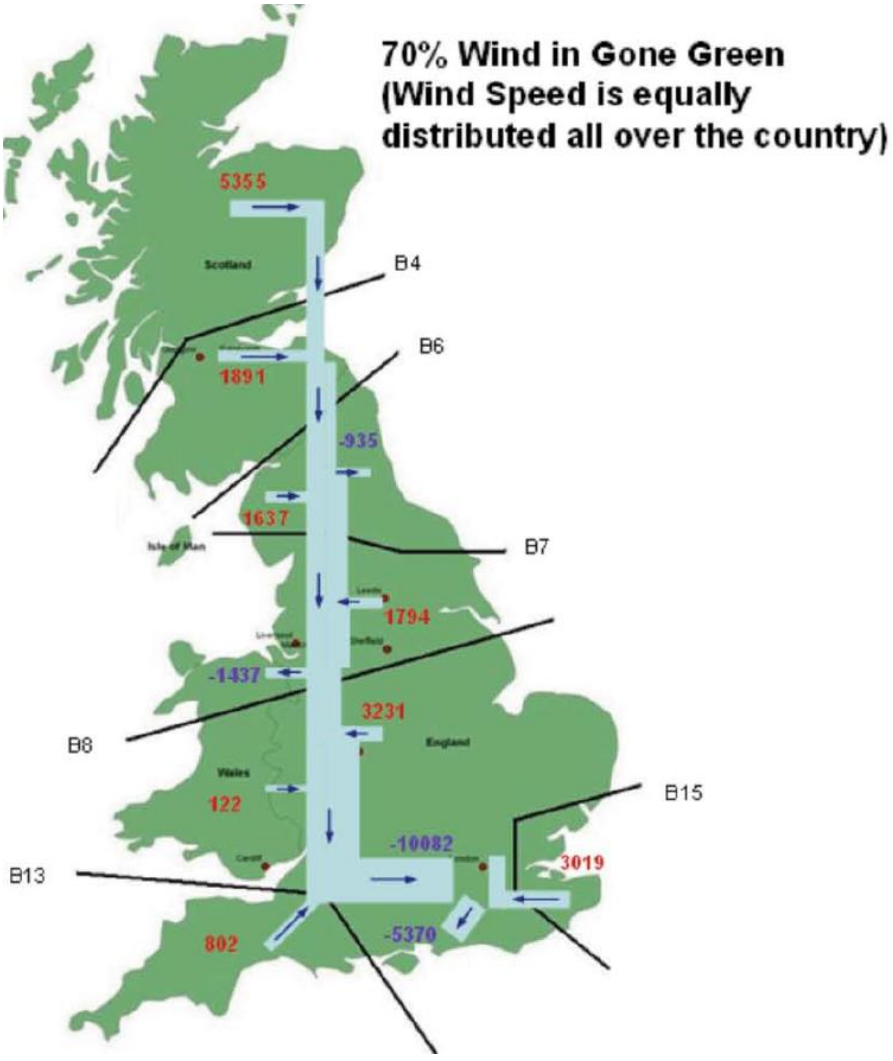

(a) Wind power plants are equally distributed all over the country

- Uneven distribution with 10% wind energy in the North and 70% in the South (NS): relatively small amount of power (1264 MW) is transferred from North to South compared with ED condition.

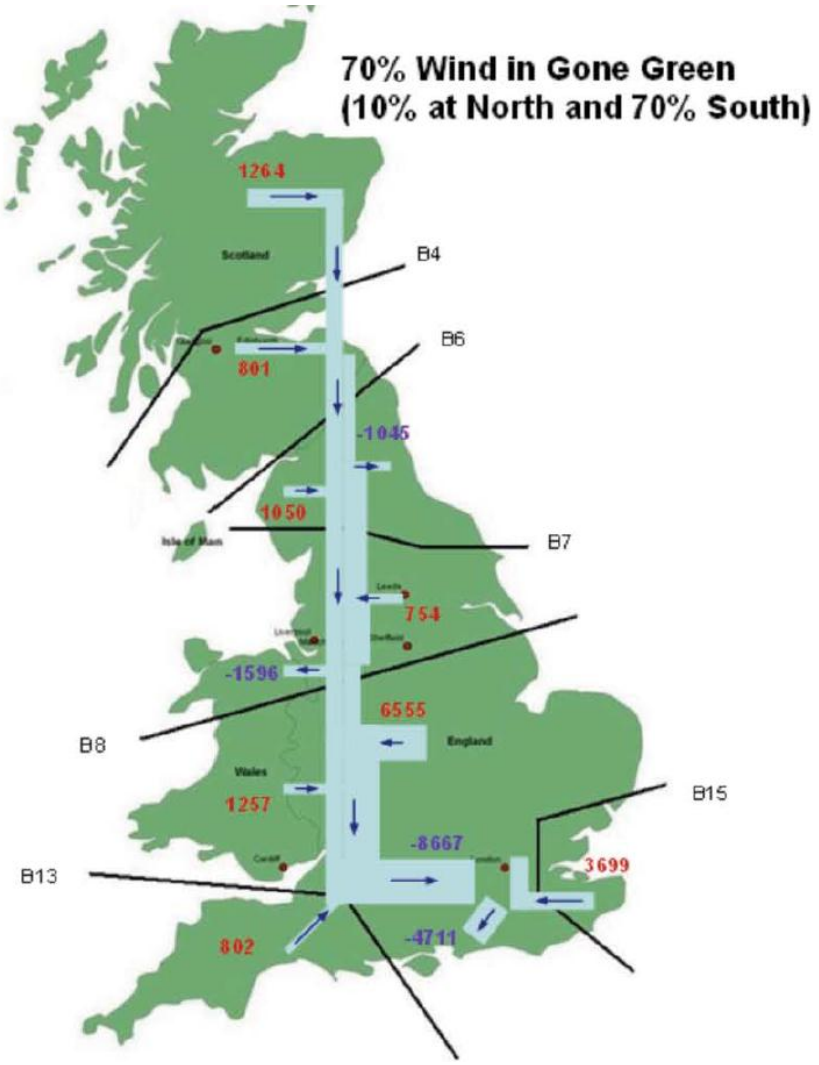

(b) Wind power plants are 10% distributed at North and 70% at South

Figure 5-13. Power flow prediction based on different wind distributed conditions [6]

5.4.7 Future frequency management plan

With the increasing penetration levels of wind power plants, the system may suffer high RoCoF during major disturbances. The distribution network may have high risk of spurious disconnection from the grid caused by the RoCoF based protection relays. To overcome this problem, two scenarios have been proposed: 1. change the current RoCoF setting; 2. introduce enough primary frequency/ Synthetic inertia response.

Before applying these two scenarios into the future application, it is important to assess the impact of each scenario on different aspects (for examples: economic cost benefit or safety of the distribution networks) for the purpose of establishing the most appropriate plan for future network operation.

Due to the economic benefits consideration, changing the existing recommended RoCoF setting (0.125 Hzs^{-1}) is much more welcome than others methods. The cost can be significant high in the later scenarios. The cost used to reduce the maximum infeed loss can be £83/MWh with a 12 GWh trading and the cost used to purchase additional synchronous generation if energy trading is not possible is even more expensive. It may cost £150/MWh to buy 240 GWh of energy [13]. National Grid has forecasted that the costs for the next 3 to 4 years used to ensure the security of the system without changing the RoCoF setting are about £10m per annum with an upper limit of £100 m per annum. In contrast, the cost of changing current RoCoF is relatively low which is estimated by less than £10 k per distributed generator site which used the RoCoF based protection. The site numbers will be 150. In addition, further cost of £125 k per site is assumed in additional assessment and mitigation measures to avoid the risk of damage to the generator. The total costs are approximate £7.5 m [13].

As previously mentioned, any loss of main event may cause hazard to the network. Hence, it is not allowed in most cases. However, to increase the RoCoF setting may result a higher possibility of unsafe islanded operation. Therefore, it is also necessary to analyses the risk assessment which reviews the risks that whether the islanding non-detection zone under different RoCoF setting is acceptable by the related policies before applying the proposed new setting. With all these considerations, the new proposed RoCoF setting in UK power system by National Grid is 1 Hzs^{-1} [13].

5.5 Summary

A new methodology of deriving an equivalent large transmission system model is described and one equivalent UK dynamic system has been established. In order to have high level of confidence in frequency performance investigation, it is crucial to employ a validated dynamic method of the system. The mode should be validated for

both steady state and dynamic studies before any future scenarios can be considered and assessed.

PMU is used as a trustful data resource to validate the proposed new method by comparing the historical event data with the simulation data. The proposed method is first compared with the Ward method based on the IEEE 14 Bus System. The results show that it can not only retain the system structure without any fictitious branches added but also have a higher accuracy in dynamic system performance compare to the Ward method. Furthermore, two known system incidents are utilized to validate the dynamic performance of the model. Both power flow and dynamic simulation results show that the equivalent UK model is able to reflect the existing system frequency response during the disturbance.

The validated system is then extended to represent a future UK system with high penetration level of wind farms for the purpose of predicting the new challenges in the system. The equivalent network is updated mainly based on the Gone Green scenario proposed by the UK National Grid. The new recommended system RoCoF setting in the future is adjusted to $1Hzs^{-1}$ by National Grid.

References

[1] S. Stavrinos, A. G. Petoussis, A. L. Theophanous, *et al.*, "Development of a validated dynamic model of Cyprus Transmission system," *7th Mediterranean Conference and Exhibition on Power Generation, Transmission, Distribution and Energy Conversion*, Agia Napa, Cyprus, 7-10 Nov. 2010, pp.1-11

[2] J. Xia, A. Dyśko, "UK transmission system modelling and validation for dynamic studies," *Innovative Smart Grid Technologies Europe (ISGT EUROPE)*, 4th IEEE/PES , Copenhagen, Denmark, 6-9 Oct.2013, pp.1-5

[3] National Grid, "*Future Operability Framework*", Sep. 2014, pp.1-34

[4] *IEEE Std C37.242-2013*, "IEEE Guide for Synchronization, Calibration, Testing, and Installation of Phasor Measurement Units (PMUs) for Power System Protection and Control," Phasor Measurement Unit (PMU) Communication Experience in a Utility Environment, March 2013, pp.1-107

[5] J. Lee; S. Lee; J. Bae, *et al*., "The PMU interface using IEC 61850," *ICT Convergence (ICTC) International Conference*, Jeju Island, Korea, 14-16 Oct. 2013, pp.1125-1128,

[6] National Grid, "*Electricity Ten Year Statement 2014*", http://www.nationalgrid.com/uk/electricity/ten-year-statement

[7] *Power Systems Test Case Archive*, Power Flow Test Case 14 bus, http://www.ee.washington.edu/research/pstca/

[8] PSS/ETM Program Application Guide, Volumes I and II, *Power Technologies International*

[9] New Electricity Trading Arrangements (neta), *Balancing Mechanism Reporting System (BMRS)*, http://www.bmreports.com

[10] National Grid, Report of the National Grid Investigation into the Frequency Deviation and Automatic Demand Disconnection that occurred on the 27th May 2008

[11] Offshore Development Information Statement, *Future Scenarios Consultation Report*, 2011 http://www.nationalgrid.com/uk/Electricity/Off-shoreTransm-ission/

[12] Operating the Electricity Transmission Networks, *Future Scenarios Consultation Report*, 2020 http://www.nationalgrid.com/uk/Electricity/Operating+in+2020/

[13] National Grid, "Frequency Change during Large Disturbances and their Impact on the Total System", *Industry Consultation Report*, Aug 2013

CHAPTER 6: UK SYSTEM FUTURE FREQUENCY PERFORMANCE EVALUTAION

The future system dynamic performances of UK are presented in this chapter through a number of cases studies. These case studies are established for the purpose of investigating the potential risks that may exist in the future [1, 2]. These challenges include:

a. The system transient performance: The system transient stability might be reduced by the increasing capacity of the wind farms together with the decommissioning of the large coal plants at the same time especially in the centre of the UK network. The reactive power control capability should be one of the most important issues need to be considered at first;

b. The RoCoF performance: The inertia-less wind farms have no ability to support the system dynamic frequency performance during disturbance, thus the system total inertia will decrease. As a result, high RoCoF may be found in the system. The impact of different influencing factors on RoCoF in the system should be investigated.

c. The system power flow volatility: According to the different wind speed distribution conditions, the pattern of power flow of UK system will have a great change in the future. It is valuable to test whether this issue will have significant influence on the system transient stability.

In section 6.1, the system transient stability is studied by way of assessing critical fault clearance time; Section 6.2 analyses system frequency performance under different demand and wind power distribution conditions. Three influencing factors related to amount of lost generation, amount of primary frequency response and frequency dependency of load are analysed. Section 6.3 gives the summary.

6.1 Transient Stability

6.1.1 Case 1: reactive power control of DFIG

In order to test the reactive power performance of the GE WT3 model, the reactive power control function is tested at first. The control method used in WT3

model was introduced in chapter 2. The test is based on the winter peak operating condition where the wind power penetration level is set to 60% and the wind speeds are equally distributed. The system critical fault clearance time (CFCT) is used for assessing the system transient stability. A three-phase to ground line fault between buses 6-7 is added at 1s, the fault is cleared by tripping a faulted transmission line (i.e. one of the two parallel circuits). The normal critical fault clearance time 80ms which is defined in grid code [3] is used. The test results (Figure 6.1) indicate that with the help of voltage control feedback loop, it is possible to maintain the system stability after the fault is cleared while the bus voltage collapse without this control loop activated.

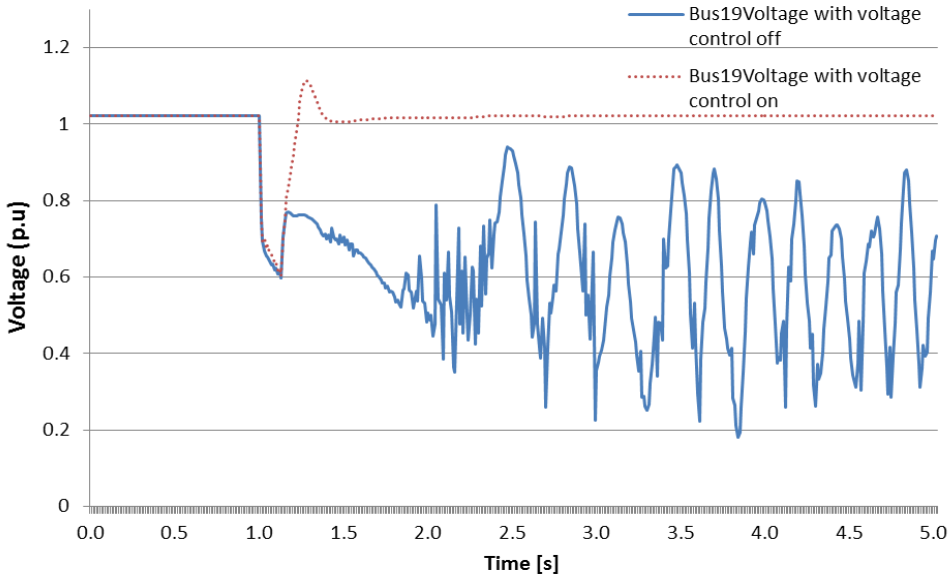

Figure 6-1. Bus 6 Voltage with voltage control on/off under 80ms fault

6.1.2 Case 2: voltage recovery: wind penetration level from 0%-70% based on winter peak demand

For the purpose of testing how the system stability is affected by the wind generations under different penetration levels, two three-phase to ground fault are applied at transmission line between bus 6 to bus 7 (the west connection between Scotland and England) and between bus 8 to bus 10 (transfer of the largest power flow in the system). The wind penetration is varied from 0% to 70%. These tests are based on the worst case: winter peak condition (highest CFCT) as mentioned in ETYS [1]. Both average distributed case and 10% north 70% south case are tested.

All the wind turbines used in this simulation have the reactive power control ability where the $vltflg$ is set to 1. The system critical fault clearance time are shown in Table 6.1.

Table 6.1. Critical fault clearance time at three-phase to ground fault with wind penetration level from 0%-70% based on winter peak

Wind Distribution	**Penetration Level**	**Fault 6-7 [ms]**	**Power Flow [MW]**	**Fault 8-10 [ms]**	**Power Flow [MW]**
ED	0%	367	214.4	176	2491.0
	10%	350	342.8	168	2611.6
	20%	328	728.0	156	2732.4
	30%	301	983.8	137	2841.2
	40%	252	1237.6	110	2944.8
	50%	188	1488.9	75	3041.4
	60%	130	1736.7	48	3129.7
	70%	58	1981.6	28	3211.2
Wind Distribution	**Penetration Level**	**Fault 6-7 [ms]**	**Power Flow [MW]**	**Fault 8-10 [ms]**	**Power Flow [MW]**
NS	0%	367	214.4	176	2491.0
	10%	360	260.7	205	2372
	20%	356	311.6	216	2227
	30%	350	362.3	224	2083.9
	40%	340	412.3	312	1936.5
	50%	322	463.2	266	1790.0
	60%	298	513.8	212	1647.3
	70%	246	563.5	142	1497.9

Form Table 6.1, it can be seen that in most cases the system critical fault clearance time are decreasing with the increasing penetration levels of wind farm. However, in the cases where the wind farms are distributed in NS condition with fault occurs on the transmission line between bus 8 and 10, the situation is different. The CFCT can be initially observed with an increase from 176 ms to 312 ms with the increasing penetration levels of wind from 0% to 40%. Changing distribution of wind generation alters the power flow pattern in the UK system which historically has always been unidirectional i.e. from the north to the south. This results the power transfers from bus 8 to bus 10 decrease even if the penetration levels of wind increase. Although the ability of DFIG to support voltage is limited by their MVAr export capability (0.95 pf) during transient period which may reduce the transient stability of the system, the reduced power flow also reduced the effect of the fault which increases the CFCT. Due to this reason, the general system transient stability

performance is much better in the case where wind farms are distributed 10% in North and 70% in South (NS) than that in the evenly distributed condition (ED).

Moreover, it should be noted some simulated the CFCTs are shorter than 80ms which is the shortest fault clearance time used in UK grid code [3] under wind ED condition when the wind penetration level is above 50% if a fault occurs at the transmission line between bus 8 and 10. In addition, CFCT is shorter than 80 ms when wind penetration level reaches 70% while a fault occurs on the line 6-7. Thus, solutions should be worked out to address this issue such as the investment in reactive power compensation devices in the centre of the network where large numbers of coal plants are decommissioned in the future.

The static var compensator (SVC) is one of the most commonly used reactive power compensators. SVCs are shunt-connected generators or absorbers whose outputs are varied with the change of network conditions. There are many types of SVC for examples: Thyristor-controlled reactor, Thyristor-switched capacitor, Thyristor-switched reactor. The general idea of SVC is a simple system which consists a shunt capacitor and a shunt reactor parallel connected [4]. Ideally, it should have unlimited var generation/absorption capability to maintain a constant voltage with no active and reactive power losses. The characteristic of SVC is illustrated in Figure 6.2 [4].

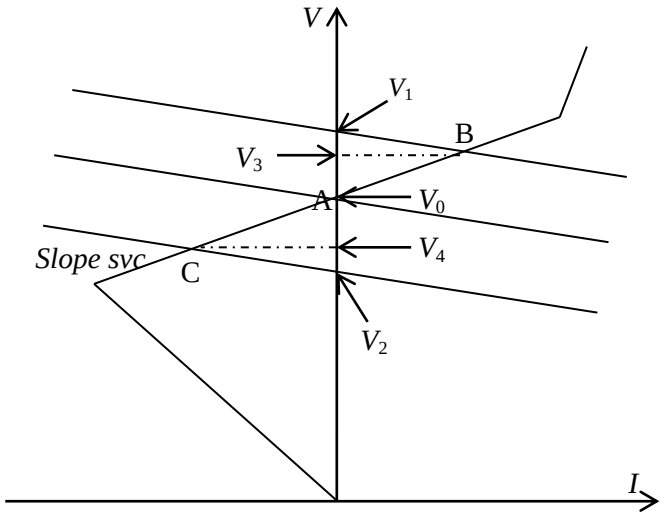

Figure 6-2. Characteristic of SVC

During the normal operating condition, the system will operate with the voltage V=V_0 and I=0 at point A. If there is a sudden disturbance occurs in the network for example, a decrease in system load, V will increase to V_1 without the help of SVC. When SVC is added, the voltage should move according to the slope direction which means the voltage should moves to point B with a lower voltage V_3 by absorbing the inductive current. Also when there is an increase in load level, the voltage can be controlled to a relatively higher voltage V_4 instead of V_2.

To verify this solution, 5 SVCs have been added to the central part of the equivalent model (buses 5, 6, 7, 8 and 9). The MVAr rating of the each SVC is set to 300 MVAr. The same three-phase to ground fault on line bus 6-7 is applied. The wind speed is evenly distributed with 70% wind penetration level condition. The voltages of bus 6 with/without SVCs added are shown in Figure 6.3.

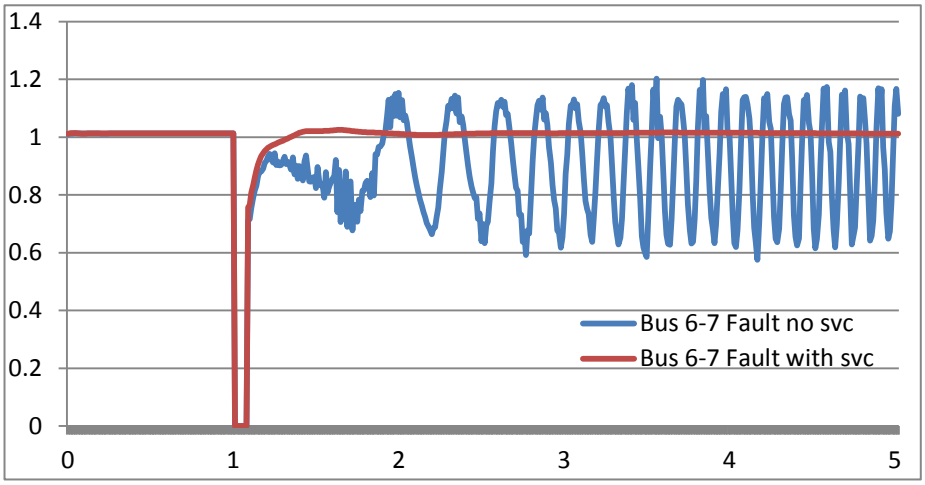

Figure 6-3. Bus 6 voltage during three-phase to ground fault: with/with no SVC

The results show that with the help of SVC, the system can remain stable and the voltage is able to recover back to its pre-fault value. The CFCT is increased to 84 ms in this case which satisfies the requirement of the minimum CFCT 80 ms.

6.1.3 Case 3: Double circuit trip of the western Scottish-English interconnector

For the purpose of analysing the effectiveness of the two new HVDC connections from Scotland to England in enhancing the transmission capability of the network, a simulation study is created where the fault mentioned in case2 is cleared

after 80ms by tripping both of the circuits connecting the Strathaven and Harker (bus 6 and bus 7) which represents the loss of western connection between Scotland and England.

From Figure 6.4 it can be seen that under ED conditions the system loses synchronism at 50% penetration level without HVDC connection added to the network. The introduced two HVDC links largely improve the transfer capacity in the middle part of the network which made the system remaining stable until the wind penetration level reaches 60%.

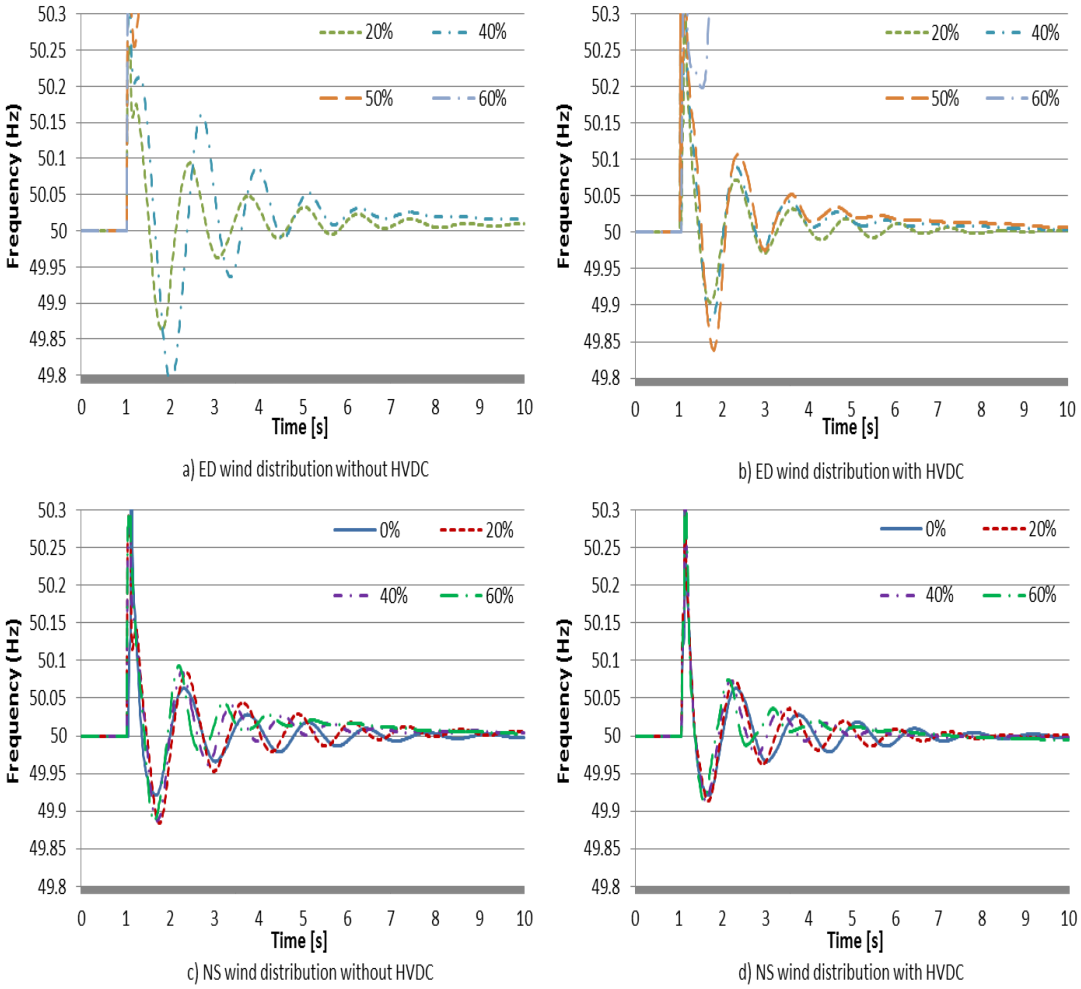

Figure 6-4. Loss of Scottish-England interconnector

However, with NS scenario condition, the system can withstand this disturbance under all the cases. Similarly to Case 6.2, the effect of different wind distribution scenarios (ED and NS) is clearly demonstrated which leads to the change of power flow throughout the UK. In NS scenario the pressure of power transfer from Scotland

to England is considerably reduced compared to that of ED scenario which improves overall transient stability of the system. Furthermore, the system damping performance is improved with the increasing levels of the wind integrated. Although the DFIG is decoupled from the network, it is still equipped with an excitation control system which can provide fast voltage regulation. Therefore, introducing the DFIG into the system can improve the system damping performance. At the same time it is known that transient stability margin is reduced [5].

A final comparison of the system CFCTs under different operating conditions which mentioned above is presented. The three-phase to ground fault is applied at the transmission line between bus 6 and 7. The highest penetration level (70%) of wind power plants is assumed. The system CFCTs corresponding to: both ED and NS operating conditions; with/without voltage control activated and introduce/not introduce the two HVDC connections are shown in Table 6.2.

Table 6.2. Critical fault clearance time comparisons with a three-phase to ground fault under different operating conditions

Wind equally distributed	DFIG with voltage control	DFIG with no voltage control
With HVDC	58 ms	50 ms
No HVDC	32 ms	20 ms
10%_north and 70% south	DFIG with voltage control	DFIG with no voltage control
With HVDC	246 ms	217 ms
No HVDC	210 ms	176 ms

The results indicate that the system transient stability can be largely improved while the HVDC connections and voltage control function are introduced. The system stability margin under NS wind speed distributed case is much better than ED case due to the relatively less transmission pressure across boundaries in NS condition.

6.2 Rate of change of frequency

6.2.1 Case 4: Frequency deviation during infeed loss

Both the winter peak & summer minimum demand conditions are tested. The future largest generation loss 1800 MW is assumed in this case. The losses are happened in the middle part (nodes N8 and N9 as indicated in Figure 5.11) of the network. The results shown in Figure 6.5 indicate that the largest frequency deviations are below 0.8 Hz which is within the infrequent infeed loss frequency drop limit defined by the UK grid code (49.2 Hz).

The RoCoF is calculated as a three cycle average based on the simulation data for the purpose of testing whether there is a risk of the protection relays to be tripped during loss of generations. The results are shown in Figure 6.6.

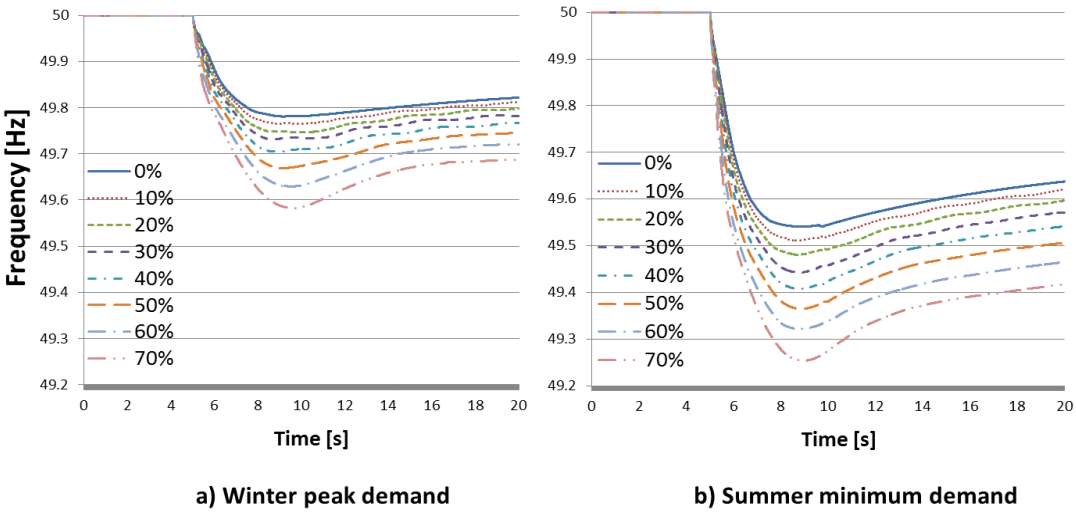

Figure 6-5. Frequency deviation with loss of 1800MW generation in middle of UK

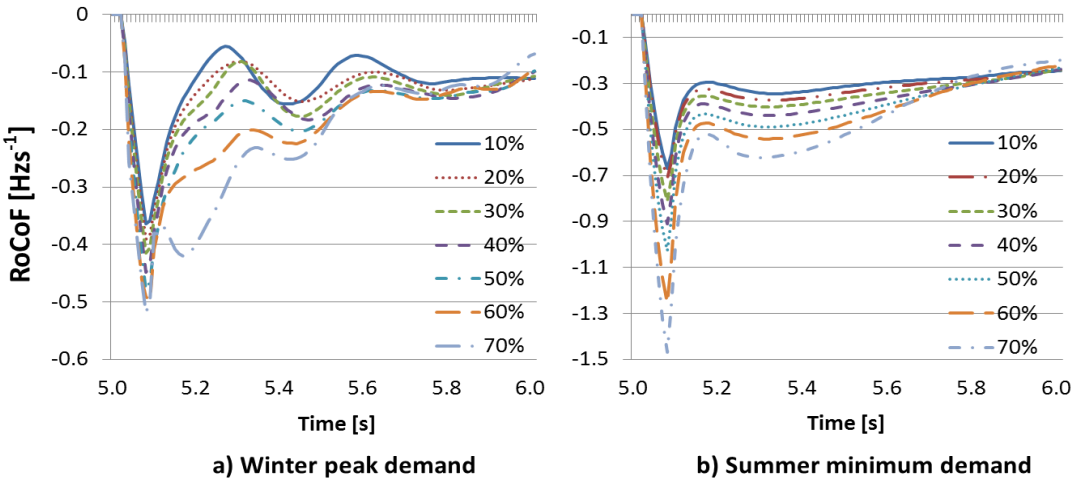

Figure 6-6. RoCoF with loss of 1800 MW generation in middle of UK

Due to the amount of total capacity of conventional generators during winter peak demand condition are still relatively high than summer minimum condition, there are not significantly increase of RoCoF. The highest RoCoF is -0.52 Hzs^{-1} which occurs at bus 9 under winter peak demand. The new recommended RoCoF setting 1 Hzs^{-1} is able to ensure that no further RoCoF-based relay will be tripped spuriously during the disturbance with the wind penetration level increased from 0%-70%. However, the highest RoCoF reaches -1.469 Hzs^{-1} under summer minimum demand condition. Under this condition, the LFDD may happen followed by further generation losses due to the spurious disconnection of the distribution networks. Hence, the following case studies are mainly focused on the RoCoF performances under summer minimum demand condition.

6.2.2 Case 5: Different amount of generation loss: RoCoF under summer minimum demand condition

During the summer minimum demand, the system total inertia is relatively lower than winter peak which may result to high rate of change of frequency. According to the ETSY [1], the minimum demand in the year 2020 is estimated as 23000 MW. The constant load is assumed for the purpose of investigating the worst case (highest RoCoF) at first. Two different amounts of generation loss are considered (1000 MW and 1800 MW) which represent the current and future largest single generator size. The loss of generation is applied in two different places: in the middle of UK (nodes N8 and N9 as indicated in Figure 5.11), and in the south of UK (nodes N12, N14 and N15). The test results are shown in Table 6.3-6.6.

Under the 1000MW loss of generation, all RoCoF values are within the new G59 recommended setting limits of 1Hzs-1 [2]. In this case there is no risk of further loss of generation due to spurious LOM protection tripping during the disturbance. However, the situations are much worse if 1800 MW generation loss is assumed.

Table 6. 3 ROCOF of the system during loss of 1000MW generation in the middle of UK

ED middle	0%	10%	20%	30%	40%	50%	60%	70%	NS middle	0%	10%	20%	30%	40%	50%	60%	70%
1	-0.332	-0.332	-0.368	-0.403	-0.452	-0.520	-0.608	-0.701	1	-0.332	-0.355	-0.378	-0.425	-0.468	-0.523	-0.625	-0.726
2	-0.332	-0.332	-0.369	-0.404	-0.452	-0.518	-0.601	-0.621	2	-0.332	-0.355	-0.357	-0.380	-0.427	-0.469	-0.523	-0.711
3	-0.336	-0.338	-0.375	-0.409	-0.456	-0.522	-0.605	-0.629	3	-0.336	-0.355	-0.362	-0.387	-0.434	-0.477	-0.533	-0.713
4	-0.331	-0.332	-0.369	-0.404	-0.452	-0.518	-0.602	-0.622	4	-0.331	-0.355	-0.356	-0.380	-0.427	-0.469	-0.524	-0.713
5	-0.334	-0.336	-0.374	-0.408	-0.456	-0.522	-0.606	-0.683	5	-0.334	-0.360	-0.385	-0.432	-0.475	-0.532	-0.628	-0.717
6	-0.339	-0.342	-0.378	-0.410	-0.456	-0.520	-0.598	-0.654	6	-0.339	-0.365	-0.390	-0.437	-0.480	-0.534	-0.625	-0.695
7	-0.349	-0.354	-0.390	-0.421	-0.465	-0.530	-0.608	-0.667	7	-0.349	-0.372	-0.401	-0.444	-0.486	-0.545	-0.631	-0.708
8	-0.367	-0.375	-0.409	-0.436	-0.477	-0.541	-0.614	-0.658	8	-0.367	-0.387	-0.419	-0.461	-0.502	-0.564	-0.642	-0.701
9	-0.351	-0.360	-0.397	-0.425	-0.468	-0.534	-0.609	-0.656	9	-0.351	-0.372	-0.406	-0.447	-0.490	-0.555	-0.633	-0.701
10	-0.360	-0.368	-0.403	-0.428	-0.469	-0.533	-0.605	-0.660	10	-0.360	-0.380	-0.412	-0.453	-0.494	-0.557	-0.634	-0.690
11	-0.326	-0.334	-0.372	-0.396	-0.437	-0.504	-0.572	-0.616	11	-0.326	-0.347	-0.383	-0.425	-0.469	-0.534	-0.608	-0.647
12	-0.298	-0.309	-0.349	-0.371	-0.413	-0.484	-0.555	-0.590	12	-0.298	-0.323	-0.361	-0.405	-0.450	-0.518	-0.573	-0.633
13	-0.262	-0.266	-0.317	-0.330	-0.372	-0.464	-0.537	-0.583	13	-0.262	-0.289	-0.329	-0.375	-0.426	-0.497	-0.561	-0.623
14	-0.278	-0.285	-0.329	-0.346	-0.385	-0.464	-0.529	-0.591	14	-0.278	-0.305	-0.345	-0.388	-0.437	-0.506	-0.579	-0.597
15	-0.267	-0.279	-0.323	-0.342	-0.385	-0.462	-0.535	-0.586	15	-0.267	-0.296	-0.335	-0.380	-0.427	-0.498	-0.576	-0.624
16	-0.252	-0.254	-0.303	-0.317	-0.358	-0.443	-0.512	-0.562	16	-0.252	-0.276	-0.315	-0.362	-0.412	-0.483	-0.560	-0.602
17	-0.260	-0.251	-0.283	-0.299	-0.342	-0.426	-0.502	-0.552	17	-0.260	-0.273	-0.293	-0.342	-0.391	-0.462	-0.544	-0.591
18	-0.336	-0.338	-0.375	-0.409	-0.456	-0.521	-0.604	-0.675	18	-0.336	-0.362	-0.387	-0.434	-0.477	-0.532	-0.627	-0.710
19	**-0.355**	**-0.357**	**-0.394**	**-0.427**	**-0.476**	**-0.545**	**-0.636**	**-0.731**	**19**	**-0.355**	**-0.395**	**-0.423**	**-0.465**	**-0.506**	**-0.565**	**-0.653**	**-0.749**
20	-0.373	-0.376	-0.411	-0.441	-0.485	-0.551	-0.635	-0.715	20	-0.373	-0.379	-0.406	-0.452	-0.495	-0.555	-0.633	-0.737
21	-0.261	-0.266	-0.315	-0.330	-0.371	-0.458	-0.527	-0.563	21	-0.261	-0.288	-0.328	-0.374	-0.424	-0.494	-0.571	-0.606

Table 6. 4 ROCOF of the system during loss of 1000MW generation in the south of UK

ED south	0%	10%	20%	30%	40%	50%	60%	70%	NS south	0%	10%	20%	30%	40%	50%	60%	70%
1	-0.244	-0.244	-0.251	-0.270	-0.287	-0.319	-0.375	-0.486	1	-0.244	-0.244	-0.248	-0.268	-0.283	-0.328	-0.448	-0.547
2	-0.243	-0.245	-0.252	-0.270	-0.287	-0.319	-0.353	-0.456	2	-0.243	-0.244	-0.247	-0.267	-0.283	-0.326	-0.445	-0.541
3	-0.240	-0.245	-0.254	-0.267	-0.285	-0.318	-0.357	-0.500	3	-0.240	-0.241	-0.247	-0.265	-0.281	-0.336	-0.456	-0.553
4	-0.243	-0.245	-0.253	-0.269	-0.287	-0.319	-0.355	-0.478	4	-0.243	-0.241	-0.248	-0.267	-0.283	-0.328	-0.447	-0.544
5	-0.240	-0.245	-0.254	-0.267	-0.286	-0.318	-0.360	-0.494	5	-0.240	-0.241	-0.247	-0.265	-0.281	-0.338	-0.458	-0.557
6	-0.237	-0.247	-0.256	-0.264	-0.283	-0.316	-0.376	-0.535	6	-0.237	-0.239	-0.247	-0.262	-0.279	-0.339	-0.457	-0.549
7	-0.232	-0.244	-0.252	-0.258	-0.286	-0.320	-0.377	-0.539	7	-0.232	-0.233	-0.241	-0.253	-0.294	-0.369	-0.489	-0.586
8	-0.240	-0.244	-0.256	-0.275	-0.325	-0.365	-0.395	-0.587	8	-0.240	-0.241	-0.248	-0.289	-0.337	-0.421	-0.541	-0.602
9	-0.229	-0.237	-0.260	-0.277	-0.327	-0.371	-0.396	-0.590	9	-0.229	-0.230	-0.251	-0.292	-0.340	-0.424	-0.543	-0.604
10	-0.237	-0.239	-0.276	-0.292	-0.343	-0.384	-0.409	-0.600	10	-0.237	-0.241	-0.265	-0.306	-0.352	-0.439	-0.557	-0.635
11	-0.241	-0.247	-0.300	-0.301	-0.359	-0.400	-0.511	-0.612	11	-0.241	-0.246	-0.279	-0.319	-0.361	-0.457	-0.537	-0.611
12	-0.272	-0.328	-0.381	-0.411	-0.433	-0.474	-0.571	-0.677	12	-0.272	-0.314	-0.343	-0.378	-0.414	-0.494	-0.557	-0.646
13	-0.364	-0.396	-0.438	-0.413	-0.481	-0.523	-0.596	-0.687	13	**-0.364**	**-0.388**	**-0.422**	**-0.460**	**-0.501**	**-0.564**	**-0.636**	**-0.728**
14	**-0.305**	**-0.450**	**-0.482**	**-0.537**	**-0.580**	**-0.627**	**-0.651**	**-0.756**	14	-0.305	-0.348	-0.372	-0.405	-0.433	-0.566	-0.609	-0.658
15	-0.328	-0.384	-0.408	-0.437	-0.484	-0.588	-0.612	-0.691	15	-0.328	-0.422	-0.462	-0.429	-0.492	-0.545	-0.607	-0.662
16	-0.347	-0.439	-0.477	-0.508	-0.537	-0.637	-0.686	-0.727	16	-0.347	-0.378	-0.410	-0.442	-0.507	-0.551	-0.614	-0.681
17	-0.350	-0.438	-0.470	-0.502	-0.528	-0.608	-0.649	-0.702	17	-0.350	-0.379	-0.418	-0.449	-0.489	-0.539	-0.599	-0.646
18	-0.239	-0.245	-0.254	-0.266	-0.285	-0.317	-0.361	-0.506	18	-0.239	-0.239	-0.247	-0.264	-0.281	-0.337	-0.457	-0.554
19	-0.229	-0.241	-0.250	-0.262	-0.290	-0.328	-0.405	-0.525	**19**	-0.229	-0.236	-0.244	-0.258	-0.293	-0.366	-0.491	-0.573
20	-0.234	-0.242	-0.250	-0.259	-0.305	-0.344	-0.404	-0.507	20	-0.234	-0.234	-0.241	-0.260	-0.310	-0.387	-0.512	-0.609
21	-0.342	-0.432	-0.467	-0.524	-0.573	-0.618	-0.642	-0.745	21	-0.342	-0.375	-0.406	-0.442	-0.509	-0.576	-0.618	-0.706

Table 6. 5 ROCOF of the system during loss of 1800MW generation in the middle of UK

ED middle	0%	10%	20%	30%	40%	50%	60%	70%	NS middle	0%	10%	20%	30%	40%	50%	60%	70%
1	-0.578	-0.6	-0.669	-0.74	-0.842	-0.988	-1.188	-1.418	1	-0.578	-0.641	0.674	-0.776	-0.875	-0.98	-1.217	-1.485
2	-0.58	-0.602	-0.671	-0.741	-0.84	-0.984	-1.178	-1.382	2	-0.58	-0.643	-0.676	-0.777	-0.874	-0.975	-1.207	-1.466
3	-0.587	-0.612	-0.681	-0.751	-0.85	-0.995	-1.188	-1.387	3	-0.587	-0.652	-0.688	-0.789	-0.887	-0.992	-1.223	-1.475
4	-0.579	-0.602	-0.671	-0.742	-0.842	-0.985	-1.18	-1.385	4	-0.579	-0.643	-0.677	-0.777	-0.875	-0.977	-1.209	-1.469
5	-0.584	-0.609	-0.679	-0.75	-0.85	-0.994	-1.188	-1.39	5	-0.584	-0.649	-0.686	-0.785	-0.884	-0.989	-1.218	-1.478
6	-0.595	-0.62	-0.689	-0.757	-0.854	-0.995	-1.18	-1.347	6	-0.595	-0.661	-0.697	-0.795	-0.892	-0.992	-1.217	-1.456
7	-0.618	-0.643	-0.712	-0.777	-0.872	-1.013	-1.197	-1.366	7	-0.618	-0.674	-0.719	-0.807	-0.902	-1.011	-1.223	-1.473
8	-0.638	-0.657	-0.727	-0.787	-0.878	-1.018	-1.193	-1.343	8	-0.638	-0.675	-0.733	-0.809	-0.903	-1.026	-1.223	-1.46
9	-0.659	-0.683	-0.752	-0.809	-0.898	-1.036	-1.21	-1.349	9	-0.659	-0.697	-0.756	-0.827	-0.918	-1.041	-1.232	-1.473
10	-0.617	-0.642	-0.713	-0.772	-0.862	-1.002	-1.176	-1.324	10	-0.617	-0.66	-0.719	-0.794	-0.887	-1.011	-1.207	-1.441
11	-0.601	-0.621	-0.693	-0.747	-0.834	-0.976	-1.142	-1.257	11	-0.601	-0.64	-0.702	-0.774	-0.866	-0.989	-1.181	-1.392
12	-0.534	-0.554	-0.6.2	-0.683	-0.772	-0.923	-1.029	-1.226	12	-0.534	-0.581	-0.645	-0.716	-0.808	-0.941	-1.139	-1.347
13	-0.48	-0.489	-0.579	-0.614	-0.702	-0.876	-1.047	-1.195	13	-0.48	-0.527	-0.594	-0.667	-0.764	-0.897	-1.089	-1.303
14	-0.5	-0.514	-0.596	-0.638	-0.723	-0.882	-1.043	-1.157	14	-0.5	-0.549	-0.615	-0.687	-0.781	-0.907	-1.102	-1.288
15	-0.48	-0.504	-0.586	-0.633	-0.723	-0.881	-1.052	-1.206	15	-0.48	-0.532	-0.599	-0.673	-0.769	-0.903	-1.1	-1.316
16	-0.45	-0.466	-0.553	-0.589	-0.676	-0.842	-1.007	-1.138	16	-0.45	-0.5	-0.567	-0.641	-0.738	-0.869	-1.061	-1.256
17	-0.412	-0.431	-0.519	-0.558	-0.647	-0.812	-0.984	-1.14	17	-0.412	-0.462	-0.529	-0.604	-0.704	-0.838	-1.032	-1.243
18	-0.588	-0.613	-0.683	-0.752	-0.851	-0.995	-1.186	-1.379	18	-0.588	-0.653	-0.689	-0.788	-0.886	-0.989	-1.218	-1.472
19	**-0.609**	**-0.634**	**-0.705**	**-0.776**	**-0.879**	**-1.017**	**-1.231**	**-1.469**	**19**	**-0.609**	**-0.67**	**-0.714**	**-0.809**	**-0.91**	**-1.026**	**-1.256**	**-1.539**
20	-0.632	-0.658	-0.727	-0.793	-0.889	-1.032	-1.225	-1.439	20	-0.632	-0.686	-0.735	-0.819	-0.917	-1.034	-1.247	-1.517
21	-0.475	-0.487	-0.575	-0.612	-0.699	-0.867	-1.034	-1.166	21	-0.475	-0.523	-0.59	-0.663	-0.759	-0.89	-1.083	-1.283

Table 6. 6 ROCOF of the system during loss of 1800MW generation in the south of UK

ED south	0%	10%	20%	30%	40%	50%	60%	70%	NS south	0%	10%	20%	30%	40%	50%	60%	70%
1	-0.421	-0.475	-0.498	-0.523	-0.553	-0.593	-0.747	-1.054	1	-0.421	-0.439	0.476	-0.525	-0.565	-0.616	-0.758	-1.021
2	-0.417	-0.474	-0.497	-0.522	-0.553	-0.593	-0.733	-0.963	2	-0.417	-0.437	-0.474	-0.525	-0.566	-0.618	-0.708	-0.996
3	-0.407	-0.463	-0.488	-0.514	-0.546	-0.593	-0.753	-0.956	3	-0.407	-0.428	-0.466	-0.517	-0.558	-0.612	-0.725	-1.017
4	-0.416	-0.472	-0.496	-0.520	-0.552	-0.592	-0.738	-0.968	4	-0.416	-0.436	-0.473	-0.524	-0.565	-0.617	-0.711	-1.004
5	-0.406	-0.464	-0.488	-0.513	-0.546	-0.597	-0.761	-0.958	5	-0.406	-0.428	-0.465	-0.517	-0.559	-0.613	-0.723	-1.029
6	-0.396	-0.456	-0.481	-0.507	-0.540	-0.591	-0.742	-1.032	6	-0.396	-0.419	-0.458	-0.510	-0.551	-0.616	-0.778	-0.991
7	-0.389	-0.434	-0.458	-0.485	-0.532	-0.654	-0.813	-1.047	7	-0.389	-0.407	-0.441	-0.493	-0.555	-0.620	-0.779	-1.069
8	-0.403	-0.422	-0.453	-0.529	-0.622	-0.752	-0.917	-1.128	8	-0.403	-0.424	-0.464	-0.521	-0.603	-0.714	-0.824	-1.157
9	-0.386	-0.407	-0.459	-0.542	-0.633	-0.763	-0.925	-1.152	9	-0.386	-0.441	-0.482	-0.538	-0.649	-0.754	-0.846	-1.172
10	-0.391	-0.422	-0.483	-0.565	-0.657	-0.786	-0.947	-1.161	10	-0.391	-0.452	-0.493	-0.572	-0.657	-0.770	-0.921	-1.173
11	-0.402	-0.476	-0.534	-0.613	-0.696	-0.815	-0.953	-1.287	11	-0.402	-0.477	-0.523	-0.652	-0.755	-0.853	-1.151	-1.149
12	-0.529	-0.605	-0.656	-0.731	-0.807	-0.925	-1.057	-1.308	12	-0.529	-0.614	-0.652	-0.708	-0.788	-0.882	-1.167	-1.228
13	-0.695	-0.704	-0.760	-0.734	-0.887	-0.920	-1.174	-1.314	13	**-0.695**	**-0.743**	**-0.781**	**-0.930**	**-1.028**	**-1.105**	**-1.314**	**-1.438**
14	**-0.619**	**-0.793**	**-0.854**	**-0.941**	**-1.032**	**-1.172**	**-1.315**	**-1.566**	14	-0.619	-0.707	-0.746	-0.811	-0.874	-0.976	-1.086	-1.219
15	-0.654	-0.732	-0.774	-0.842	-0.912	-1.032	-1.161	-1.442	15	-0.654	-0.740	-0.757	-0.767	-0.831	-0.905	-1.197	-1.327
16	-0.671	-0.845	-0.894	-0.969	-1.045	-1.169	-1.289	-1.436	16	-0.671	-0.762	-0.830	-0.894	-0.963	-1.018	-1.176	-1.399
17	-0.664	-0.828	-0.887	-0.946	-1.024	-1.138	-1.274	-1.419	17	-0.664	-0.761	-0.843	-0.907	-0.987	-1.008	-1.103	-1.392
18	-0.405	-0.462	-0.486	-0.512	-0.545	-0.594	-0.753	-0.969	18	-0.405	-0.426	-0.464	-0.516	-0.557	-0.612	-0.733	-1.016
19	-0.395	-0.450	-0.474	-0.499	-0.533	-0.659	-0.842	-1.121	19	-0.395	-0.449	-0.474	-0.554	-0.596	-0.699	-0.802	-1.139
20	-0.387	-0.430	-0.453	-0.481	-0.562	-0.693	-0.872	-1.034	20	-0.387	-0.404	-0.437	-0.485	-0.528	-0.592	-0.732	-1.153
21	-0.669	-0.834	-0.895	-0.975	-1.057	-1.186	-1.313	-1.516	21	-0.669	-0.758	-0.868	-0.879	-0.932	-0.989	-1.109	-1.430

For the disturbance applied near the middle part of the network, the higher RoCoF can be found in the north and central part in both ED and NS distribution conditions. Under the ED condition, the highest RoCoF occurred at bus 19 (-1.469 Hzs^{-1}) while under NS condition, it reaches (-1.539 Hzs^{-1}). It should be noted that these values are much higher than the new proposed setting 1 Hzs^{-1}. The test results indicate that the RoCoF can potentially exceed the planned new setting when the wind penetration level reaches approximately 50%.

Additionally, an interesting issue should be noticed that the RoCoF are relative smaller under ED condition than that under NS condition in this case. Although the DFIG is partially decoupled from the grid, it is not completely inertia-less if the wind turbine is P regulated according to [6]. The decrease of the ω_s is compensated by the i_{qr} which may lead to an increase in electrical torque T_e. Since the mechanical torque is unchanged, this creates the decelerating torque. Thus, the onshore DFIG may still have little inertia support to the grid during disturbance even if the contribution is relatively small. Under high wind penetration conditions, the amount of inertia support may have a significant influence on the system frequency performance.

The results are somewhat different when the disturbance occurs in the south part. The RoCoF under ED condition are much higher than that under NS condition. Due to the lack of conventional generation inertia support and less capacity of DFIG generating in south region under ED, the highest RoCoF occurs at bus 14 (London with a value -1.566 Hzs^{-1}) among all the cases. Similar to above test, more DFIG capacity distributed in the south made the RoCoF lower under NS condition than that under ED condition. The system may have a higher RoCoF (exceeds 1 Hzs^{-1}) if the wind penetration level is reached 40% in this case.

To further investigate the influence of the amount of generation loss on the RoCoF, the amount of generation loss was increased gradually from 1000 MW while the wind penetration level was fixed to 70%. The worst cases (fault occurs in south under ED condition & fault occur in middle under NS condition) are analysed. It was found that the RoCoF reaches 1 Hzs-1 when the generation loss is 1335 MW and 1370 MW for ED and NS conditions respectively as shown in Table 6.7.

Table 6.7. Generation loss limit with RoCoF reaches 1 Hzs^{-1}

ED South 1335MW Loss	70% Bus 14	NS Middle 1370MW Loss	70% Bus 19
1	-0.688	1	-0.967
2	-0.633	2	-0.951
3	-0.663	3	-0.955
4	-0.636	4	-0.953
5	-0.655	5	-0.959
6	-0.698	6	-0.938
7	-0.706	7	-0.952
8	-0.759	8	-0.944
9	-0.765	9	-0.950
10	-0.777	10	-0.930
11	-0.878	11	-0.887
12	-0.893	12	-0.863
13	-0.812	13	-0.841
14	**-1.008**	14	-0.820
15	-0.884	15	-0.845
16	-0.946	16	-0.804
17	-0.895	17	-0.799
18	-0.670	18	-0.953
19	-0.735	19	**-1.005**
20	-0.696	20	-0.992
21	-0.894	21	-0.824

Hence, additional actions needed to be considered in order to maintain system integrity in the future. One option is to further increase the protection setting value in order to avoid spurious tripping under this kind of disturbance or introduce a time delay on the relay during the transient high peak value occurred. However, by doing so may, the non-detection zone of the anti-islanding protection will be increased which can cause undesirable hazards in the network.

6.2.3 Case 6: Different amount of primary frequency response

The above case shows the potential risk that high RoCoF (higher than 1 Hzs-1) may occur when the largest loss of generation limit increases to 1800 MW. This case explores if the provision of additional primary frequency response can somewhat help this situation (perhaps provided by non-synchronous generators as a special service in the future [2]). Therefore, in the UK model the amount of primary frequency response (PFR) was increased from 10% to 20% in order to verify if this

may help to reduce the RoCoF. The loss of generation is assumed to occur in the middle part. The results are shown in Table 6.8 and illustrated in Figure 6.7.

It can be seen that the RoCoF has been reduced with the additional 10% primary frequency response. For both ED and NS distribution conditions, the highest RoCoF is contained within 1Hzs-1 even with wind penetration level reaching 50%.

Table 6.8. RoCoF of system during loss of 1800 MW generation: 10%(PFR) vs 20%(PFR)

PFR	10% vs 20% (10% Penetration)		10% vs 20% (30% Penetration)		10% vs 20% (50% Penetration)		10% vs 20% (70% Penetration)	
ED	-0.635	-0.592	-0.776	-0.745	-1.028	-0.955	-1.470	-1.305
NS	-0.671	-0.645	-0.809	-0.776	-1.027	-0.963	-1.539	-1.378

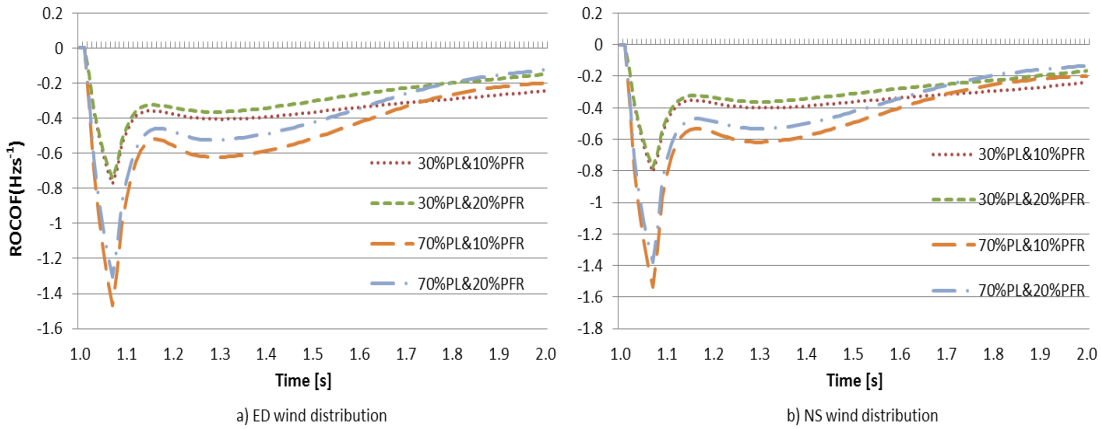

Figure 6-7. System RoCoF during loss of 1800 MW generation at changing PFR

However, it is evident that even at 20% PFR the improvement is not significant and the RoCoF values are still higher than 1 Hzs-1 if wind penetration level increases above 50%. Therefore, in the future it may be necessary to seek additional transient active power support during the loss of generation using other techniques capable of providing near instantaneous response. The synthetic inertia may be an alternative solution to provide transient active power support during the loss of generation [2, 7]. The UK grid code has mentioned that all the onshore/offshore wind farms (larger than 50 MW) should provide speed droop support to the system (normally 10% of its rated power output) in the future. Since the additional speed droop control signal is controlled by the electronic device in rotor sider converter control, it can provide faster response than the conventional turbine governor control.

6.2.4 Case 7: Load response to frequency deviation

In this section frequency dependency of loads is investigated. The IEELBL load frequency model is used [8]. It is assumed that 1% frequency deviation results in 1%-4% active power demand variation (APD) [9]. The tests are based on ED wind distributed condition. The disturbances are applied in the middle section of the network. The highest RoCoF values for increasing wind penetration level are presented in Table 6.9.

Table 6.9. System RoCoF during loss of 1800MW generation under varying APD

ED Middle	0%	10%	20%	30%	40%	50%	60%	70%
Constant	-0.609	-0.634	-0.705	-0.776	-0.879	-1.017	-1.231	-1.469
1%APD	-0.603	-0.628	-0.698	-0.767	-0.867	-1.010	-1.209	-1.441
2%APD	-0.598	-0.623	-0.690	-0.758	-0.856	-0.995	-1.188	-1.418
3%APD	-0.593	-0.617	-0.683	-0.750	-0.845	-0.981	-1.168	-1.394
4%APD	-0.587	-0.611	-0.676	-0.741	-0.834	-0.967	-1.149	-1.372

Results indicate that the frequency dependent load has a definite ability to reduce the RoCoF even though the improvement does not appear dramatic. Therefore, the amount of change in active power demand corresponding to 1% frequency deviation was further increased to 20% in order to determine whether more significant reduction of RoCoF is achievable. It is envisaged that higher values of APD may be implemented in the future using, for example, fast demand shedding [2, 10].

Table 6.10. RoCoF during loss of 1800 MW generation at increasing frequency dependency of demand (70% wind penetration)

2% APD	4% APD	6% APD	8% APD	10% APD	12% APD	14% APD	16% APD	18% APD	20% APD
-1.418	-1.372	-1.331	-1.293	-1.258	-1.226	-1.197	-1.169	-1.142	-1.114

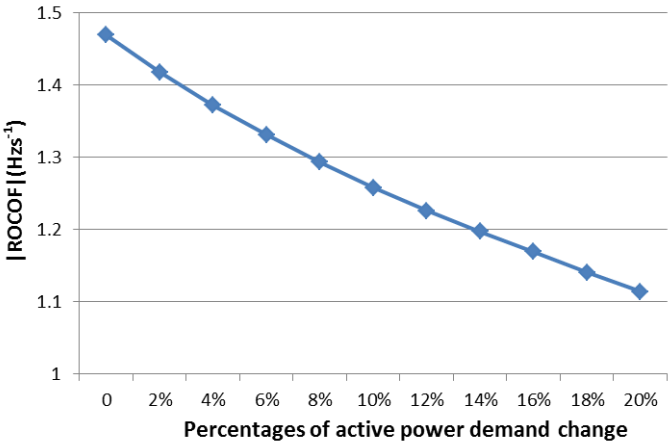

Figure 6-8. RoCoF at increasing frequency dependency of demand (70% wind penetration)

It can be seen from Figure 6.8, the relation between the amount of active power demand response and RoCoF is generally not linear. The improvement is more significant within the first 6% and gradually reduces as the demand response is increased. Nonetheless, the highest ROCOF under 70% wind penetration is still higher than 1Hzs-1 which indicates that frequency dependent demand response alone cannot provide a complete solution to the issue of high RoCoF.

6.3 Summary

The future frequency performances are analysed in two major areas: rate of change of frequency and transient stability. Testing results show that the reactive power control system built-in the WT3 model can have significant help on system transient stability. With the increasing penetration level of wind farms, the system transient stability decrease quite a lot. There are several cases with the network CFCT is less than 80ms (ED 70% fault at line 6-7, 58 ms/ 50%, 60%&70% fault at line 8-10, 75 ms, 48 ms&28 ms). The reactive power control in the future is one of the major challenges. The reactive power compensator is one option to improve the transient stability. The results indicate that with the additional 5 SVC added in the central part of the network, the system can remain stable and voltage is able to recover back.

The two new HVDC connections provide a strong support to the transmission capacity between Scotland and England. It is demonstrated that the system is able to remain stable with suddenly loss of western connections from Scotland to England in

most cases except for the 60% and 70% equal distribution conditions. Also, it is concluded that the north south wind distribution condition has better transient stability than the equal distribution condition since the power flow pressures across each boundary are relatively small.

The system RoCoF is another important issue need to be resolved. In all cases, there is no risk of LFDD may happen with 1000 MW generation loss. However, the RoCoF during loss of 1800 MW generation will be above 1 Hzs^{-1} when the wind penetration level is higher than 40%. With additional primary frequency response or frequency dependent load, it is possible to reduce the RoCoF. However, none of them can address the problem of high RoCoF under high wind penetration level (above 60%) alone. Hence, whether selecting a new RoCoF setting, introducing inertia support from the non-synchronous generators (DFIG) or introduce frequency dependent demand or even utilise a combination of all those factors will remain a challenge for future studies. Detailed cost benefit analysis is needed to determine the best course of action.

References

[1] National Grid, "*Electricity Ten Year Statement 2014*", http://www.nationalgrid.com/uk/electricity/ten-year-statement

[2] National Grid, "*Future Operability Framework*", Sep. 2014, pp.1-34

[3] National Grid, "*Grid code Report*", November 2011, pp.11-61, http://www2.nationalgrid.com/UK/Industry-information/Electricity-codes/Grid-code/The-Grid-code/

[4] P. Kundur, "*Power System Stability and Control*", McGraw-Hill, Inc., NY, 1993

[5] G. J W. Dudgeon, W.E. Leithead, A. Dysko, J. O'Reilly, *et al*., "The Effective Role of AVR and PSS in Power Systems: Frequency Response Analysis," *Power Systems, IEEE Transactions on* , vol.22, no.4, Nov. 2007, pp.1986-1994

[6] M. Kayikci, J.V. Milanović, "Dynamic Contribution of DFIG-Based Wind Plants to System Frequency Disturbances," *Power Systems, IEEE Transactions on* , vol.24, no.2, May 2009, pp.859-867

[7] G. Ramtharan, J.B. Ekanayake, N. Jenkins, "Frequency support from doubly fed induction generator wind turbines," *IET Renewable Power Generation,* vol.1, no.1, March 2007, pp.3-9

[8] *PSS/ETM Program Application Guide*, Volumes I and II, Power Technologies International

[9] M.Y. Akhtar, "Frequency-dependent dynamic, representation of induction-motor loads," *Proceedings of the Institution of Electrical Engineers*, vol. 115, no. 6, June 1968, pp.802-812

[10] M.Q. Ahsan, A.H. Chowdhury, S.S. Ahmed, *et al*., "Technique to Develop Auto Load Shedding and Islanding Scheme to Prevent Power System Blackout," *Power System, IEEE Transaction on*, vol. 27, no. 1, Jan. 2012, pp.198-205

CHAPTER 7: CONCLUSIONS AND RECOMMENDATION FOR FUTURE WORK

7.1 General Conclusion

Wind energy has been developed rapidly during the past decades due to its no-carbon emission characteristic. In many countries, electricity companies already considered clean energy as one of the most important elements of their future energy plans. For example, the National Grid has mentioned that the UK transmission network will face significant changes in the next few decades, as new generation and network operation technologies (including demand side management) gradually change the pattern of electricity transmission in UK.

Up until recently power systems have been primarily energised by thermal plants which have relatively high inertia constants, and the ability to provide primary and secondary frequency response during frequency deviations. However, the converter-connected variable speed wind turbines cannot provide similar frequency response. In the past, when penetration levels of such sources were relatively low, the lack of frequency response was not considered important. Even the prospect of spurious disconnection of these sources during the system wide disturbance was not of major concern. The system frequency and voltage could be maintained within acceptable limits by using the existing conventional synchronous generators. However, when the penetration level of these non-synchronous sources increases to a certain level, a new set of problems occurs.

Hence, the research presented in this thesis aims to systematically assess the frequency performance of the transmission system with a high penetration level of wind power plants which are represented as Doubly Fed Induction Generators (DFIG). One of the key novel contributions of this research is to quantify the potential risks in the system with the increasing penetration level of wind plants. The evaluation is undertaken using an equivalent model of the UK system with the inclusion of the anticipated future system scenarios. The system performance is assessed by analysing following factors: load flow, reactive power capability, transient stability and RoCoF.

Good understanding of wind energy is necessary before analysing the system frequency performance. The reasons why the DFIG based source cannot provide inertia support to the system are explained through the introduction of the aerodynamic characteristic, rotor side converter control system, and pitch angle control system of the wind turbine. The built-in GE WT3 model in PSS/E software is used.

In order to achieve an accurate prediction of the system frequency response, a reduced representative UK dynamic model has been developed and validated. Because the contemporary power system is very large, it is impractical to model the system in full detail. Therefore, appropriate network reduction methods were sought to reduce the size of the system by eliminating or aggregating bus nodes. There are two system equivalencing methods, referred to as: modal method and coherency method. The modal method analyses the various modes of oscillations which exist in the system by linearizing the non-linear differential equations. This way the non-dominant modes are eliminated. However, such equivalent model may not guarantee acceptable performance during the major system disturbances. Hence, coherency method is also used. The coherent groups of generators are identified and the elimination of the buses is accomplished by the network reduction method. In 1980s, there were three main approaches in network reduction area: Dimo's method, Zhukov's method and Ward method. The core concept of these node reduction methods is to remove/aggregate external nodes in such a way that they will not change the current and voltage (I_R and V_R) at retained buses. Dimo's method was usually applied for steady-state analysis, however it may create fictitious impedances as the transfer matrix changes during the reduced network nodal matrix calculation. Zhukov's method was suitable for transient study. Unlike Dimo's method, the calculation of the equivalent network does not create fictitious connections. Among these methods, Ward's method was the simplest network reduction method and was widely used. Its principle was to eliminate selected nodes (termed external nodes) and retain all the remaining nodes (termed internal nodes). Later, extended Ward equivalent was developed with all generator nodes retained for the purposes of improving accuracy.

However, all the methods mentioned above have their disadvantages and limitations: need the original system data in order to create the state-space linear model or electrical transmission network nodal matrix. Therefore, in this thesis, it was considered impractical to establish the equivalent UK system using these methods. Hence, a new network equivalent method was developed. The processes of this method can be summarised in three main steps:

1) Development of the equivalent model for load flow studies. In this step, the coherent groups of generators and the retained nodes should be defined; also the method used to calculate the equivalent transmission line must be carried out.
2) Dynamic parameter setting which determines the parameters of the transfer functions of control devices with the assistance of small signal analysis and Bode frequency analysis.
3) The last important step is to validate this reduced model by comparing the simulation results to several historical data records of actual system events.

According to the National Grid Ten Year Statement (ETYS), the UK transmission system is divided into 17 study zones. Hence, each zone is represented by one node. The nodes which are close to large power plants or main transmission lines are chosen as the aggregated nodes. Four extra nodes are added depending on the power transfers to adjacent zones and network density. Transmission line impedance is calculated through the known sending and receiving end power flow information which can be obtained from the ETYS. In order to calculate the required parameters in a more efficient way, a Matlab based tool with convenient Graphical User Interface is developed. The 21-bus UK equivalent transmission system is finally established.

Through eigenvalue analysis, one unstable real mode and two lightly damped interarea modes were initially identified before any control device was attached to the generators. With the help of automatic voltage regulators (AVR), the unstable real mode was eliminated. However, new oscillatory modes appeared due to the negative impact on system damping after the application of these excitation systems. These oscillatory modes were analysed using eigenvectors to demonstrate that there were three major oscillation modes present among the generators in Scotland,

England (middle part) and England (South) &Wales. In order to decouple the cross-coupling effects between control loops, the individual channel analysis and design (ICAD) method was introduced. The multivariable system structure was decomposed into several single-input and single-output individual channels. This greatly helped to make the decision on choosing the appropriate locations and transfer functions of the power system stabiliser (PSS). There were eight PSSs in total attached to the generators. The transient stability margin of the system was significantly improved with the implementation of these PSSs. A final check was performed by the time domain case study which indicated that the installation of the PSSs provided a robust damping performance compared to the system without them.

The proposed method was compared with the Ward method by using the well-known IEEE 14 buses system. The power flow simulation indicated that the proposed method could not only maintain the system transmission structure without adding any fictitious branches but also had similar load flow results compared to those based on the original system data. Moreover, the dynamic time domain simulation was assessed under loss of generation condition. The result demonstrated that the proposed method could accurately replicate well-matched swing curves simulated from original system, and at the same time, also delivered slightly higher accuracy compared to Ward method.

In addition, two known system incidents were utilized to validate the dynamic performance of the equivalent UK system model: The first one was based on the Phasor Measurement Unit (PMU) data records and the other is based on the well-known “UK loss of generation incident on May 2008” incident. In order to test the system performance under different loading conditions, a dedicated method was proposed which utilized the Balancing Mechanism Reporting System (BMRS). Through BMRS website the historical generation and demand distribution profiles on any specific day are accessible. The close match of frequency traces between the equivalent system and the real system event records was observed which confirmed that the established equivalent UK system was able to reflect the existing system response during the disturbance.

For the purpose of analysing the future system frequency performance, the model was extended to represent a future UK transmission system with planned

reinforcements and high penetration of wind according to the UK Gone Green scenario. Reinforcements in the transmission system taken into account include rebuilding the transmission lines in Scotland and installation of two new HVDC connections between Scotland and England. Test results showed that although the built-in reactive power control systems of the DFIG model can provide considerable support and improve the system transient stability, the critical fault clearance time (CFCT) of system is still significantly reduced with the increasing penetration level of wind farms. In some cases, it can be less than 80ms. Appropriate amount of reactive power compensation should be added to ensure the security of transient performance of the system. For a fault on west coast connection with (evenly distributed) ED 70% condition, the minimum CFCT requirement was achieved by installing additional 5 static var compensators (300MVAr rating) to the central part of England.

Nevertheless, the system transmission capacity across the boundaries is largely enhanced by the two new HVDC connections. The sudden loss of the western connection between Scotland and England was tested where both of the circuits were tripped 80ms after a three-phase fault. The results showed that the system was able to remain stable during the disturbance with the help of two HVDC lines except for 60% & 70% ED wind generation scenario. Also, it was concluded that the 10% North and 70% South (NS) wind power distribution condition had better transient stability than the ED condition since the power flow pressures across each boundary are relatively small.

With increasing penetration levels of converter-connected wind turbines, the system rate of change of frequency (RoCoF) gradually increases which will pose a major challenge in the future, especially under summer minimum demand condition. Among all the simulation results, the highest RoCoF during loss of 1800MW generation can be observed. In some cases the values can exceed $1\mathrm{Hz}s^{-1}$ (new proposed setting limit) if the wind penetration level is higher than 40%. The distribution networks may have high risk of spurious disconnection from the grid if no additional support is provided. Although the system RoCoF can be reduced with the help of increasing amount of primary frequency response or by introducing frequency dependent demand in the network, none of them can secure a reliable

solution alone. The system may still face the risk of high RoCoF if the wind penetration level reaches 60%. Cost benefit analysis is needed to determine the best actions in the future.

7.2 Recommendations for Future Work

The work presented in this thesis has proposed a modelling framework as well as achieved many interesting observations regarding future UK system frequency performance. Based on the outcome of this work, there are still a number of interesting research avenues which should be explored in the future. These could be summarised as follows:

- More detailed dynamic modelling of the HVDC connections. The current equivalent model does not fully represent the effect from the offshore wind farms which have been modelled as negative loads. Such detailed HVDC modelling could lead to the development of frequency support solutions based on the synthetic inertia control technique.
- Application of the frequency response control loop within the wind turbine system in order to achieve fast frequency response and to support system stability.
- Investigation of the scenarios associated with other types of system reinforcements providing reactive power compensation such as: SVC, STATCOM, series compensators, etc. The analysis would identify appropriate locations to install these devices with the consideration of how they may influence the oscillatory performance.
- Analysis of system RoCoF with the assistance of synthetic inertia response from wind power plants, introduction of more rapid frequency response services, or utilisation of a combination of all those influencing factors based on cost benefit analysis.

APPENDIX A : GB TRANSMISSION SYSTEM WITH LARGE POWER STATIONS

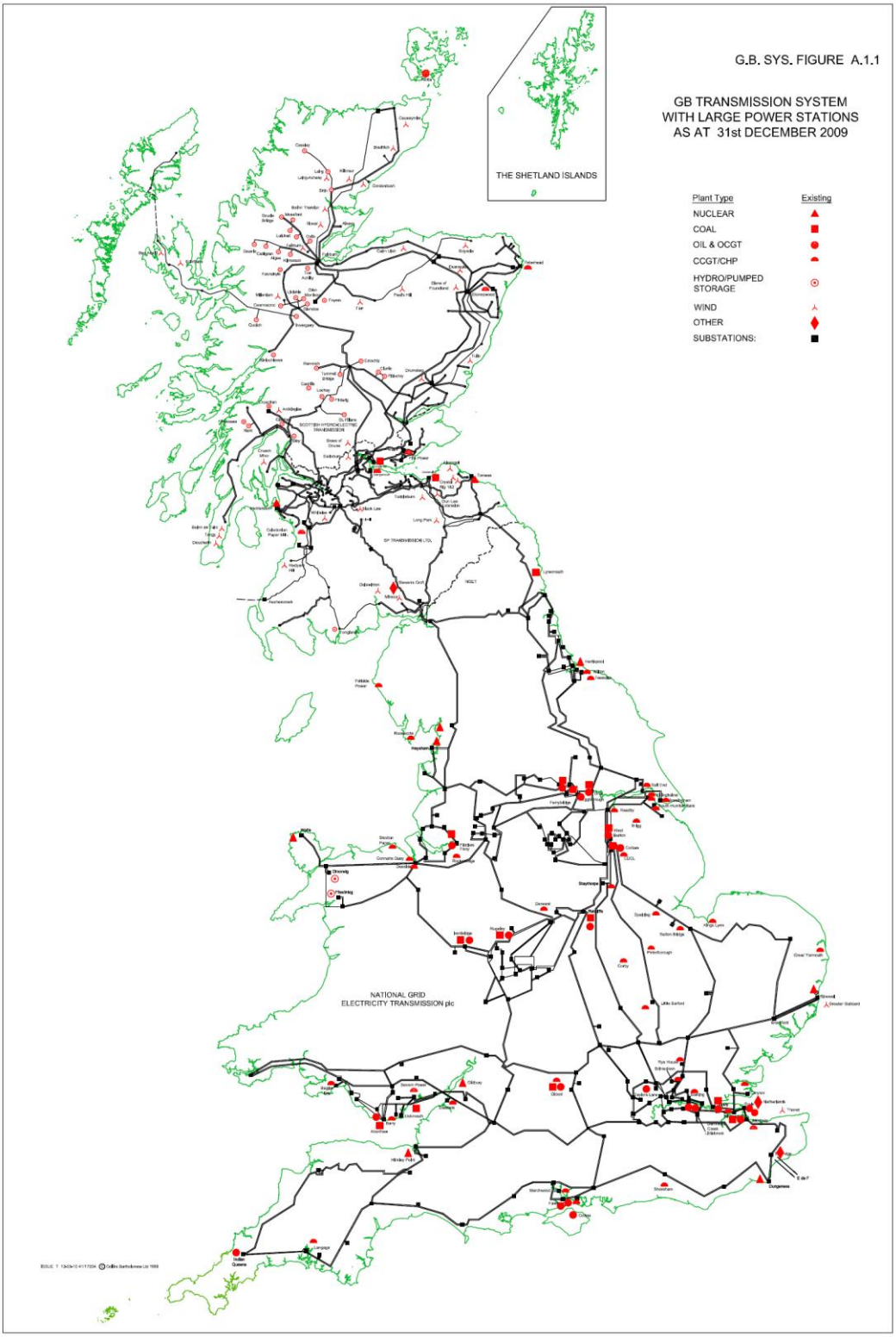

Figure a: GB Transmission system with large power station 2010

APPENDIX B : GB TRANSMISSION BOUNDARIES AND SYS STUDY ZONES

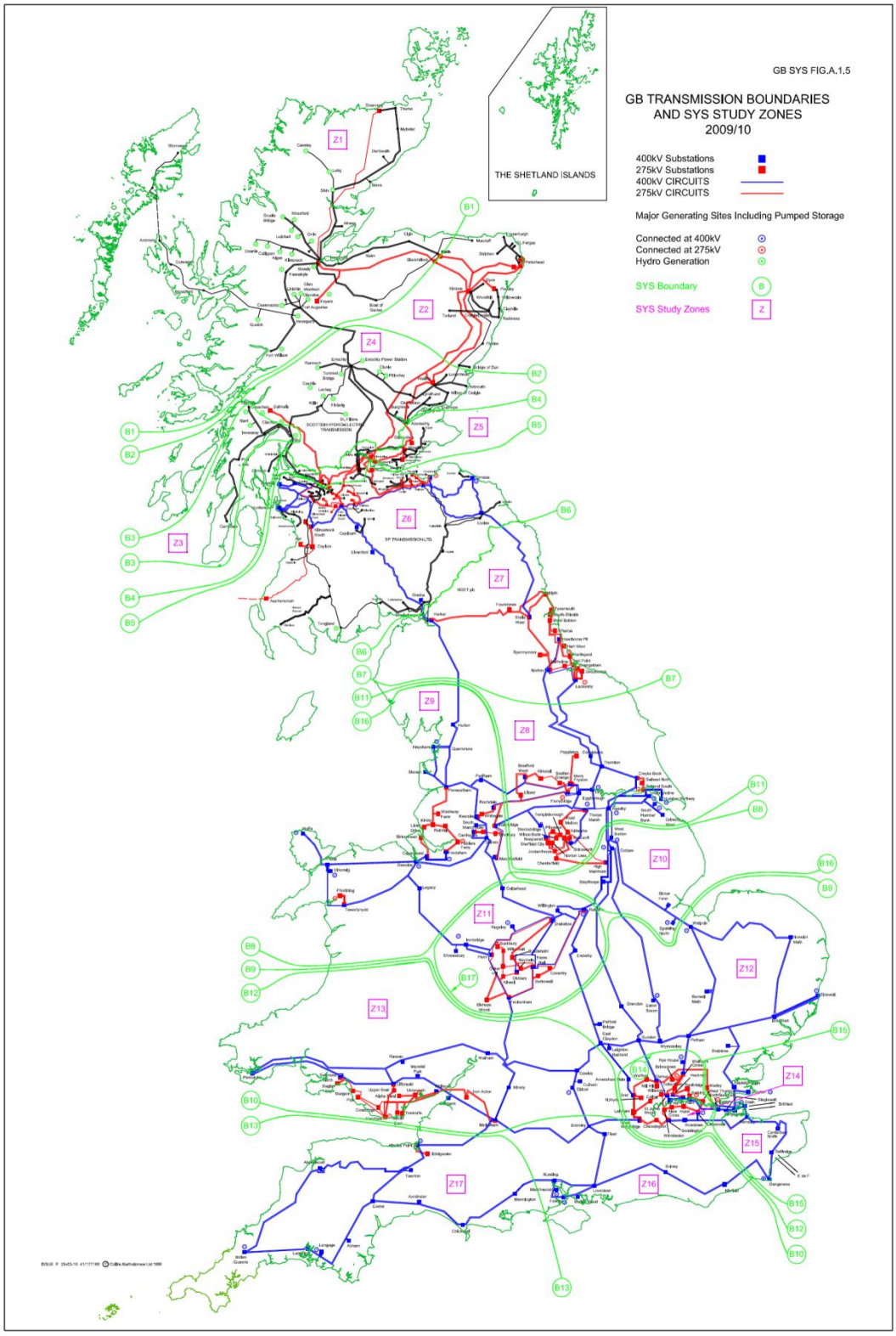

Figure b : GB Transmission boundaries and SYS study zones

APPENDIX C : GENERATION AND DEMAND PROFILE: STUDY BOUNDARY BASED

Generation and Demand Profile

Studied Boundary Generation, Demand and Transfer (MW)								
Boundary	Name	Quantity (MW)	10/11	11/12	12/13	13/14	14/15	15/16
B1	SHETL	Effective Generation	870	899	887	1131	1453	1444
B1	SHETL	Demand	479	490	489	483	492	496
B1	SHETL	Planned Transfer	391	409	398	648	961	948
B2	SHETL	Effective Generation	2120	2143	2160	2393	2906	2888
B2	SHETL	Demand	1051	1054	1055	1043	1063	1055
B2	SHETL	Planned Transfer	1069	1089	1105	1350	1843	1833
B3	SLOY	Effective Generation	306	305	301	327	323	321
B3	SLOY	Demand	59	51	51	52	52	58
B3	SLOY	Planned Transfer	247	254	250	275	271	263
B4	SHETL	Effective Generation	2894	2914	2921	3199	3760	3736
B4	SHETL	Demand	1632	1628	1628	1608	1639	1630
B4	SHETL	Planned Transfer	1262	1286	1293	1591	2121	2106
B5	SPT	Effective Generation	5140	5257	5053	5187	5766	5746
B5	SPT	Demand	2854	2849	2837	2843	2889	2892
B5	SPT	Planned Transfer	2286	2408	2198	2344	2877	2854
B6	SPT	Effective Generation	9038	9468	9638	9770	10419	10165

Generation and Demand Profile								
Boundary	Name	Quantity (MW)	10/11	11/12	12/13	13/14	14/15	15/16
B6	SPT	Demand	5684	5684	5685	5707	5935	5928
B6	SHETL	Planned Transfer	3354	3784	3953	4063	4484	4237
B7	Upper North	Effective Generation	11957	12465	12737	13226	14204	14006
B7	Upper North	Demand	8432	8394	8364	8404	8647	8543
B7	Upper North	Planned Transfer	3525	4071	4373	4822	5556	5463
B8	Upper North	Effective Generation	11957	12465	12737	13226	14204	14006
B8	Upper North	Demand	8432	8394	8364	8404	8647	8543
B8	Upper North	Planned Transfer	3525	4071	4373	4822	5556	5463
B9	Midlands	Effective Generation	40318	40500	40676	40389	40399	39575
B9	Midlands	Demand	28736	28761	28846	28914	29169	29064
B9	Midlands	Planned Transfer	11582	11739	11829	11475	11230	10512
B10	South Coast	Effective Generation	2996	2789	2607	3016	3400	3366
B10	South Coast	Demand	6816	6737	6676	6656	6632	6644
B10	South Coast	Planned Transfer	-3820	-3948	-4069	-3641	-3232	-3278
B11	North East	Effective Generation	23284	23235	23040	23242	23861	23279
B11	North East	Demand	14218	14049	13902	14055	14407	14311
B11	North East	Planned Transfer	9066	9186	9139	9186	9454	8969
B12	South East	Effective Generation	9231	8959	8761	8936	9044	8912

Generation and Demand Profile								
Boundary	Name	Quantity (MW)	10/11	11/12	12/13	13/14	14/15	15/16
B12	South East	Demand	11631	11532	11463	11441	11411	11433
B12	South East	Planned Transfer	-2400	-2573	-2702	-2506	-2367	-2521
B13	South East	Effective Generation	1757	1734	1725	2140	2537	2511
B13	South East	Demand	2605	2567	2535	2529	2522	2528
B13	South East	Planned Transfer	-848	-833	-811	-390	15	-17
B14	London	Effective Generation	1723	1700	1691	1863	2021	1846
B14	London	Demand	9824	9902	10005	10089	10165	10252
B14	London	Planned Transfer	-8101	-8202	-8314	-8226	-8143	-8406
B15	Thames Estuary	Effective Generation	2497	2457	2438	2316	2178	3217
B15	Thames Estuary	Demand	2004	2013	2028	2022	2016	2008
B15	Thames Estuary	Planned Transfer	493	444	410	294	163	1209
B16	North East	Effective Generation	28921	29159	29298	29212	29501	28864
B16	North East	Demand	14923	14765	14633	14772	15109	15003
B16	North East	Planned Transfer	13998	14394	14665	14439	14392	13861
B17	West Midlands	Effective Generation	3397	3685	4002	3785	3541	3490
B17	West Midlands	Demand	6594	6738	6899	6884	6864	6878
B17	West Midlands	Planned Transfer	-3197	-3053	-2897	-3099	-3323	-3389

APPENDIX D : SUBTOTALS OF CAPACITY (MW) BY PLANT TYPE AND SYS STUDY ZONE, 2010/11

Subtotals of Capacity (MW) by Plant Type and SYS Study Zone					
Zone	**Node Name**	**Generation Type**	**Installed Active Power Capacity (MW)**	**Planned transfer condition available active power capacity (MW)**	**Total Capacity(MW)**
1	Beauly	Hydro	577	536	
		Pumped Storage	300	0	1528
		Wind Onshore	651	340	
2	KINTORE	CCGT	1380	1294	
		CHP	12	0	1410
		Hydro	18	0	
3	SLOY	Hydro	230	214	403
		Wind Onshore	172	0	
4	TEAL	Hydro	559	537	662
		Wind Onshore	103	74	
5	LOAN	CHP	139	0	
		LARGE COAL	2284	2220	2898
		Pumped Storage	440	430	
		Wind Onshore	35	0	
6	STHA	NUCLEAR	2289	1770	2289
	ECCL	COAL	1102	1000	
		Wind Onshore	1327	886	
		CCGT	20	0	2647
		Hydro	33	0	
		Biomass	45	0	
		CHP	120	0	
7	STEW	CCGT	1974	1800	
		Nuclear	1207	1070	3601
		Pumped Storage	420	0	
8	KEADBY	CCGT	4945	4250	
		CHP	1218	521	13995

Subtotals of Capacity (MW) by Plant Type and SYS Study Zone					
Zone	**Node Name**	**Generation Type**	**Installed Active Power Capacity (MW)**	**Planned transfer condition available active power capacity (MW)**	**Total Capacity(MW)**
9	DAINE	CCGT	2934	2320	
		CHP	365	0	
		COAL	4395	3610	10840
		NUCLEAR	960	800	
		OIL	2004	1600	
		Wind Offshore	182	0	
10	COTTAM	CCGT	2975	1815	6962
		COAL	3987	3200	
11	DARKELOW	CHP	228	0	4231
		COAL	4003	3402	
12	SUNDON	CCGT	3050	2304	
		Nuclear	1207	1000	5072
		Wind Offshore	815	600	
13	MELK	CCGT	4431	2860	
		COAL	3723	3400	
		Nuclear	430	400	9047
		OCGT	100	0	
		Pumped Storage	363	0	
14	WESTHAM	CCGT	2123	1455	
		OCGT	144	0	3512
		OIL	1245	0	
15	KINO	CCGT	3165	1000	
		COAL	3097	2100	
		Nuclear	1081	574	8899
		OIL	1355	0	
		Wind Offshore	201	0	
16	LOVEDEAN	CCGT	1320	1120	
		CHP	158	0	2709
		OCGT	195	0	
		OIL	1036	967	
17	MANN	CCGT	905	719	
		Nuclear	1261	1160	2306
		OCGT	140	0	

APPENDIX E : POWER FLOW DATA FOR TRANSMISSION LINE CALCULATION

Power Flow Data for transmission line calculation

Node From	Voltage (p.u.)	Angle (Deg)	Node To	Voltage (p.u.)	Angle (Deg)	Sending End Active Power	Sending End Reactive Power	Receiving End Active Power	Receiving End Reactive Power
1	1.0295	84.2	**2**	1.0021	79.2	247.1	-17.5	246.3	-9.6
1	1.0295	84.2	**4**	1.0041	76.1	151.7	-7	151.7	-13.4
2	1.0021	79.2	**4**	1.0041	76.1	674	-80.4	666.6	-90.8
2	1.0021	79.2	**5**	1.0367	66.3	288	-66	281.9	-82.1
3	1.0122	66.9	**18**	1.0069	64.6	209.3	-5.7	207.6	-6.3
4	1.0041	76.1	**3**	1.0122	66.9	57.2	-10.9	57.1	-11.4
4	1.0041	76.1	**5**	1.0367	66.3	461	-121	458	-125
4	1.0041	76.1	**18**	1.0069	64.6	420	-121	417	-125
5	1.0367	66.3	**6**	1.013	56.6	1291.2	182	1278.5	77.2
5	1.0367	66.3	**18**	1.0069	64.6	356	69.6	355	50.8
18	1.0069	64.6	**6**	1.013	56.6	576.5	-34.1	572.1	-25.7
6	1.013	56.6	**7**	0.9995	46.5	1782.8	-142.6	1775	-202.6
7	0.9995	46.5	**9**	0.9923	22.1	1514	-135	1495.2	-217.2
7	0.9995	46.5	**20**	0.9946	45.4	166.6	11.7	165.9	51.5
8	1.005	27	**9**	0.9923	22.1	2118.2	-67.1	2111	12.2
8	1.005	27	**10**	0.9987	24	5575	-165.4	5540.4	-370.5
9	0.9923	22.1	**11**	1.0031	11.5	4416.5	-454.2	4399.8	-585
10	0.9987	24	**11**	1.0031	11.5	2369	14.3	2342.4	-199.8
10	0.9987	24	**12**	1.0052	2.3	7543.6	-56.4	7428	-1139.9
11	1.0031	11.5	**12**	1.0052	2.3	1743	-184	1732.8	-250.2
11	1.0031	11.5	**13**	1.0081	-6	1743.8	-32.7	1724.3	-150.3
12	1.0052	2.3	**13**	1.0081	-6	502	-16.1	501	-30.3
12	1.0052	2.3	**14**	0.998	-11.4	5309.3	98	5273.7	-133.6
12	1.0052	2.3	**15**	1.012	-4.4	1402.7	-115.4	1396.1	-125.4
13	1.0081	-6	**17**	1.0123	-14.7	467.6	-103.6	466	-13.4
13	1.0081	-6	**21**	1.0087	-9.4	3583.6	-193	3560.8	-123.6
15	1.012	-4.4	**14**	0.998	-11.4	2462.6	-496.3	2461.3	-438.6
15	1.012	-4.4	**16**	1.0106	-13.6	510	-84.8	509.5	-31.9
19	1.0178	59.8	**20**	0.9946	45.4	1971.8	179.6	1970.2	164.8
20	0.9946	45.4	**8**	1.005	27	2051.3	-317.6	2041.7	171.7
21	1.0087	-9.4	**14**	0.998	-11.4	828	-97.5	824.5	-70.8
21	1.0087	-9.4	**16**	1.0106	-13.6	1873.2	-320.8	1869.8	-348.2
5	1.0367	66.3	**19**	1.0178	59.8	900.1	158.3	899.8	132
19	1.0178	59.8	**6**	1.013	56.6	53.9	28.4	53.8	75.8
16	1.0106	-13.6	**17**	1.0123	-14.7	258.9	-118.4	258.7	-53.2

APPENDIX F : EQUIVALENT TRANSMISSION LINE PARAMETERS

Equivalent Transmission Line Parameters

Node From	Node Name	Node To	Node Name	Resistance	Reactance	Capacitor
1	Beauly	2	KINTORE	0.0131827	0.0357304	0.14094
1	Beauly	4	TEAL	0.0232493	0.0944381	0.0717394
2	KINTORE	4	TEAL	0.000725854	0.00802517	0.129429
2	KINTORE	5	LOAN	0.0084387	0.0791794	0.244741
3	SLOY	18	WIYH	0.00312718	0.0195322	0.037958
4	TEAL	3	SLOY	0.039842	0.276557	0.0432212
4	TEAL	5	LOAN	0.00178785	0.0196683	0.724215
5	LOAN	6	STHA	0.000481853	0.0138213	0.553344
5	LOAN	18	WIYH	0.00359654	0.00427573	0.0284837
18	WIYH	6	STHA	0.000225073	0.0247056	0.43579
6	STHA	7	Harker	0.00170638	0.00981566	1.24496
7	Harker	9	DAINE	0.00357765	0.0268128	2.85932
7	Harker	20	STEW	0.000723123	0.0116172	0.217016
8	kEADBY	9	DAINE	0.000648777	0.00402015	1.30311
8	kEADBY	10	COTTAM	0.00015872	0.00093751	0.419851
9	DAINE	11	DARKELOW	0.000245273	0.00412473	3.47949
10	COTTAM	11	DARKELOW	0.000177761	0.00919722	1.50879
10	COTTAM	12	SUNDON	0.000311051	0.00493358	8.91499
11	DARKELOW	12	SUNDON	0.00102268	0.00914841	1.06073
11	DARKELOW	13	MELK	0.000643995	0.0175015	2.06014
12	SUNDON	13	MELK	0.000770538	0.0291332	0.289352
12	SUNDON	14	WESTHAM	0.000148217	0.00448969	5.18134
12	SUNDON	15	KINO	0.000240943	0.00846026	0.760088
13	MELK	17	MANN	0.0032082	0.0326645	0.791082
13	MELK	21	BRLE	5.78012E-05	0.00168566	1.38432
15	KINO	14	WESTHAM	0.00146298	0.00472198	1.74452
15	KINO	16	LOVEDEAN	0.00389277	0.0316322	0.659251
19	ECCL	20	STEW	3.17952E-05	0.0127756	2.40618
20	STEW	8	kEADBY	8.65229E-05	0.0154137	5.76743
21	BRLE	14	WESTHAM	0.00171314	0.00407798	0.271424
21	BRLE	16	LOVEDEAN	0.000591822	0.00388345	0.541884
5	LOAN	19	ECCL	0.0005	0.0132736	0.372344
6	STHA	19	ECCL	0.00042	0.0441124	0.236302
16	LOVEDEAN	17	MANN	0.00166948	0.00703486	0.34365

APPENDIX G: SYNCHRONOUS GENERATOR BLOCKS

Round Rotor Generator Model

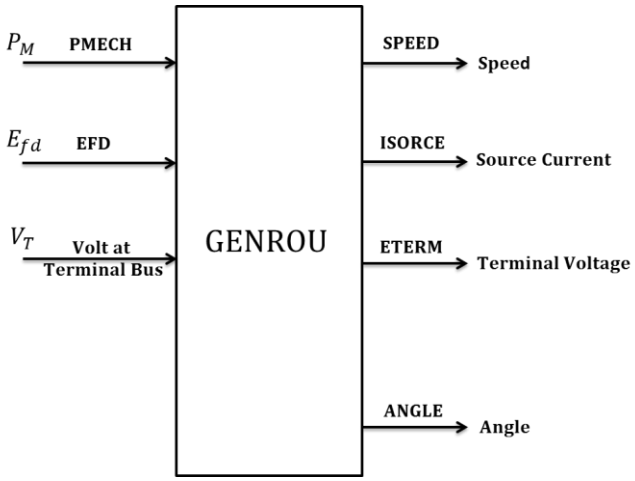

Dynamic Data Description **State Description**

CONs	Description	STATES	Description
J	T'_{d0} (>0) (sec)	K	E'_q
J+1	T''_{d0} (>0) (sec)	K+1	E'_d
J+2	T''_{q0} (>0) (sec)	K+2	ψkd
J+3	T''_{q0} (>0) (sec)	K+3	ψkq
J+4	H, inertia	K+4	Δ, speed (pu)
J+5	D, Speed damping	K+5	Angle (radians)
J+6	X_d		
J+7	X_q		
J+8	X'_d		
J+9	X'_q		
J+10	$X''_d = X''_q$		
J+11	X_I		
J+12	S(1.0)		
J+13	S(1.2)		

APPENDIX H: TURBINE GOVERNOR BLOCKS

Steam Turbine-Governor

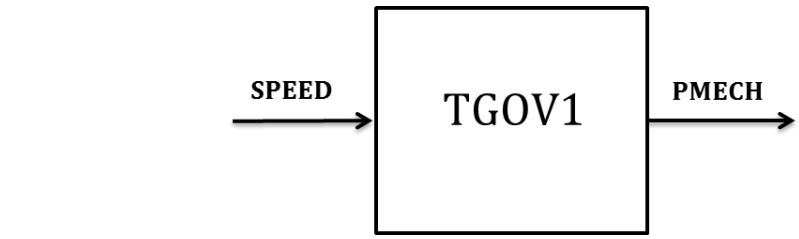

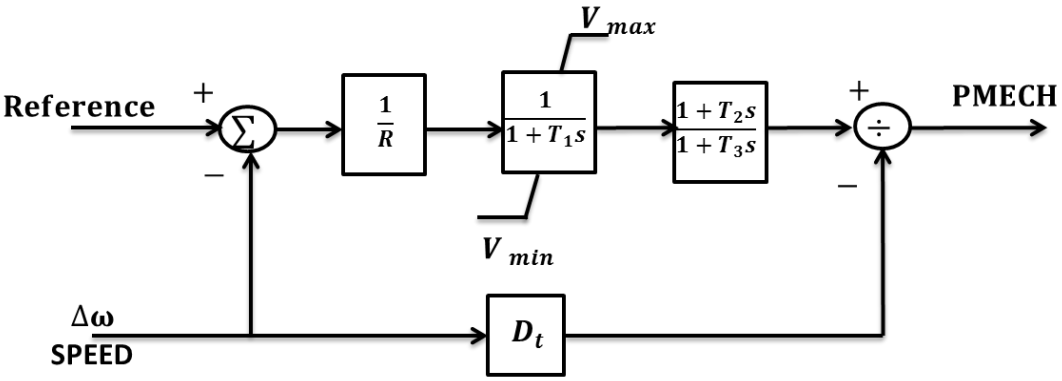

Dynamic Data Description **State Description**

CONs	Description	STATES	Description
J	R	K	Valve opening
J+1	T_1(>0) (sec)	K+1	Turbine power
J+2	V_{MAX} (>0) (sec)		
J+3	V_{MIN}(>0) (sec)		
J+4	T_2 (>0) (sec)		
J+5	T_3 (>0) (sec)		
J+6	D_t		

APPENDIX I: EXCITATION SYSTEM

SEXS

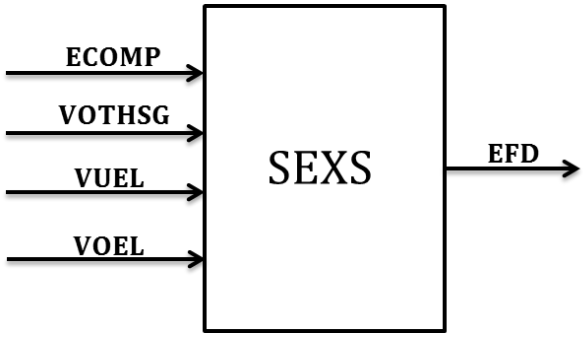

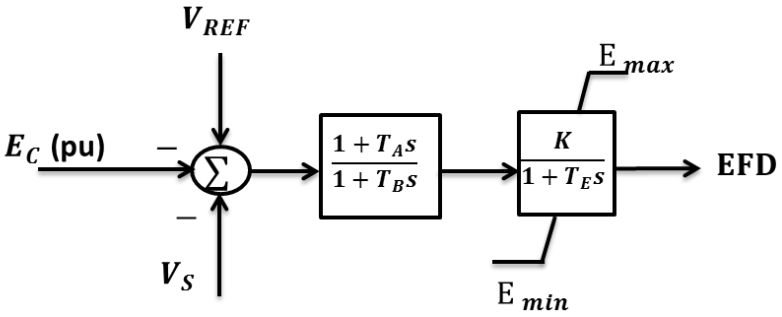

Dynamic Data Description **State Description**

CONs	Description	STATES	Description
J	T_A/T_B	K	First integrator
J+1	T_B(>0) (sec)	K+1	Second
J+2	K		
J+3	T_E(>0) (sec)		
J+4	E_{MIN} (pu on EFD base)		
J+5	E_{MAX} (pu on EFD base)		

APPENDIX J: POWER SYSTEM STABILIZER

Speed Sensitive Stabilizing Model

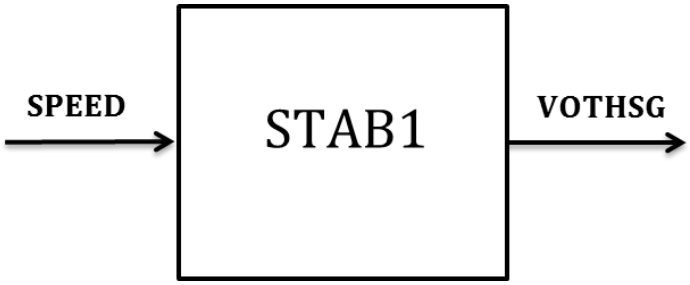

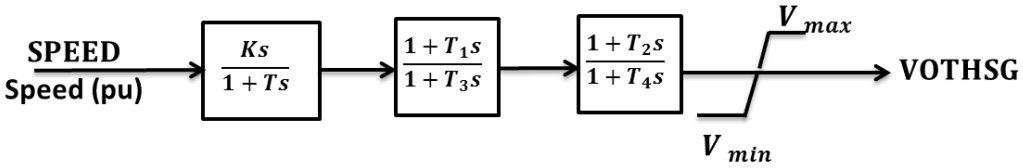

Dynamic Data Description **State Description**

CONs	Description	STATES	Description
J	$K/T\ (sec)^{-1}$	K	Washout
J+1	T(>0) (sec)	K+1	First lead-lag
J+2	T_1/T_3	K+2	Second lead-lag
J+3	T_3(>0) (sec)		
J+4	T_2/T_4		
J+5	T_4(>0) (sec)		
J+6	H_{LIM}		

APPENDIX K: WT3 DFIG MODEL DATA

WT3G1 Model			
J	X_{eq}	Equivalent reactance	0.8
J+1	K_{pll}	PLL first integrator gain	30
J+2	K_{ipll}	PLL second integrator gain	0
J+3	P_{llmax}	PLL maximum limit	0.1
J+4	P_{rated}	Turbine MW rating	1.5
WTE3 Model			
J	T_{fv}	Filter time constant in voltage regulator	0.15
J+1	K_{pv}	Proportional gain in voltage regulator	18
J+2	K_{IV}	Integrator gain in voltage regulator	5
J+3	X_c	Line drop compensation reactance	0.05
J+4	T_{FP}	Filter time constant in torque regulator	0.05
J+5	K_{IP}	Integrator gain in torque regulator	0.6
J+6	P_{MX}	Min limit in torque regulator	1.12
J+7	P_{MN}	Max limit in voltage regulator	0.1
J+9	Q_{MX}	Max limit in voltage regulator	0.296
J+10	Q_{MN}	Min limit in voltage regulator	-0.436
J+11	IP_{MAX}	Max active current limit	1.1
J+12	T_{RV}	Voltage sensor time constant	0.05
J+13	RP_{MX}	Max power order derivative	0.45
J+14	RP_{MN}	Min power order derivative	-0.45
J+15	$T_{\_Power}$	Power filter time constant	5
J+16	K_{qi}	MVAR/Voltage gain	0
J+17	V_{MNCL}	Min voltage limit	0.9
J+18	V_{MXCL}	Max voltage limit	1.2
J+19	K_{qv}	Voltage/MVAR gain	40
J+20	XIQ_{MN}	XIQmin	-0.5
J+21	XIQ_{MX}	XIQmax	0.4

J+22	T_V	Lag time constant in windVar controller	0.05
J+23	T_P	Pelec filter in fast PF controller	0.05
J+24	F_n	A proportion of online wind turbines	1
J+25	ωP_{min}	Shaft speed at Pmin	0.69
J+26	ωP_{20}	Shaft speed at 20% rated power	0.78
J+27	ωP_{40}	Shaft speed at 40% rated power	0.98
J+28	ωP_{60}	Shaft speed at 60% rated power	1.12
J+29	P_{min}	Minimum power for operating at ωP_{100} speed	0.74
J+30	ωP_{100}	Shaft speed at 100% rated power	1.2
WT3T Model			
J	VW	Initial wind	1.25
J+1	H	Total inertia constant	4.95
J+2	DAMP	Machine damping factor	0
J+3	K_{aero}	Aerodynamic gain factor	0.007
J+4	Theta2	Blade pitch at twice rated wind speed	21.98
J+5	H_{tfrac}	Turbine inertia fraction	0.875
J+6	$Freq_1$	First shaft torsional resonant frequency	1.8
J+7	D_{shaft}	Shaft damping factor	1.5
WT3P1			
J	T_p	Blade response time constant	0.3
J+1	K_{pp}	Proportional gain of PI controller	150
J+2	K_{ip}	Integrator gain of PI controller	25
J+3	K_{pc}	Proportional gain of the compensator	3
J+4	K_{ic}	Integrator gain of the compensator	30
J+5	TetaMn	Lower pitch angle limit	0
J+6	TetaMx	Upper pitch angle limit	27
J+7	RTetaMx	Upper pitch angle rate limit	10
J+8	P_{MX}	Power reference	1

APPENDIX L: HVDC MODEL DATA

VSC DC Model with Two VSC Converters			
J	T_{po_1}	Time constant of active power order controller	0.05
J+1	AC_VC_Limit_1	Reactive power limit for ac voltage control	0
J+2	AC_Vctrl_kp_1	Voltage control proportional gain	2.4
J+3	T_{ac_1}	Time constant for AC voltage PI integral	0.01
J+4	T_{acm_1}	Time constant of the ac voltage transducer	0.01
J+5	Lacmax_1	Current Limit	1
J+6	Droop_1	Voltage control droop	0
J+7	VCMX_1	Maximum VSC Bridge Internal Voltage	1.07
J+8	XREACT_1	Reactance of the ac series reactor	0.17
J+9	QMAX_1	Maximum system reactive limits in Mvars	60
J+10	QMIN_1	Minimum system reactive limits in Mvars	-60
J+11	AC_VC_KT_1	Adjustment Parameter for the feedback from reactive power limiter to ac voltage controller	1.2
J+12	AC_VC_KTP_1	Adjustment Parameter for the feedback from current order limiter to ac voltage controller	1
J+13	T_{po_2}	Time constant of active power order controller	0.05
J+14	AC_VC_Limit_2	Reactive power limit for ac voltage control	0
J+15	AC_Vctrl_kp_2	Voltage control proportional gain	2.4
J+16	T_{ac_2}	Time constant for AC voltage PI integral	0.01
J+17	T_{acm_2}	Time constant of the ac voltage transducer	0.01
J+18	Lacmax_2	Current Limit	1
J+19	Droop_2	Voltage control droop	0
J+20	VCMX_2	Maximum VSC Bridge Internal Voltage	1.07
J+21	XREACT_2	Reactance of the ac series reactor	0.17
J+22	QMAX_2	Maximum system reactive limits in Mvars	60
J+23	QMIN_2	Minimum system reactive limits in Mvars	-60
1	AC_VC_KT_2	Adjustment Parameter for the feedback from reactive power limiter to ac voltage controller	1.2
J+25	AC_VC_KTP_2	Adjustment Parameter for the feedback from current order limiter to ac voltage controller	1
J+26	$T_{po\_}DCL$	Time constant of the power order controller	0.05
J+27	$T_{po\_}lim$	Time constant of the power order limit controller	0.05